Consequences of Altered Short-Chain Carbon Metabolism in Heart Failure

2017

Julie Horton
University of Central Florida

CONSEQUENCES OF ALTERED SHORT-CHAIN CARBON METABOLISM IN HEART FAILURE

by

JULIE L. HORTON
B.S. University of Central Florida, 2011
M.S. University of Central Florida, 2013

A dissertation submitted in partial fulfillment of the requirements
for the degree of Doctor of Philosophy
in the Burnett School of Biomedical Sciences
in the College of Medicine
at the University of Central Florida
Orlando, Florida

Spring Term
2017

Major Professor: Daniel P. Kelly

ABSTRACT

Cardiovascular disease is currently the foremost cause of death within the United States. Heart failure (HF) is a syndrome defined by the inability of the heart to adequately execute requisite pump function in order to deliver nutrients and oxygen to peripheral tissues, irrespective of etiology. One of the most common causes of HF is chronic pressure overload due to hypertension. Ischemic heart disease is also a common driver of HF, often in conjunction with hypertension. Pressure overload initially causes compensatory metabolic changes. Structural changes follow shortly thereafter typically resulting in left ventricular hypertrophy. Eventually, the heart loses the ability to compensate for the aberrant hemodynamic load and begins failing. The failing heart is unable to supply adequate adenosine triphosphate (ATP) for contractile function as evidenced by falling phosphocreatine (PCr) levels. This energy deficit occurs concurrently with a metabolic re-programming that results in a fuel utilization pattern resembling the fetal heart. Notably, enzymes involved in catabolism of fatty acids, the chief fuel substrate for ATP generation in the normal adult heart, are downregulated in the failing heart. However, the extent to which alternative fuels compensate for decreased fatty acid oxidation (FAO) is not well-known. Furthermore, consequences of the fuel substrate switches that occur in heart failure are not well established.

In this work, we discover a new paradigm for alternate fuel utilization in the failing heart and define consequences of altered fuel metabolism in HF. We discovered a post-translational modification resultant from an accumulation of acetyl groups (C2) present in a mouse model of early-stage HF and human HF. Mitochondrial proteins were found

to be hyperacetylated in the failing heart, and at least some of these alterations result in diminished electron-transport chain (ETC) capacity as shown by mutagenesis studies on succinate dehydrogenase A (SDHA). We also found an accumulation of C4-OH carnitine, a by-product of ketone oxidation in HF. This metabolite aggregation occurred alongside an increase in β-hydroxybutyrate dehydrogenase 1 (BDH1) transcript and protein levels. This signature suggested that the failing heart shifted to ketone bodies as a fuel. Subsequent experiments confirmed increased capacity for myocardial ketone oxidation in compensated cardiac hypertrophy and in HF. The consequences of increased ketone oxidation were then assessed using a cardiac-specific BDH1 knockout (BDH1 KO) mouse. Despite not having any apparent defect at baseline, we found BDH1 KO mouse hearts are completely unable to oxidize 3-hydroxybutyrate. The deficit for ketone oxidation capacity became consequential upon subjugation to transverse aortic constriction with a small apical myocardial infarction (TAC/MI). The BDH1 KO mice exhibit altered pathological cardiac remodeling compared to wild-type controls. These latter data suggest the increased reliance on ketone oxidation in HF, mediated by BDH1, is an adaptive response.

Together the results of these studies provide important information regarding the consequences of altered fuel metabolism in HF. Recent reports of reduced HF mortality and elevated circulating ketone levels in patients prescribed Empagliflozin make cardiac ketone metabolism research in this dissertation particularly apropos.

ACKNOWLEDGMENTS

First and foremost, I would like to thank Dr. Daniel Kelly for giving me the opportunity of a lifetime. Taking a chance on me truly changed the world for the better. I will be forever grateful. Not only did Dr. Kelly give me the chance to pursue my dreams, but he also showed tremendous dedication to my training.

Dr. Alvaro Estevez has been one of the largest influences in molding my scientific thinking. He has also been one of the most supportive people in my life. His guidance, help, and advice are invaluable.

I have been honored to have Dr. Sampath Parthasarathy serve on my committee. His advice and suggestions are always insightful. His amicable nature is much appreciated; it gives me confidence when I need it most.

I was very lucky to have Dr. Peter Crawford accept a position on my committee. His unapologetic foray into the frontiers of science is truly inspirational. People like Dr. Crawford are paving the way for junior scientists like me to break barriers of possibility.

I would also like to thank Dr. Steven Ebert. Dr. Ebert has been an important mentor in my life since I was an undergraduate. He has been a constant source of sage advice. His honesty and sincerity have been very helpful throughout the years.

I am eternally grateful to Dr. Rick Vega. He has been an amazing mentor and friend. Talking with Dr. Vega is always enlightening, as he truly is a brilliant scientist. He gives fantastic advice as well. His help with everything I have done has been critical to my success.

I would like to express my immense gratitude to Teresa Leone. She has more grit and dedication than anyone I have ever met, and I really admire that. She has been essential in every aspect of my graduate training. Her influence in the Kelly lab is world-renowned (seriously), and I have benefited tremendously from all of her assistance.

My lab mates including; Ling Lai, Jeanne Brooks, Rosa Rosario, Tomoya Sakamoto aka my favorite postdoc, Byungyong Ahn, Michelle Trevino, and Emily Smith have all been critical players in everything I have accomplished during my graduate career.

Finally, I would like to acknowledge other major influences in my career to date: Ola Martin, Greg Aubert, Mangala Soundarapandian, Karl Chai, Roseann White, William Self, Muthu Periasamy, Craig Venter, Maynard James Keenan, Charles Darwin, Leonardo da Vinci, Dinesh Shamdasani, Salvador Dali, Jim Henson, my Dad, Jared, Miki, Bear, Pickle, and all things unknown.

TABLE OF CONTENTS

LIST OF FIGURES x
LIST OF TABLES xi
CHAPTER ONE: INTRODUCTION 1
CHAPTER TWO: AN OVERVIEW OF LITERATURE REGARDING HEART METABOLISM IN PHYSIOLOGICAL AND PATHOPHYSIOLOGICAL STATES 6
Cardiac Function 7
The Heart is an Essential Organ to Life 7
Oxidative Phosphorylation in the Cardiac Myocyte 8
Maintenance of ATP Levels in the Heart 10
Physiological Metabolic Plasticity in the Heart 11
Cardiac Metabolism during Development 11
Fuel Substrate Preference in the Healthy Adult Heart 14
Metabolism in the Failing Heart 17
Demand for Energy Exceeds Supply in Heart Failure 17
Fuel Shifts in the Failing Heart: Culprit or Innocent Bystander? 19
References 23
CHAPTER THREE: MITOCHONDRIAL PROTEIN HYPERACETYLATION IN THE FAILING HEART[1] 30
Abstract 30
Introduction 31
Results 33
Increased Lysine Acetylation of Mitochondrial Proteins in the Failing Mouse Heart 33
Increased Acetylation of Mitochondrial Proteins in the Failing Human Heart 37
Altered NAD^+ Homeostasis in Failing Heart 39
Evidence that Lysine Acetylation Affects Activity of Succinate Dehydrogenase A, a Key Component of the TCA Cycle and ETC Complex II 42
Discussion 45
Methods 50
Animal Studies 50
Human Studies 50

Western Blotting 51
Metabolomic Analysis of NAD^+ Metabolites 52
Acetylproteomics 53
Chemicals and Supplies 54
Mitochondrial Preparation 54
Sample Preparation 55
Fractionation and Enrichment 56
LC/MS/MS 57
Database Search, FDR filtering, and Acetylation Analysis 59
Protein Normalization 60
Mitochondrial Assignment 60
Mitochondrial Respiration 61
Vector Construction 61
Cellular Oxygen Consumption Rates 61
SDHA Activity 62
Statistics 63
Study Approval 63
Author Contributions 63
Acknowledgements 64
Footnotes 64
Conflict of Interest: 64
Reference Information: 65
References 65
Supplemental Material 70
CHAPTER FOUR: THE FAILING HEART RELIES ON KETONE BODIES AS A FUEL[2] 85
Abstract 85
Background 85
Methods and Results 85
Conclusions 86
Keywords: 86
Introduction 86
Methods 88

Animal Studies 88
Proteomics using Stable Labeling by Amino Acids (SILAC) 89
Substrate Oxidation Measurements 89
RNA Analyses 90
Western Blot 90
Metabolomic Analysis of Organic Acids and Acylcarnitines 90
Plasma Biochemistry Measurements 91
Statistical Analyses 91
Results 91
Mitochondrial Proteomic Profiling Reveals Evidence for Altered Fuel Utilization in the Hypertrophied and Early Stage Failing Mouse Heart 91
The Hypertrophied Heart Re-programs to Utilize Ketone Bodies as an Alternate Fuel Source 94
Identification of Metabolite Signatures of Ketone Utilization in the Myocardium of the Failing Heart 96
Discussion 100
Conclusions 104
Clinical Perspective 104
Acknowledgments 105
References 105
Data Supplement 111
Supplemental Methods 111
Supplemental References 128
CHAPTER FIVE: CONSEQUENCES OF INCREASED KETONE OXIDATION IN HEART FAILURE 129
Introduction 129
Results 131
Generation of Cardiac-specific BDH1 KO Mouse 131
BDH1 deficiency results in worsened pathologic cardiac remodeling in context of a pressure-overload stress 134
Discussion 137
Methods 144
Animal Studies 144
Cardiac specific BDH1 Knockout Mouse Production 144

Genotyping 144
Heart failure model 145
RNA Isolation 146
RT-qPCR 146
Metabolite Analysis 147
Substrate Oxidation Measurements 147
References 148
CHAPTER SIX: CONCLUSION 150
APPENDIX 153
Copyright Permission for Content in Chapter 3 154
Copyright Permission for Content in Chapter 4 157

LIST OF FIGURES

Figure 1. Increased lysine acetylation of mitochondrial proteins involved in multiple mitochondrial energy transduction pathways in cardiac tissue of mice from the heart failure group. 36

Figure 2. Increased acetylation of mitochondrial proteins in failing human heart. 38

Figure 3. Hyperacetylated mitochondrial proteins in failing human heart are involved in multiple energy transduction pathways. 39

Figure 4. Evidence for altered NAD+ homeostasis in failing mouse and human heart. 41

Figure 5. Evidence for acetylation effects on succinate dehydrogenase A function relevant to heart failure. 44

Figure 6. Schematic depicting a conceptual model for the impact of mitochondrial protein lysine acetylation as a driver of the progressive decline in capacity for mitochondrial oxidative flux and ATP synthesis known to occur during the development of heart failure. 49

Figure 7. Mitochondrial proteomic profiling in the hypertrophied and failing mouse heart. 93

Figure 8. *Bdh1* expression is induced in the hypertrophied and failing mouse heart. 95

Figure 9. Increased βOHB oxidation in the hypertrophied heart. 96

Figure 10. The myocardial metabolite profile of the failing heart is indicative of increased ketone utilization in the failing heart. 97

Figure 11. Myocardial metabolite profile on a ketogenic diet is similar to that observed for the HF mice on a standard chow diet. 99

Figure 12. Generation of cardiac-specific (cs) BDH1 KO mice. 132

Figure 13. csBDH1 KO mice are unable to oxidize 3OHB. 133

Figure 14. Survival rates following TAC/MI. 135

Figure 15. BDH1 KO mice exhibit severe pathological remodeling. 136

Figure 16. The gene expression signature indicates severe pathological remodeling in the BDH1 KO mouse 138

Figure 17. Proposed models for cardiac remodeling in csBDH1 KO mice. 143

LIST OF TABLES

Table 1. Mendelian ratios for offspring from *Cre*$^{-}$, *Bdh1* $^{f/f}$ crossed with *Cre*$^{+}$, *Bdh1* $^{f/f}$. 133
Table 2. Echocardiography data 4-weeks post-TAC/MI or sham procedure 135
Table 3. Genotyping Primers 145
Table 4. . RT-qPCR Primers 147

CHAPTER ONE: INTRODUCTION

Heart failure (HF) is a major worldwide health problem. The prevalence and mortality associated with this syndrome are significant (1). Etiology of heart failure varies widely, but the unifying characteristic is the inability of the heart to sufficiently pump enough blood throughout the body in order to meet the nutritive and oxygen demands of peripheral tissues. During the development of common forms of heart failure, contractile dysfunction occurs concurrently with energy metabolic alterations (2). The failing heart has diminished high-energy phosphate reserves suggesting inadequate capacity to supply adenosine triphosphate (ATP) relative to demand (3). Therefore, investigating the metabolic derangements of the failing heart and delineating the corresponding changes in fuel utilization and energy production could lead to new strategies for treatment of the syndrome. Whether metabolic derangements in heart failure are causative or consequential is a subject of intense investigation. Substantial evidence supports the conclusion that metabolic derangements serve as an aggravating element of heart failure, if not outright causative. In some genetic forms of heart failure, metabolic abnormalities clearly play a primary role as the causative factor (4).

Most heart failure patients in the United States have antecedent hypertension and/or ischemic heart disease (5). Aberrant hemodynamics increase the amount of pressure and consequently the requisite work the heart must do to maintain circulation. Pressure overload of the heart results in early metabolic changes preceding structural alterations. Chronic high-blood pressure eventually leads to hypertrophy of cardiac myocytes (6). Cardiac hypertrophy occurs concomitantly with a fuel shift to a more

“fetal” pattern including decreased reliance on fatty acids as a fuel substrate for ATP generation. This decrease in fatty acid oxidation (FAO) persists into heart failure. Downregulation in transcriptional factors and target FAO genes has been well-described by our lab and others as a driver in the altered fuel oxidation response in the hypertrophied and failing heart (4, 7). However, the degree to which alternative fuels compensate for the decreased FAO and consequences of the fuel substrate switch remain unknown. This is especially true for early-stage heart failure which is the subject of relatively few inquiries to date. Research into the compensated hypertrophic heart and early stages of heart failure is particularly important because earlier treatment in disease progression, prior to significant myocyte loss, would undoubtedly benefit patients.

In an effort towards understanding the metabolic events in the hypertrophied and early-stage failing heart, our lab conducted unbiased systems profiling of the transcriptome and metabolome in well-defined mouse models of compensated hypertrophy (CH) and early-stage heart failure (8). The transcriptional profiles of compensated hypertrophy and HF in this study showed strong positive correlation. The data corroborated previous findings of downregulated FAO genes in the hypertrophic and failing heart. However, the results also revealed the rather surprising finding that expression of genes involved in oxidative phosphorylation (OXPHOS) is not altered in either hypertrophy or early-stage heart failure (8). This finding contrasted studies detailing global downregulation of OXPHOS gene programs in late-stage heart failure (9-12).

While the transcriptional profile was similar between CH and HF, the metabolome exposed profound differences. The CH samples did not show a differential metabolite profile compared to sham controls. Conversely, there were multiple alterations in the HF samples including an accumulation of medium and long-chain acylcarnitines and decreased tricarboxylic acid cycle (TCA cycle) intermediates (8). In heart failure, the discrepancy between the unaltered gene expression profile and the changes in the metabolite profile suggested regulation of metabolism occurring at a post-transcriptional level. This dissertation seeks to investigate the potential source of these metabolite alterations and consequences in the failing heart.

Chapter 3, a first author manuscript, "*Mitochondrial Protein Hyperacetylation in the Failing Heart"*, investigates post-transcriptional changes in CH and HF. This work tests the hypothesis that lysine acetylation levels of mitochondrial proteins change in the failing heart. Indeed, we found dramatic lysine hyperacetylation of mitochondrial proteins not only in mouse models of HF but also in human HF. We then sought to determine if these hyperacetylation events had functional relevance. To this end, we focused on lysine 179 (K179) on succinate dehydrogenase, subunit A (SDHA), a hyperacetylated residue in the failing heart. We report loss-of-function in complex II of the ETC and SDHA specific catalytic deficiency resulting from K179 acetylation suggesting that at least some of the hyperacetylation observed in HF is consequential.

Chapter 4, a co-authored manuscript, "*The Failing Heart Relies on Ketone Bodies as a Fuel"*, initially describes the proteome in hearts from CH and HF mouse models. One of the findings in this unbiased query was that β-hydroxybutyrate

dehydrogenase 1 (BDH1) protein, a ketone metabolism enzyme, is upregulated in the failing heart. This inspired the hypothesis that the failing heart increasingly depends on ketone oxidation. Subsequent experiments provided additional support for this hypothesis. Interestingly, a separate group arrived at the same conclusion in late-stage human HF.

In Chapter 5, a first-author manuscript in preparation titled "*Consequences of Increased Ketone Oxidation in Heart Failure"*; we examine the consequences of the aforementioned ketone oxidation in HF. This investigation uses a novel cardiac-specific BDH1 knockout (KO) mouse to directly interrogate ramifications of ketone oxidation in the failing heart. An experiment utilizing isolated hearts perfused with labeled ketones show BDH1 is necessary for 3-hydroxybutyrate oxidation in the heart. BDH1 KO mice subject to transverse aortic constriction combined with a small apical myocardial infarction (TAC/MI) exhibit a more severe degree of pathological cardiac remodeling compared to BDH1 wild-type (WT) leading us to hypothesize that increased ketone oxidation in HF is an adaptive response. Delineation of the mechanism governing the BDH1-mediated ketone oxidation benefit in HF remains an active area of investigation.

In summary, this dissertation project was designed to explore the metabolic derangements in the failing heart. The overall objective was to identify new candidate therapeutic targets or biomarkers that could aid in treating patients with HF. The following specific aims were pursued to accomplish this goal:

1.) To define significant and functional consequences of elevated mitochondrial acetyl pools in the failing heart.

2.) To determine alternative fuel substrates utilized in the failing heart in context of reduced fatty acid oxidation.

3.) To determine consequences of elevated ketone oxidation, as an alternate fuel, in heart failure.

CHAPTER TWO:
AN OVERVIEW OF LITERATURE REGARDING HEART METABOLISM IN PHYSIOLOGICAL AND PATHOPHYSIOLOGICAL STATES

Cardiovascular disease (CVD) kills more people in the United States than any other cited cause of death. One in nine death certificates implicate heart failure (HF) as a primary or corollary causation. Individuals diagnosed with HF face daunting odds for long-term survival. After a patient is initially hospitalized for heart failure, 10.4% die within a month, 22% die within a year, and 42.3% die within five years (1). It is noteworthy that current mortality rates signify improvement. Thirty-four years ago, 50% of HF patients died within *two years* of initial hospitalization (13). Similarly, in most of the world, ischemic heart disease mortality rates declined significantly over the last 30 years (14). The decrease in mortality is largely attributed to changes in treatment regimens and developments in implantable devices (15).

However, the incidence of heart failure has not similarly improved (1). The fact that CVD remains the leading cause of death reflects the substantial prevalence of HF; afflicting almost 6 million adults in the United States alone. Furthermore, the health burden is expected to grow with an almost 50% increase in prevalence by 2030 (1). Therefore, it is essential to expand current knowledge of HF pathology and continue developing strategies for prevention and treatment.

Cardiac Function

The Heart is an Essential Organ to Life

All living things must meet basic requirements of cellular processes in order to survive. At the most fundamental level, a cell must receive requisite nutrients and conversely dispose of generated waste products. A prokaryotic organism can accomplish this task by utilizing a variety of mechanisms including passive diffusion and active transport to move nutrients and waste across a cell membrane and/or cell wall. In single cell eukaryotes, these processes occur similarly across membranes of the various organelles, and compartmentalization allows for appreciable specificity in deliverance of proper nutrients and removal of appropriate waste. The transport of nutrients and waste becomes more complex in multicellular organisms as the surface area of the cell decreasingly interfaces with the environment. As the level of organismal complexity increases, the requirements to specifically transport nutrients and waste to proper physical locations must correspondingly evolve (17). In large multicellular organisms like humans, the process to transport nutrients and waste throughout the body is mediated by a closed circulatory system.

A closed circulatory system accommodates the blood that carries oxygen and nutrients to all the cells of the body and similarly carries waste away from origination cells to sites of disposal. Blood, like all physical substances on Earth, must adhere to the physical limitations imposed by gravity; and as such, circulation requires an input of mechanical energy. In closed circulatory systems, the energy to move blood throughout the body is provided by a biotic pump called a heart. The heart pumps blood throughout

the body by contracting and relaxing, emptying and filling the chambers with blood respectively. The rhythm and force of contraction must precisely provide temporal and spatial regulation of blood flow. Thus, preservation of vertebrate life relies on faithful operation of the heart (18).

The pump function of the heart results from deliberately coordinated contractions produced within cardiac myocytes. The contractions made within an individual myocyte result from force generation produced by proteins in the extracellular matrix. The proteins involved in myocyte contraction constitute the intracellular contractile apparatus. The mechanical energy of contraction is derived from transformation of chemical energy released during adenosine triphosphate (ATP) hydrolysis (6).

Oxidative Phosphorylation in the Cardiac Myocyte

Since contraction of cardiac myocytes depends on ATP, a sufficient supply of ATP is of paramount importance. The healthy, developed heart generates ATP largely through oxidative phosphorylation (OXPHOS), which occurs in the mitochondria (16). ATP production from OXPHOS takes advantage of an electrochemical gradient called the proton motive force (19). Complexes I, III, and IV of the electron-transport chain (ETC) pump protons obtained from oxidation of reducing equivalents into the space between the inner and outer mitochondrial membranes (20). The electrons obtained from oxidation of reducing equivalents move through the ETC in a series of redox reactions that leave the electrons and corresponding complexes in a lower energetic state. This continues until the electrons reduce oxygen and form water. The energy released during

the transfer of electrons is used to pump protons into the intermembrane space against the concentration gradient (21). The requirement of oxygen as a terminal electron acceptor in the ETC is absolute. In absence of oxygen, electrons cannot proceed to lower energy states, and the proton-pumping complexes, in turn, will not have sufficient energy to send protons to the intermembrane space (6). For this reason, the importance of sufficient delivery of oxygenated blood to cardiac myocytes cannot be overstated.

The collection of protons in the intermembrane space of the mitochondria create a charge differential across the inner membrane. The F_o component of complex V, also called ATP synthase, functions as an ion channel and allows reflux of the protons into the mitochondrial matrix. The reflux of protons releases free energy previously stored as potential energy in the electrochemical gradient. The chemical energy released by proton flow into the mitochondrial matrix is transformed into mechanical energy rotating the stalk and F_o subunit of ATP synthase. The rotation causes conformational changes in the F_1 subunit of ATP synthase resulting in the shape required to catalyze phosphorylation of adenosine diphosphate (ADP) using an inorganic phosphate and produce ATP (22).

Reducing equivalents employed by the ETC are nicotinamide adenine dinucleotide plus hydrogen (NADH) and flavin adenine dinucleotide plus hydrogen ($FADH_2$). NADH and $FADH_2$ are formed from a variety of redox reactions occurring in the cytoplasm and mitochondria. Redox enzymes catalyze the removal of hydrogens from carbon based substrates, often referred to as fuels, and subsequent reduction of either nicotinamide adenine dinucleotide (NAD^+) or flavin adenine dinucleotide (FAD).

The NADH made in the cytoplasm must be transported to the mitochondria, and this process occurs via the malate-aspartate shuttle (23).

The collected pool of NADH in the mitochondria is oxidized by NADH dehydrogenase (complex I), a large membrane-bound flavoprotein. Mammalian respiratory complex I contains 45 subunits with 14 of those catalytically involved in the oxidation of NADH, transfer of electrons, and pumping of protons (24). The electrons from NADH are transferred through flavin mononucleotide co-factors to iron-sulfur clusters and eventually reach ubiquinone at the ubiquinone binding site.

$FADH_2$ oxidation occurs at the site of the dehydrogenase reaction. $FADH_2$ generated from fatty acid oxidation (FAO) involves the electron transfer flavoprotein (ETF). ETF conducts electrons from $FADH_2$ to ubiquinone in the respiratory chain. FAD is directly reduced to $FADH_2$ by succinate dehydrogenase (SDH) in a reaction coupled with succinate oxidation. The electrons are transferred through iron-sulfur clusters of SDH to ubiquinone. The reduced ubiquinone pool is oxidized by complex III (25).

Maintenance of ATP Levels in the Heart

In summary, proper function of the ETC requires sufficient: 1) oxygen, 2) catabolic substrates, and 3) mitochondrial oxidative capacity. The quantity of the aforementioned factors deemed sufficient depends completely on the demand for ATP. The cardiac demand for ATP is dictated primarily by the needs of the contractile apparatus, but anabolic processes also require ATP, albeit a much smaller amount. The heart must respond virtually instantaneously to the needs of cells, and consequently cardiac

workload is dynamic. An expeditious mechanism is in place to accommodate fluctuations in ATP demand (26).

The mitochondrial creatine kinase (MtCK) functions to generate a high-energy phosphate reservoir in the heart. The creatine kinase reaction works in tandem with adenylate kinase (AK) to regulate ATP levels and localization. When the heart produces more ATP than is required, it stores the high-energy phosphate in the form of phosphocreatine (PCr). PCr also serves to transfer ATP from mitochondria to the myofibrils, the main site of ATP utilization in the cardiac myocyte. Conversely, when the energetic demands exceed the rate of ATP production, the heart uses the phosphate stored in PCr to phosphorylate ADP and make requisite ATP (27). The PCr reserves, though, only provide momentary compensation. Typical concentrations of ATP and PCr in a healthy heart can only sufficiently supply no more than a few heart beats before depletion (6). This fact underscores the importance of flawless cardiac bioenergetics.

Physiological Metabolic Plasticity in the Heart

Cardiac Metabolism during Development

The heart is an energetic omnivore capable of utilizing a variety of substrates to produce ATP depending on its physiological or pathophysiological circumstances. One of the most well-described fuel substrate switches occurs in the developing heart. The heart is the first functional organ in the embryo. It continues to grow in order to meet the circulatory demands of a growing fetus. Cellular growth, proliferation, and limited

oxygen availability disproportionally favor anaerobic glycolysis and lactate oxidation as lipids are needed for biosynthesis of daughter cells.

An embryonic heart primarily uses glycolysis to generate ATP independently of the mitochondria. The catalytic machinery necessary for OXPHOS is not yet well-developed, and lactate oxidation accounts for the majority of fetal oxygen consumption. Only 15% of the ATP generated in the fetal heart is acquired from FAO (28). Another major determinant of fetal heart metabolism is substrate availability. Circulating fatty acids are scarce in the fetus whereas lactate is abundant. The fetal heart readily consumes lactate and predominately expresses the A isomer of lactate dehydrogenase (LDHA), which converts pyruvate to lactate (29). The metabolic phenotype of the fetal heart can be summarized as primarily deriving ATP from glycolysis and lactate oxidation with fatty acids playing a relatively minor role.

Immediately preceding birth, the fetal heart undergoes a surge of mitochondrial biogenesis, exponentially increasing the number of mitochondria in the heart (30, 31, 32). Recent work also implicated mitophagy of fetal mitochondria as an essential element in cardiac maturation (33). In the early neonatal period, approximately half of cardiac ATP is derived from glycolysis. The levels of circulating lactate decrease dramatically, and consequently lactate oxidation contributes far less to ATP production. Ketone bodies are believed to be transiently oxidized in the postnatal period. The remaining ATP is derived from a dramatic increase in capacity for FAO (34). During the neonatal period, mitochondrial content expands and matures through a process that involves both biogenesis and fusion/fission dynamics (35).

Within days of birth, the heart reaches maturation with respect to its bioenergetic profile. Rates of cardiac FAO are approximately 10-times levels present at birth concomitant with the ingestion of milk. The increased reliance on fatty acids for ATP production accompanies a parallel decrease in glycolysis (35, 36).

A network of transcription factors facilitates metabolic gene expression changes in the postnatal developing heart. Work in the Kelly lab demonstrated that peroxisome proliferator-activated receptor gamma coactivator 1-alpha (PGC-1α) is necessary and sufficient for perinatal mitochondrial biogenesis (35, 36). PGC-1α works as a master regulator by co-activating several critical transcription factors: the peroxisome proliferator-activated receptors (PPARα, β/δ, and γ), the estrogen related receptors (ERRα, β, γ), and the nuclear respiratory factors (NRF1/2) (37, 38, 39). PPARα and ERR, in coordination with PGC-1α, induce FAO gene expression allowing for the shift to increased reliance on fatty acids for ATP generation (40). The ERR transcription factors are also essential for inducing expression of multiple tricarboxylic acid cycle (TCA cycle) and OXPHOS genes. They are also at least partially responsible for regulating expression of developmentally appropriate excitation-contraction coupling proteins (41, 42, 43). NRF-1 and NRF-2 control expression of critical subunits that form ETC complexes. They also regulate gene expression necessary for mitochondrial deoxyribonucleic acid (mtDNA) replication and transcription (44, 45).

Contrary to the mitochondrial dynamism seen in the developing heart, rates of mitochondrial turnover in the adult heart are relatively slow, occurring once every two weeks. Existing mitochondria must instead adjust their oxidative capacity and fuel

substrate preference to alterations in physiology (46). Under normal physiological conditions, OXPHOS supplies approximately 90% of the heart's ATP and fatty acids are the preferential fuel substrate. However, the developed myocardium maintains substantial metabolic plasticity and can use amino acids, glucose, lactate, and ketones to generate energy (47). This flexibility allows the heart to maintain adequate cardiac power provided enough substrate is available (48, 49).

Fuel Substrate Preference in the Healthy Adult Heart

In a physiological setting, the heart encounters a variety of potentially competing substrates. Under these conditions, the healthy heart preferentially oxidizes fatty acids to form acetyl-CoA and reducing equivalents for the ETC (50). FAO accounts for 60-90% of the ATP generated in the adult heart (30). Demonstrating the indelible preference for FAO, providing the heart with excessive glucose does not stimulate increased pyruvate-derived acetyl-CoA. Similarly, contribution to the acetyl-CoA pool from the oxidation of fatty acids is not curtailed when uptake of glucose is elevated with insulin. One can surmise that in the healthy heart, levels of glucose entering the myocardium do not precipitate decreased FAO (51).

Despite preferentially using fatty acids, the heart will continually import glucose. The import of glucose does not depend on rates of FAO. Instead, when FAO provides adequate acetyl-CoA, the pyruvate formed from glycolysis will be converted to lactate or glycogen (51, 48). The Randle cycle explains this fuel substrate prioritization, implicating products of FAO as short-term graduated inhibitors of glycolysis (52).

The normal heart maintains the capacity to oxidize glucose if necessary. The heart appears to maintain its voracious appetite for glucose as a preparatory measure for acute metabolic stress. With rapid elevations in workload, the heart will increasingly use pyruvate to form acetyl-CoA. Also, in hypoxic environments, the heart continues to import circulating glucose, anaerobically producing ATP through glycolysis and generating lactate (49, 51). Nonetheless, the heart's ability to import glucose does encounter an upper limit, necessitating at least a second fuel substrate in cases of long-term metabolic stress (49).

Ketone oxidation is considerably limited in the normal, adult heart. Unlike glucose in the presence of competing substrates, rates of ketone oxidation do not increase with an increase in cardiac workload (49, 51). However, under experimental conditions fully suppressing FAO, there is an elevation in ketone oxidation. In fact, an increase in myocardial ketone oxidation in absence of FAO is preferential to increased glucose oxidation. The rate of myocardial ketone oxidation is inversely proportional to the rate of FAO. When provided adequate glucose and ketones, the heart can maintain constant ATP production in absence of FAO by using ketones as a primary fuel and glucose as a secondary fuel (49). It is important to note, though, that cardiac ketone metabolism has not been extensively studied *in vivo*, and the aforementioned studies were largely conducted in artificial conditions.

Much of the predilection for FAO in the heart can be attributed to gene regulation by nuclear receptor transcription factors acting as metabolic sensors. The Kelly laboratory defined this network in heart. A variety of endogenous fatty acids serve as

activating ligands for PPARs. Therefore, in the presence of fatty acids, PPARs will regulate expression of target genes in an isoform specific manner. PPARα and PPARβ/δ both activate FAO enzyme expression, and PPARβ/δ additionally activates expression of glucose oxidation enzymes (53, 54, 40).

The importance of PPARα as a metabolic sensor was demonstrated in experiments with cardiac-specific overexpression of PPARα in mice. These mice have increased rates of cardiac FAO. This substantial increase in FAO occurred concurrently with an accumulation of triglycerides in the heart. Interestingly, the PPARα overexpressing mice develop left ventricular hypertrophy (LVH) and dysfunction. This cardiac pathology can then be prevented by deletion of the fatty acid import protein cluster of differentiation 36 (CD36). These experiments provide clear evidence that the levels of PPARα expression are carefully calibrated for optimal rates of import and oxidation of fatty acids (55).

Other experiments provided further elucidation of the complex gene program governing FAO. ERRα has been shown to activate expression of PPARα amongst other metabolic genes (43). ERRα is coactivated by PGC-1α to regulate FAO enzyme expression such as the medium chain acyl-CoA dehydrogenase (MCAD). MCAD catalyzes the first step in oxidation of medium-chain fatty acids and is a necessary intermediate enzyme for oxidation of long and very-long chain fatty acids (42, 56). Furthermore, ERRα has been shown to regulate nearly all other aspects of oxidative energy transduction including transcription of TCA cycle genes and ETC related genes (57, 42).

Metabolism in the Failing Heart

Demand for Energy Exceeds Supply in Heart Failure

Heart failure in adults is a progressive syndrome that begins when the healthy heart encounters stress. Chronic pressure-overload of the heart, as occurs in hypertension, typically results in LVH if left untreated (58, 5). Indeed, high-blood pressure is a notorious risk factor for heart failure; 75% of HF patients have antecedent hypertension (1, 5).

The mechanism by which hypertension causes hypertrophy occurs at a cellular level. As afterload (blood pressure) increases, velocity of myocyte shortening decreases. Ventricles with myocytes enduring these conditions become less effective at ejecting blood against the elevated systemic pressures (6). To compensate, the heart increases the number of sarcomeres and mitochondria to supplement contractile function. This, in turn, triggers a hypertrophic growth response resulting in enlarged myocytes (59). The auxiliary contractile function in the pathological hypertrophic growth response is associated with reactivation of gene programs encoding fetal forms of contractile proteins (60). The increased workload placed upon the heart from abnormal hemodynamics intrinsically alters left ventricular function and consequently energy metabolism (2). In fact, hypertension in absence of hypertrophy results in PCr levels equitable to normotensive individuals, suggesting sufficient capacity for the heart to accommodate *acute* elevations in workload (2).

The alterations in cardiac metabolism begin at onset of pressure-overload and precede myocyte hypertrophy. In human heart failure, considerable evidence exists to

support the hypothesis that the failing heart cannot produce sufficient ATP for energetic demand. One study found concentrations of ATP and PCr reduced by 35% and 51% respectively in the failing human heart (3). Other studies have reported significant declines in PCr with no change in ATP. These latter studies concluded the discrepant data likely reflected an earlier stage of heart failure (61). These findings in humans have also been recapitulated in experimental models of HF (62).

Taken together, these data suggest progressive deterioration in the ability of the failing heart to meet energetic demand. In early stages of HF, the heart cannot sufficiently produce ATP. The existing PCr high-energy phosphate stores compensate, resulting in lower PCr levels but maintenance of ATP concentrations. As heart failure progresses, PCr levels continue to decline, unable to compensate for insufficient ATP production. Additionally, significant decreases in creatine and MtCK activity in the failing heart have been reported, potentially accounting for declining ATP concentrations before total exhaustion of PCr (63).

In addition to the “energy-starved” condition accompanying heart failure, many lines of evidence support the notion that metabolic perturbations can cause heart failure. One of the most compelling pieces of evidence exists in the way of inherited genetic conditions. Inborn errors in FAO genes cause early onset cardiomyopathy (PMID: 8114864). Defects in mitochondrial encoded genes cause a variety of myopathies. Mutations in nuclear encoded genes involved in metabolism also cause hypertrophy and heart failure (64). A number of knockout and transgenic mice designed with perturbations in cardiac OXPHOS enzymes develop heart failure as well (65). For

instance, in loss-of-function experiments deleting ERRα in a mouse, pressure-overload results in decompensated heart failure (66).

Interestingly, not all transcription factors appear independently critical as many important regulatory functions have biological “fail-safe” compensatory strategies. For example, PGC-1α knockout mice do not display overt dysfunction under basal conditions (35). However, following pressure-overload, loss of PGC-1α results in accelerated cardiac remodeling (PMID: 16775082). Knockout of peroxisome proliferator-activated receptor gamma coactivator 1-beta (PGC-1β) results in a similarly normal phenotype. Further investigation elucidated PGC-1β as functionally redundant, essentially assuming the role of PGC-1α in the knockout (PMID: 16775082, PMID:18628400). However, the ability for PGC-1-mediated compensation to maintain function only applies to non-stressed conditions. Mice lacking both isoforms of PGC-1 lose compensatory phenotype seen in single KO, resulting in an early perinatal lethality accompanied by a late fetal arrest of mitochondrial biogenesis in the heart(PMID:18628400). The decrease in FAO that occurs in HF, which is discussed in detail in the next section, is especially striking given the redundancy in the oxidative metabolism gene program.

Fuel Shifts in the Failing Heart: Culprit or Innocent Bystander?

The metabolic plasticity of the heart permits rapid changes in fuel substrate utilization. Onset of hypertension triggers a decreased reliance on fatty acids as an oxidative fuel (2). Interestingly, decreased myocardial FAO in hypertensive patients is an independent

predictor of LVH (66). The rationale for the heart decreasing fatty acid utilization upon pressure-overload is not well-understood. Furthermore, it is not known if the correlative decreases in FAO observed during hypertension are causal or consequential of hypertrophy and eventual failure.

As discussed previously, there is substantial evidence supporting the idea that the failing heart cannot adequately meet ATP demand. Generally, there is also agreement that worsening heart failure accompanies reductions in FAO rates. In end-stage human heart failure particularly, there is well-established impairment in FAO (4). This is supported by multiple reports of dramatic downregulation in FAO enzymes including significant reductions in long-chain acyl-CoA dehydrogenase (LCAD) and MCAD (7).

Early-stage idiopathic dilated cardiomyopathy patients also consistently have lower FAO rates (4). Experimental models of pressure-overload induced HF repeatedly show decreases in FAO enzyme expression as well (67, 68, 7, 8). Furthermore, some studies equate decreased FAO enzyme levels with decreased FAO rates. For example, in a canine model of HF, 40% reductions in MCAD protein levels are correlated with an equivalent 40% decrease in FAO capacity (69).

There are a few caveats regarding the downregulation of FAO in HF. Some etiologies of HF demonstrate elevated FAO capacity *early* in disease progression and only exhibit downregulation of FAO in late-stage HF (4). Still other etiologies have a completely opposite metabolic signature; the diabetic failing heart, as an example, does not display the characteristic decreased FAO. Instead, diabetic hearts experience an

upregulation of FAO in hypertrophy, likely reflective of the high levels of free fatty acids activating PPARs (55, 70). The majority of HF, though, occurs as a result of pressure-overload and consistently presents a decreased degree of FAO.

The regulatory mechanisms dictating the decrease in FAO during pressure-overload induced HF are relatively well-described. Similar to the reactivation of fetal isoforms of contractile genes, the metabolic profile in HF is often referred to as a reversion to a “fetal” program (30). The ability of the heart to compensate under hemodynamic stress depends on the same gene regulatory mechanisms responsible for the cardiac fuel substrate switch that takes place during development. PPARα levels and activity decline in human HF and animal models of pressure-overload induced cardiac hypertrophy (7, 71). Also in human HF, expression of ERR target genes are significantly downregulated (66). Notably, the depression of FAO gene expression starts in hypertrophy preceding overt dysfunction and persists through heart failure (30).

While evidence for lower FAO rates in HF is well-documented, the degree to which the failing heart compensates with an alternative fuel substrate is more enigmatic. Moreover, considerable questions regarding the *consequences* of a fuel substrate switch in HF remain unanswered. The failing heart appears to, at least in part, compensate for decreased FAO with elevated glycolysis. A few studies report elevated glucose oxidation gene expression (55, 70). However, the vast majority of studies report no change in levels of enzymes involved with import of glucose, glycolysis, or conversion of pyruvate into acetyl-CoA (4). The absence of altered glycolytic molecular machinery implicates regulation of glycolytic enzyme activity, potentially via

mechanisms employed by the Randle cycle. Therefore, the most plausible explanation for increased glycolysis in HF is not a deliberate compensation but instead occurs fortuitously by virtue of decreased FAO. Additionally, the degree to which glycolysis can effectively augment ATP production is not clear (4).

The research directly describing lactate utilization and ketone oxidation in the failing heart is scarce. Rodent models of heart failure are consistently reported to have increases in monocarboxylate transporter 1 (MCT-1), which import both lactate and ketones (72). Multiple studies also report elevated plasma ketone levels and hepatic ketogenesis in heart failure patients (73). Additionally, strong positive correlation exists between acetone concentrations in exhalation and severity of HF (74). Another investigation directly measured myocardial ketone extraction rates between healthy and failing human hearts reporting no difference (75). This summarization of the current literature epitomizes the lack of robust research conducted to date regarding alternative fuel substrate utilization in the failing heart.

There is no doubt that metabolism plays a critical role in heart function and dysfunction. Thus, examining the metabolism of the failing heart will certainly provide valuable insight to inform treatment decisions. Some of the intricacies of metabolism in the failing heart have been described. It is well-established that downregulation of FAO occurs in HF. Elucidation of the transcriptional circuitry regulating FAO during HF has provided insight into the mechanisms governing this process. However, very little is known about the role of alternative fuel substrates in HF. Questions remain such as, what happens when FAO is downregulated? What fuel substrates power the failing

myocardium? What dictates preference for one substrate versus another in HF? How does alternative fuel substrate utilization affect prognosis of heart failure?

Thus, the objective of this dissertation aims to begin delineating the consequences of altered short-chain carbon metabolism in heart failure. This dissertation specifically tests the hypotheses that during heart failure: 1) metabolite derangements, namely increases in acetyl-pools, result in post-translational modifications of key metabolic proteins, 2) metabolic reprogramming occurs that increases myocardial ketone oxidation capacity, and 3) the increased capacity for ketone oxidation is an adaptive mechanism.

References

1. Mozaffarian D, Benjamin EJ, Go AS, et al. Heart Disease and Stroke Statistics-2016 Update: A Report From the American Heart Association. Circulation. 2016;133(4):e38-60.

2. Taegtmeyer H, Overturf ML. Effects of moderate hypertension on cardiac function and metabolism in the rabbit. Hypertension. 1988;11(5):416-26.

3. Beer M, Seyfarth T, Sandstede J, et al. Absolute concentrations of high-energy phosphate metabolites in normal, hypertrophied, and failing human myocardium measured noninvasively with (31)P-SLOOP magnetic resonance spectroscopy. J Am Coll Cardiol. 2002;40(7):1267-74.

4. Lopaschuk GD, Ussher JR, Folmes CD, Jaswal JS, Stanley WC. Myocardial fatty acid metabolism in health and disease. Physiol Rev. 2010;90(1):207-58.

5. Johnson FL. Pathophysiology and etiology of heart failure. Cardiol Clin. 2014;32(1):9-19, vii.

6. Iaizzo PA. Handbook of Cardiac Anatomy, Physiology, and Devices. Springer; 2015.

7. Sack MN, Rader TA, Park S, Bastin J, Mccune SA, Kelly DP. Fatty acid oxidation enzyme gene expression is downregulated in the failing heart. Circulation. 1996;94(11):2837-42.

8. Lai L, Leone TC, Keller MP, et al. Energy metabolic reprogramming in the hypertrophied and early stage failing heart: a multisystems approach. Circ Heart Fail. 2014;7(6):1022-31.

9. Gao Z, Xu H, DiSilvestre D, Halperin VL, Tunin R, Tian Y, Yu W, Winslow RL, Tomaselli GF. Transcriptomic profiling of the canine tachycardia-induced heart failure model: global comparison to human and murine heart failure. J Mol Cell Cardiol. 2006;40:76–86.
10. Bugger H, Schwarzer M, Chen D, Schrepper A, Amorim PA, Schoepe M, Nguyen TD, Mohr FW, Khalimonchuk O, Weimer BC, Doenst T. Proteomic remodelling of mitochondrial oxidative pathways in pressure overload-induced heart failure. Cardiovasc Res. 2010;85:376–384.
11. Barth AS, Kumordzie A, Frangakis C, Margulies KB, Cappola TP, Tomaselli GF. Reciprocal transcriptional regulation of metabolic and signaling pathways correlates with disease severity in heart failure. Circ Cardiovasc Genet. 2011;4:475–483.
12. Xu J, Nie HG, Zhang XD, Tian Y, Yu B. Down-regulated energy metabolism genes associated with mitochondria oxidative phosphorylation and fatty acid metabolism in viral cardiomyopathy mouse heart. Mol Biol Rep. 2011;38:4007–4013.
13. Merlo M, Pivetta A, Pinamonti B, et al. Long-term prognostic impact of therapeutic strategies in patients with idiopathic dilated cardiomyopathy: changing mortality over the last 30 years. Eur J Heart Fail. 2014;16(3):317-24.

14. Moran AE, Forouzanfar MH, Roth GA, et al. Temporal trends in ischemic heart disease mortality in 21 world regions, 1980 to 2010: the Global Burden of Disease 2010 study. Circulation. 2014;129(14):1483-92.

15. Hunt SA, Abraham WT, Chin MH, et al. ACC/AHA 2005 Guideline Update for the Diagnosis and Management of Chronic Heart Failure in the Adult: a report of the American College of Cardiology/American Heart Association Task Force on Practice Guidelines (Writing Committee to Update the 2001 Guidelines for the Evaluation and Management of Heart Failure): developed in collaboration with the American College of Chest Physicians and the International Society for Heart and Lung Transplantation: endorsed by the Heart Rhythm Society. Circulation. 2005;112(12):e154-235.

16. Mootha VK, Arai AE, Balaban RS. Maximum oxidative phosphorylation capacity of the mammalian heart. Am J Physiol. 1997;272(2 Pt 2):H769-75.

17. Margulis L. Origin of Eukaryotic Cells, Evidence and Research Implications for a Theory of the Origin and Evolution of Microbial, Plant, and Animal Cells on the Precambrian Earth. New Haven, Yale University Press, 1970.; 1970.

18. Adshead J. Our Present Gaol System Deeply Depraving to the Prisoner and a Positive Evil to the Community, Some Remedies Proposed. 1847.

19. Mitchell P. Coupling of phosphorylation to electron and hydrogen transfer by a chemi-osmotic type of mechanism. Nature. 1961;191:144-8.

20. Sazanov LA. A giant molecular proton pump: structure and mechanism of respiratory complex I. Nat Rev Mol Cell Biol. 2015;16(6):375-88.

21. Nelson DL, Cox MM. Lehninger Principles of Biochemistry. W. H. Freeman; 2012.

22. Boyer PD, Cross RL, Momsen W. A new concept for energy coupling in oxidative phosphorylation based on a molecular explanation of the oxygen exchange reactions. Proc Natl Acad Sci USA. 1973;70(10):2837-9.

23. Lanoue KF, Williamson JR. Interrelationships between malate-aspartate shuttle and citric acid cycle in rat heart mitochondria. Metab Clin Exp. 1971;20(2):119-40.

24. Zhu J, Vinothkumar KR, Hirst J. Structure of mammalian respiratory complex I. Nature. 2016;536(7616):354-8.

25. Rutter J, Winge DR, Schiffman JD. Succinate dehydrogenase - Assembly, regulation and role in human disease. Mitochondrion. 2010;10(4):393-401.

26. Wallimann T, Wyss M, Brdiczka D, Nicolay K, Eppenberger HM. Intracellular compartmentation, structure and function of creatine kinase isoenzymes in tissues with high and fluctuating energy demands: the 'phosphocreatine circuit' for cellular energy homeostasis. Biochem J. 1992;281 (Pt 1):21-40.

27. Scholz TD, Laughlin MR, Balaban RS, Kupriyanov VV, Heineman FW. Effect of substrate on mitochondrial NADH, cytosolic redox state, and phosphorylated compounds in isolated hearts. Am J Physiol. 1995;268(1 Pt 2):H82-91.

28. Lopaschuk GD, Spafford MA, Marsh DR. Glycolysis is predominant source of myocardial ATP production immediately after birth. Am J Physiol. 1991;261(6 Pt 2):H1698-705.

29. Iyer NV, Kotch LE, Agani F, et al. Cellular and developmental control of O2 homeostasis by hypoxia-inducible factor 1 alpha. Genes Dev. 1998;12(2):149-62.

30. Dorn GW, Vega RB, Kelly DP. Mitochondrial biogenesis and dynamics in the developing and diseased heart. Genes Dev. 2015;29(19):1981-91.

31. Smolich JJ, Walker AM, Campbell GR, Adamson TM. Left and right ventricular myocardial morphometry in fetal, neonatal, and adult sheep. Am J Physiol. 1989;257(1 Pt 2):H1-9.

32. Marin-garcia J, Ananthakrishnan R, Goldenthal MJ. Heart mitochondrial DNA and enzyme changes during early human development. Mol Cell Biochem. 2000;210(1-2):47-52.

33. Gong G, Song M, Csordas G, Kelly DP, Matkovich SJ, Dorn GW. Parkin-mediated mitophagy directs perinatal cardiac metabolic maturation in mice. Science. 2015;350(6265):aad2459.

34. Bartelds B, Gratama JW, Knoester H, et al. Perinatal changes in myocardial supply and flux of fatty acids, carbohydrates, and ketone bodies in lambs. Am J Physiol. 1998;274(6 Pt 2):H1962-9.

35. Martin OJ, Lai L, Soundarapandian MM, et al. A role for peroxisome proliferator-activated receptor γ coactivator-1 in the control of mitochondrial dynamics during postnatal cardiac growth. Circ Res. 2014;114(4):626-36.

36. Lehman JJ, Barger PM, Kovacs A, Saffitz JE, Medeiros DM, Kelly DP. Peroxisome proliferator-activated receptor gamma coactivator-1 promotes cardiac mitochondrial biogenesis. J Clin Invest. 2000;106(7):847-56.

37. Huss JM, Kopp RP, Kelly DP. Peroxisome proliferator-activated receptor coactivator-1alpha (PGC-1alpha) coactivates the cardiac-enriched nuclear receptors estrogen-related receptor-alpha and -gamma. Identification of novel leucine-rich interaction motif within PGC-1alpha. J Biol Chem. 2002;277(43):40265-74.

38. Scarpulla RC. Nuclear control of respiratory chain expression by nuclear respiratory factors and PGC-1-related coactivator. Ann N Y Acad Sci. 2008;1147:321-34.

39. Puigserver P, Wu Z, Park CW, Graves R, Wright M, Spiegelman BM. A cold-inducible coactivator of nuclear receptors linked to adaptive thermogenesis. Cell. 1998;92(6):829-39.

40. Gulick T, Cresci S, Caira T, Moore DD, Kelly DP. The peroxisome proliferator-activated receptor regulates mitochondrial fatty acid oxidative enzyme gene expression. Proc Natl Acad Sci USA. 1994;91(23):11012-6.

41. Schreiber SN, Emter R, Hock MB, et al. The estrogen-related receptor alpha (ERRalpha) functions in PPARgamma coactivator 1alpha (PGC-1alpha)-induced mitochondrial biogenesis. Proc Natl Acad Sci USA. 2004;101(17):6472-7.

42. Sladek R, Bader JA, Giguère V. The orphan nuclear receptor estrogen-related receptor alpha is a transcriptional regulator of the human medium-chain acyl coenzyme A dehydrogenase gene. Mol Cell Biol. 1997;17(9):5400-9.

43. Huss JM, Torra IP, Staels B, Giguère V, Kelly DP. Estrogen-related receptor alpha directs peroxisome proliferator-activated receptor alpha signaling in the transcriptional control of energy metabolism in cardiac and skeletal muscle. Mol Cell Biol. 2004;24(20):9079-91.

44. Scarpulla RC, Vega RB, Kelly DP. Transcriptional integration of mitochondrial biogenesis. Trends Endocrinol Metab. 2012;23(9):459-66.

45. Gleyzer N, Vercauteren K, Scarpulla RC. Control of mitochondrial transcription specificity factors (TFB1M and TFB2M) by nuclear respiratory factors (NRF-1 and NRF-2) and PGC-1 family coactivators. Mol Cell Biol. 2005;25(4):1354-66.

46. Lai L, Wang M, Martin OJ, et al. A role for peroxisome proliferator-activated receptor γ coactivator 1 (PGC-1) in the regulation of cardiac mitochondrial phospholipid biosynthesis. J Biol Chem. 2014;289(4):2250-9.

47. Lopaschuk GD, Jaswal JS. Energy metabolic phenotype of the cardiomyocyte during development, differentiation, and postnatal maturation. J Cardiovasc Pharmacol. 2010;56(2):130-40.

48. Bøtker HE, Goodwin GW, Holden JE, Doenst T, Gjedde A, Taegtmeyer H. Myocardial glucose uptake measured with fluorodeoxyglucose: a proposed method to account for variable lumped constants. J Nucl Med. 1999;40(7):1186-96.

49. Sharma N, Okere IC, Brunengraber DZ, et al. Regulation of pyruvate dehydrogenase activity and citric acid cycle intermediates during high cardiac power generation. J Physiol (Lond). 2005;562(Pt 2):593-603.

50. Lanoue K, Nicklas WJ, Williamson JR. Control of citric acid cycle activity in rat heart mitochondria. J Biol Chem. 1970;245(1):102-11.

51. Taegtmeyer H, Hems R, Krebs HA. Utilization of energy-providing substrates in the isolated working rat heart. Biochem J. 1980;186(3):701-11.

52. Hales CN, Walker JB, Garland PB, Randle PJ. Fasting Plasma Concentrations Of Insulin, Non-Esterified Fatty Acids, Glycerol, and Glucose in the Early Detection of Diabetes Mellitus. Lancet. 1965;1(7376):65-7.

53. Aoyama T, Peters JM, Iritani N, et al. Altered constitutive expression of fatty acid-metabolizing enzymes in mice lacking the peroxisome proliferator-activated receptor alpha (PPARalpha). J Biol Chem. 1998;273(10):5678-84.

54. Djouadi F, Brandt JM, Weinheimer CJ, Leone TC, Gonzalez FJ, Kelly DP. The role of the peroxisome proliferator-activated receptor alpha (PPAR alpha) in the control of cardiac lipid metabolism. Prostaglandins Leukot Essent Fatty Acids. 1999;60(5-6):339-43.

55. Finck BN, Lehman JJ, Leone TC, et al. The cardiac phenotype induced by PPARalpha overexpression mimics that caused by diabetes mellitus. J Clin Invest. 2002;109(1):121-30.

56. Vega RB, Kelly DP. A role for estrogen-related receptor alpha in the control of mitochondrial fatty acid beta-oxidation during brown adipocyte differentiation. J Biol Chem. 1997;272(50):31693-9.

57. Wang T, Mcdonald C, Petrenko NB, et al. Estrogen-related receptor α (ERRα) and ERRγ are essential coordinators of cardiac metabolism and function. Mol Cell Biol. 2015;35(7):1281-98.

58. Mcmullen JR, Jennings GL. Differences between pathological and physiological cardiac hypertrophy: novel therapeutic strategies to treat heart failure. Clin Exp Pharmacol Physiol. 2007;34(4):255-62.

59. Zak R. Growth of the Heart in Health and Disease. Raven Pr; 1984.

60. Rajabi M, Kassiotis C, Razeghi P, Taegtmeyer H. Return to the fetal gene program protects the stressed heart: a strong hypothesis. Heart Fail Rev. 2007;12(3-4):331-43.

61. Weiss RG, Gerstenblith G, Bottomley PA. ATP flux through creatine kinase in the normal, stressed, and failing human heart. Proc Natl Acad Sci USA. 2005;102(3):808-13.

62. Sorokina N, O'donnell JM, Mckinney RD, et al. Recruitment of compensatory pathways to sustain oxidative flux with reduced carnitine palmitoyltransferase I activity characterizes inefficiency in energy metabolism in hypertrophied hearts. Circulation. 2007;115(15):2033-41.

63. Nascimben L, Ingwall JS, Pauletto P, et al. Creatine kinase system in failing and nonfailing human myocardium. Circulation. 1996;94(8):1894-901.

64. Morita H, Seidman J, Seidman CE. Genetic causes of human heart failure. J Clin Invest. 2005;115(3):518-26.

65. Karamanlidis G, Lee CF, Garcia-menendez L, et al. Mitochondrial complex I deficiency increases protein acetylation and accelerates heart failure. Cell Metab. 2013;18(2):239-50.

66. Aubert G, Vega RB, Kelly DP. Perturbations in the gene regulatory pathways controlling mitochondrial energy production in the failing heart. Biochim Biophys Acta. 2013;1833(4):840-7.

67. Osorio JC, Stanley WC, Linke A, et al. Impaired myocardial fatty acid oxidation and reduced protein expression of retinoid X receptor-alpha in pacing-induced heart failure. Circulation. 2002;106(5):606-12.

68. Lei B, Lionetti V, Young ME, et al. Paradoxical downregulation of the glucose oxidation pathway despite enhanced flux in severe heart failure. J Mol Cell Cardiol. 2004;36(4):567-76.

69. Panchal AR, Stanley WC, Kerner J, Sabbah HN. Beta-receptor blockade decreases carnitine palmitoyl transferase I activity in dogs with heart failure. J Card Fail. 1998;4(2):121-6.

70. Finck BN, Han X, Courtois M, et al. A critical role for PPARalpha-mediated lipotoxicity in the pathogenesis of diabetic cardiomyopathy: modulation by dietary fat content. Proc Natl Acad Sci USA. 2003;100(3):1226-31.

71. Barger PM, Brandt JM, Leone TC, Weinheimer CJ, Kelly DP. Deactivation of peroxisome proliferator-activated receptor-alpha during cardiac hypertrophic growth. J Clin Invest. 2000;105(12):1723-30.

72. Stanley WC, Recchia FA, Lopaschuk GD. Myocardial substrate metabolism in the normal and failing heart. Physiol Rev. 2005;85(3):1093-129.

73. Cotter DG, Schugar RC, Crawford PA. Ketone body metabolism and cardiovascular disease. Am J Physiol Heart Circ Physiol. 2013;304(8):H1060-76.

74. Yokokawa T, Sugano Y, Shimouchi A, et al. A case of acute decompensated heart failure evaluated by series of exhaled acetone concentrations as noninvasive biomarker of heart failure severity. Int J Cardiol. 2016;204:112-3.

75. Janardhan A, Chen J, Crawford PA. Altered systemic ketone body metabolism in advanced heart failure. Tex Heart Inst J. 2011;38(5):533-8.

CHAPTER THREE:
MITOCHONDRIAL PROTEIN HYPERACETYLATION IN THE FAILING HEART[1]

[1]This chapter has been published as JL Horton, OJ Martin, L Lai, NM Riley, AL Richards, RB Vega, TC Leone, DJ Pagliarini, DM Muoio, KC Bedi Jr., KB Margulies, JJ Coon, and DP Kelly. Mitochondrial protein hyperacetylation in the failing heart. *JCI Insight.* 2016;1(2):e84897

Abstract

Myocardial fuel and energy metabolic derangements contribute to the pathogenesis of heart failure. Recent evidence implicates posttranslational mechanisms in the energy metabolic disturbances that contribute to the pathogenesis of heart failure. We hypothesized that accumulation of metabolite intermediates of fuel oxidation pathways drives posttranslational modifications of mitochondrial proteins during the development of heart failure. Myocardial acetylproteomics demonstrated extensive mitochondrial protein lysine hyperacetylation in the early stages of heart failure in well-defined mouse models and the in end-stage failing human heart. To determine the functional impact of increased mitochondrial protein acetylation, we focused on succinate dehydrogenase A (SDHA), a critical component of both the tricarboxylic acid (TCA) cycle and respiratory complex II. An acetyl-mimetic mutation targeting an SDHA lysine residue shown to be hyperacetylated in the failing human heart reduced catalytic function and reduced complex II–driven respiration. These results identify alterations in mitochondrial acetyl-CoA homeostasis as a potential driver of the development of energy metabolic derangements that contribute to heart failure.

Introduction

The adult mammalian heart requires enormous amounts of energy to sustain contractile function. Given that cardiomyocyte energy stores are limited, ATP must be continually generated by oxidation of carbon fuels, necessitating a high-capacity finely tuned mitochondrial system (1–5). Significant evidence suggests that insufficient capacity for mitochondrial fuel oxidation and ATP production is causally linked to the development of heart failure (HF). For example, human genetic defects in mitochondrial fatty acid oxidation (FAO), the chief fuel utilization pathway in heart, or derangements in oxidative phosphorylation (OXPHOS)/electron transport complex (ETC), cause cardiomyopathy (6). Studies conducted in animal models of HF have shown reduced capacity for mitochondrial FAO and increased reliance on glycolysis (7–16). Cardiac magnetic resonance spectroscopy studies in humans have shown that myocardial “high-energy” phosphocreatine (PCr) stores are reduced with pathological ventricular hypertrophy and decline further during the transition to HF (17–21). Notably, the [PCr]/[ATP] ratio correlates with HF severity and is a strong predictor of cardiovascular mortality (22, 23).

The mechanisms involved in curtailing the ability of the failing heart to satisfy its voracious appetite for ATP are a subject of intense investigation. To date, most studies have focused on late-stage HF. The results of such studies have identified widespread changes in energy metabolic gene expression associated with structural and functional mitochondrial abnormalities, cardiomyocyte death, and fibrosis, likely reflecting the final common pathway of late-stage disease (24–27). However, the primary events involved in energy metabolic remodeling en route to HF have not been well characterized.

Recently, we employed an unbiased systems biology approach to identify molecular signatures of altered energy metabolism in the hypertrophied and early-stage failing mouse heart using integrated transcriptomics and metabolomics (28). This strategy unveiled the surprising finding that transcription of the majority of genes involved in mitochondrial energy transduction and OXPHOS is not altered in the hypertrophied and failing heart, with the notable exception of a progressive downregulation of genes involved in FAO. In striking contrast, tissue metabolite pools were broadly perturbed in the failing heart and distinguished the onset of contractile dysfunction and ventricular remodeling. These integrated profiling results strongly suggest that posttranslational mechanisms are an important contributor to the derangements in mitochondrial carbon flux during development of HF.

The results of our recent metabolomic profile of the failing mouse heart (28) revealed a potential mechanism whereby mitochondrial proteins may be altered at the posttranslational level. Notably, levels of acetylcarnitine (C2-carnitine), which are thought to reflect changes in the mitochondrial pool of acetyl-CoA, were increased in the failing heart but not in compensated cardiac hypertrophy (28). Consistent with this finding, acetyl-CoA levels were recently shown to be increased in the failing human heart (29). There is evidence that increased acetyl-CoA concentration can drive acetylation of nonhistone proteins (30, 31). In addition, emerging evidence indicates that increased lysine acetylation may result in enzymatic dysfunction (30, 32, 33). Accordingly, the observed expansion of the acetyl-CoA pool in the failing heart suggests that increased mitochondrial protein acetylation may contribute to derangements in

mitochondrial energy metabolism in the failing heart. To address this possibility, we conducted unbiased, mass spectrometric–based, acetylproteomic studies on heart samples from well-defined mouse models of cardiac remodeling and in the failing human heart. The results demonstrate a striking increase in mitochondrial protein lysine acetylation in the failing heart. Our results also suggest that alterations in protein acetylation can affect mitochondrial fuel oxidation and respiration, contributing to the vicious cycle of “energy starvation” that contributes to the syndrome of HF.

Results

Increased Lysine Acetylation of Mitochondrial Proteins in the Failing Mouse Heart

The mitochondrial acetylproteome was profiled in cardiac samples from well-defined mouse models of compensated pathologic cardiac hypertrophy and HF using mass spectrometry. Established mouse models of pressure overload–induced cardiac hypertrophy and failure were used for these studies. In brief, transverse aortic constriction (TAC) was performed on C57BL/6J mice (34). TAC performed on 8- to 12-week-old C57BL/6J mice resulted in significant left ventricular (LV) hypertrophy, with preserved systolic function and no evidence of chamber volume remodeling or reduced ejection fraction at the 4-week time point, referred to here as compensated hypertrophy (CH). In a second age-matched experimental group, termed the HF group, TAC was combined with a small apical myocardial infarction (MI) achieved by placing a ligature in the distal portion of the left anterior descending coronary artery, which resulted in predictable global LV systolic and diastolic dilatation and significantly reduced LV

ejection fraction (LVEF) 4 weeks after the procedure (28, 35). This approach allowed us to define molecular profiles in the early stages of CH and HF at a similar age and duration of pressure overload.

Cardiac ventricular mitochondria were purified from the samples taken from CH and HF groups and corresponding sham-operated controls. Acetylated peptides were enriched from the extracted mitochondrial proteins via anti-acetyl lysine antibodies. A total of 244 unique acetylated lysine sites situated in 82 mitochondrial proteins (from a total of 383 mitochondrial proteins identified) were identified (Supplemental Table 1). 57% of the identified acetylated proteins exhibited two or more acetylated lysine residues. Considering fold changes greater than ± 1.5 as compared to control samples, 42 mitochondrial protein acetylation sites were differentially decorated in the HF samples (increased acetylation in 37 residues and decreased acetylation in 5 residues; Supplemental Table 2). Of the 37 residues with increased acetylation, 16 of these sites were identified previously as potential targets of sirtuin 3 (SIRT3) deacetylase activity in mouse heart (32) (Supplemental Table 2).

Pathway analysis (Ingenuity Pathway Analysis) demonstrated that acetylated mitochondrial proteins involved in mitochondrial energy transduction were highly represented (Supplemental Table 3). Notably, a significant number of hyperacetylated proteins in the HF samples were embedded in key fuel catabolic and ATP synthetic pathways, including FAO, tricarboxylic acid (TCA) cycle, and ETC (Figure 1A and Supplemental Table 3). In contrast to the acetylproteomic profile of the HF samples, the CH group exhibited fewer hyperacetylated proteins and greater directional

heterogeneity (hyperacetylated and hypoacetylated proteins) in the FAO, TCA, and ETC pathways (Figure 1B and Supplemental Table 4). Taken together, these findings suggest that, during the progression from compensated cardiac hypertrophy to HF, net mitochondrial protein acetylation increases.

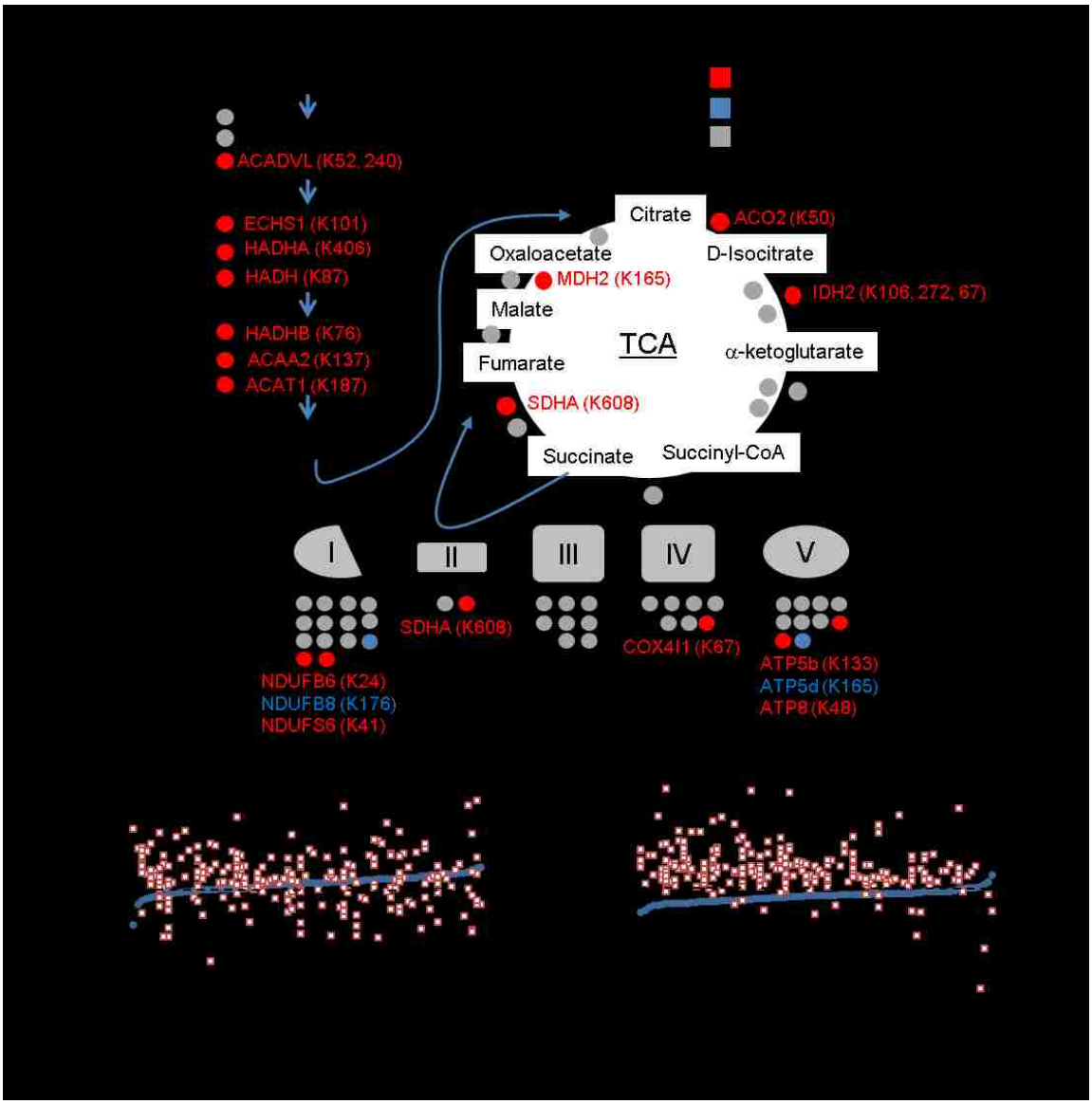

Figure 1. Increased lysine acetylation of mitochondrial proteins involved in multiple mitochondrial energy transduction pathways in cardiac tissue of mice from the heart failure group.

(A) Lysine-acetylated proteins (indicated by circles, protein symbols are noted) identified by mass spectrometry in both heart failure (HF) samples and sham-operated control samples (n = 2/group) in each of the 3 main mitochondrial fuel oxidation/ATP synthesis pathways (β-oxidation, tricarboxylic acid [TCA] cycle, and electron transport complex [ETC]). All acetylated residues with at least ± 1.5 fold change for mean HF/control values are shown. Specific lysine acetylation sites are noted in parentheses. Acetylation status is indicated by color coding: proteins with increased acetylation (HF/sham) are in red; proteins with decreased acetylation are in blue; and proteins with no change are in gray. **(B)** All detected acetylated mitochondrial proteins were rank ordered according to log2 fold change between compensated hypertrophy (CH) or HF and their corresponding sham controls in mean protein abundance along the x axis (blue circles). The log2 fold change between CH or HF and corresponding sham controls of each detected acetyl isoform (red squares, normalized to corresponding protein abundance) is plotted on the y axis in the same position on the x axis as the corresponding protein. The dashed line represents no change in acetylation level. Additional numerical data is provided in Supplemental Tables 2-4. SDHA, succinate dehydrogenase A.

Increased Acetylation of Mitochondrial Proteins in the Failing Human Heart

To determine the relevance of the cardiac acetylproteomic findings in mice to human HF, we interrogated the cardiac acetylproteome of the failing human heart. For these studies, we conducted proteomics on samples prepared from LV of 5 cardiac transplant recipients with end-stage dilated cardiomyopathy (DCM group, LVEF = 10%) and 5 nonfailing (NF) organ donors with normal LV function (NF group, LVEF = 47%–80%). Significant acetylation changes were defined as a cutoff of ± 1.5 fold change or $P < 0.05$ based on a Student's *t* test when comparing mean values of the DCM versus NF groups. Similar to the findings in the mouse HF samples, failing human heart samples exhibited a marked increase in mitochondrial protein acetylation (Supplemental Table 5). The general increase in mitochondrial protein acetylation in the DCM samples is shown in heat map (Figure 2A) and graphic (Figure 2B) formats. Whereas many of the hyperacetylated lysine residues are shared between mouse and human HF samples, a substantial number were species-specific (as seen in the comparison between Supplemental Tables 3 and 5). The reason for this latter observation is unclear but likely relates to differences in the relative acetylome coverage in each study and, in some cases, nonconserved residues between mice and humans. Importantly, similar to the mouse heart results, enzymes and proteins involved in multiple mitochondrial energy transduction pathways exhibited increased lysine acetylation, including FAO, TCA, ETC, and OXPHOS (Figure 3).

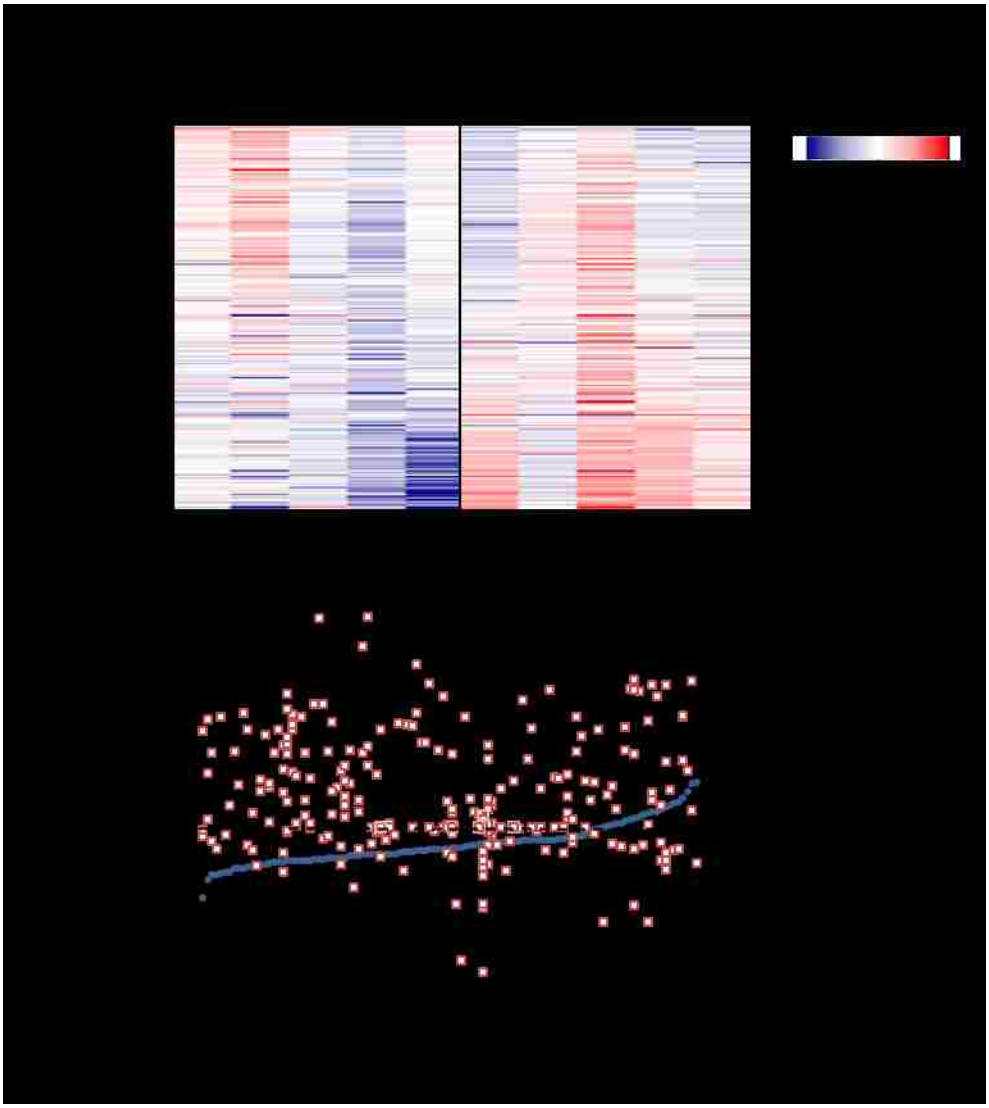

Figure 2. Increased acetylation of mitochondrial proteins in failing human heart.

(A) Heat map of the acetylproteomics data set representing the log2-transformed value of mitochondrial acetyl isoforms from cardiac biopsies of dilated cardiomyopathy (DCM) patients (n = 5) or nonfailing (NF) controls (n = 5). Acetylation events were normalized to corresponding protein abundance. The horizontal data lines represent the normalized value for each patient relative to the mean value across all 10 samples. The color coding indicates the direction and magnitude of the normalized log2-transformed value for each detected acetyl form, blue indicates low and red indicates high, in each patient sample. **(B)** All detected acetylated mitochondrial proteins were individually rank ordered according to the log2 fold change in mean protein abundance (DCM/NF) along the x axis (blue circles). The log2 fold change between DCM and NF controls of each detected acetyl isoform (red squares, normalized to corresponding protein abundance) is plotted on the y axis in the same position on the x axis as the corresponding protein. The dashed line represents no change in acetylation level.

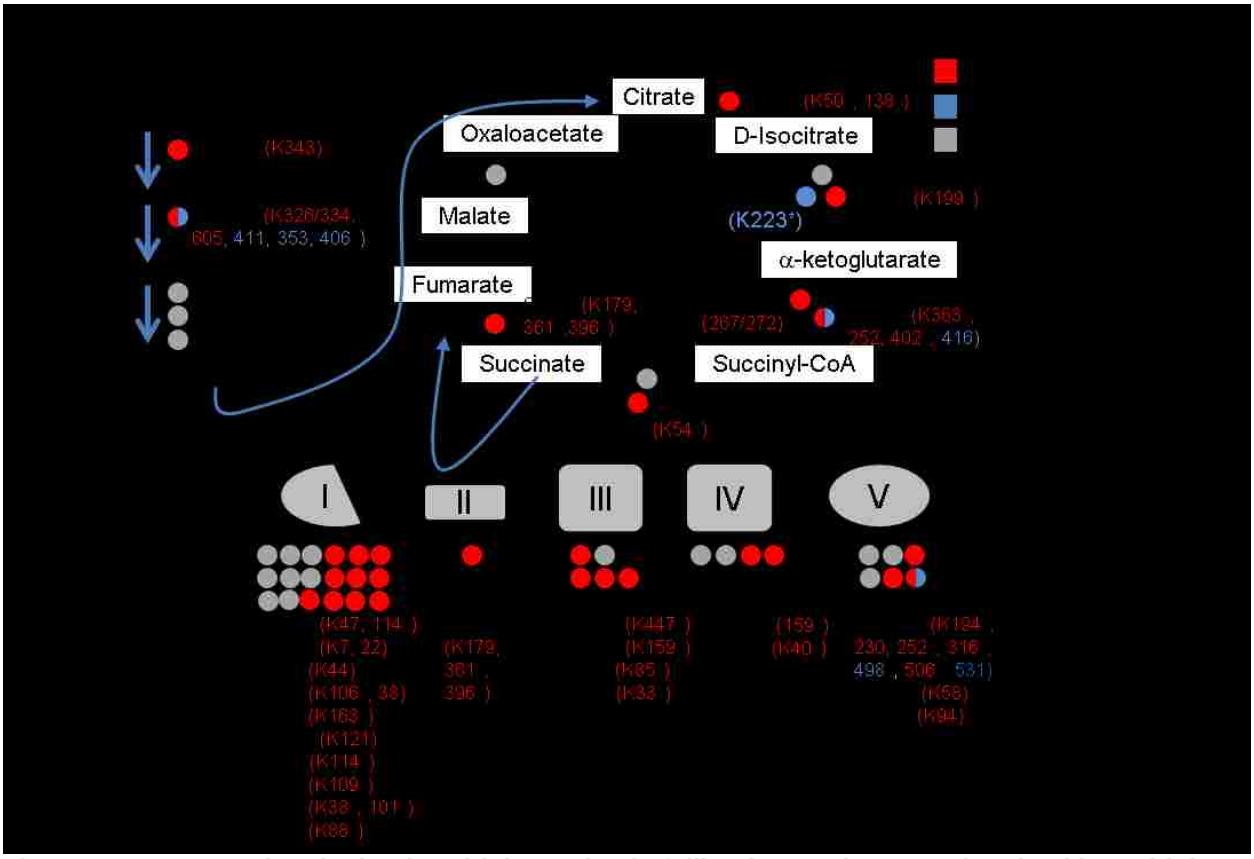

Figure 3. Hyperacetylated mitochondrial proteins in failing human heart are involved in multiple energy transduction pathways.

Lysine-acetylated proteins (indicated by circles, protein symbols are noted) identified by mass spectrometry in dilated cardiomyopathy (DCM) patients and nonfailing (NF) control samples (n = 5/group) in each of the 3 main mitochondrial fuel oxidation/ATP synthesis pathways (β-oxidation, tricarboxylic acid [TCA] cycle, and electron transport complex [ETC]) are shown. All acetylated residues with at least ± 1.5 fold change for mean DCM/NF values are shown. Mean DCM acetylation levels that were significantly different compared to NF control values based on Student's t test are also indicated (*P < 0.05). Specific lysine acetylation sites are noted in parentheses. Acetylation status is indicated by color coding: proteins with increased acetylation (DCM/NF) are in red; proteins with decreased acetylation are in blue; and proteins with no significant change are in gray. All acetylation levels were normalized to corresponding protein abundance. SDHA, succinate dehydrogenase A.

Altered NAD^+ Homeostasis in Failing Heart

SIRT3, a mitochondrial-localized NAD^+-dependent deacetylase, has been shown to play an important role in mitochondrial protein acetylation status (32, 36, 37). Therefore, we sought to assess NAD^+ levels in the mouse and human HF samples to determine

whether, in addition to increased acetyl-CoA levels, capacity for enzymatic deacetylation was altered in the failing heart. Quantitative mass spectrometric assays revealed that myocardial levels of NAD^+ were reduced in the mouse HF group but not the CH group (HF, 1,990 ± 80.27 vs. control, 2,532 ± 174.56 pmol/mg tissue; *P* = 0.018; Figure 4A). Moreover, NAD^+ was significantly reduced in the human DCM samples compared to NF controls (Figure 4B). Measurements of additional NAD^+ metabolite species in the human heart samples demonstrated that NADH levels were not significantly altered in the DCM samples but that NAD phosphate ($NADP^+$) levels were decreased and nicotinamide mononucleotide (NMN) increased in the DCM samples compared to NF controls (Figure 4B). Taken together, these results suggest regulation at several points, including NAD^+ biosynthesis and salvage pathways (Figure 4C) in the failing heart.

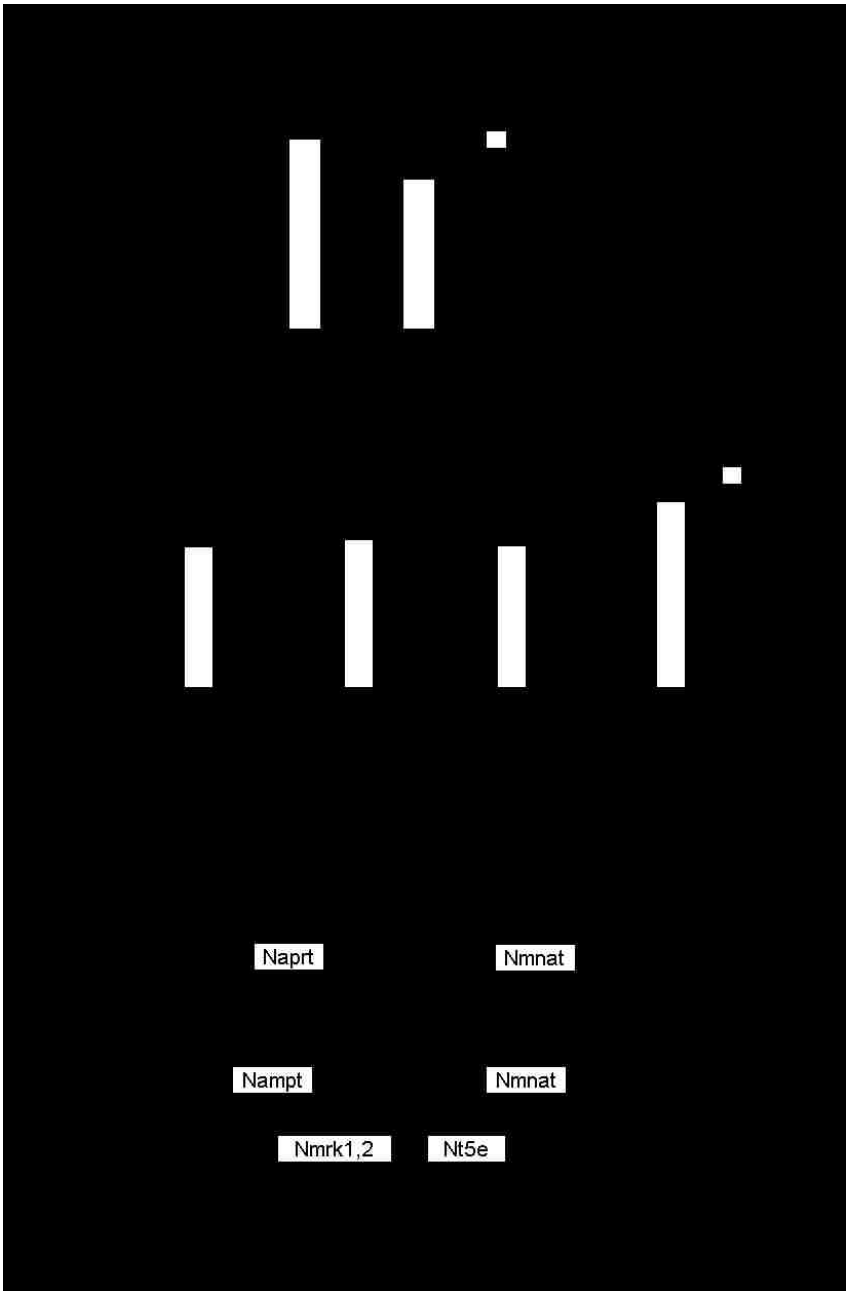

Figure 4. Evidence for altered NAD+ homeostasis in failing mouse and human heart.

(A) NAD+ was measured in mouse cardiac tissue by quantitative mass spectrometry (n = 6/group). The values shown are normalized to mg of dry weight of tissue (mg dw). CH, compensated hypertrophy; HF, heart failure; TAC, transverse aortic constriction; MI, myocardial infarction. **(B)** Levels of NAD+, NADH, NAD phosphate (NADP+), and nicotinamide mononucleotide (NMN) in human failing (dilated cardiomyopathy [DCM]) and nonfailing (NF) control hearts (n = 5 per group). The values shown are normalized to mg of wet weight of tissue. **(C)** Schematic of NAD+ biosynthesis and salvage (within dashed line) pathways. NA, nicotinic acid; Naprt, nicotinate phosphoribosyltransferase; NaMN, NA mononucleotide; Nmnat, nicotinamide mononucleotide adenylyltransferase; Nadsyn, glutamine-dependent NAD+ synthetase; Nampt, nicotinamide phosphoribosyltransferase; Nmrk, nicotinamide riboside kinase 1;2; Nt5e, 5'-nucleotidase ecto; NR, nicotinamide riboside. *P < 0.05 based on Student's t test. Bars represent mean ± SEM.

Evidence that Lysine Acetylation Affects Activity of Succinate Dehydrogenase A, a Key Component of the TCA Cycle and ETC Complex II

As an initial step to explore the functional impact of the altered mitochondrial protein acetylation pattern observed in the HF samples, we focused on subunit A of succinate dehydrogenase A (SDHA), an enzyme that serves a critical role in both the TCA cycle and ETC (as part of complex II). SDHA exhibited increased acetylation at several residues in the mouse and human HF samples (Figures 1A and Figure 3), and its protein levels were not different between failing heart and controls in the mouse and human samples (data not shown). We first measured the activity of complex II in saponin-skinned myocardial LV fibers prepared from HF mice and controls. Complex II–driven state 3 respiration (succinate plus rotenone) was significantly lower in the HF samples compared to sham-operated controls (Figure 5A). In contrast, complex I–driven respiration rates were shown to be normal in the mouse HF samples (28). These results are consistent with reduced SDHA activity in the failing heart. In further support of this conclusion, we have shown that succinate levels are increased in mouse HF samples, consistent with reduced SDHA activity in the TCA cycle (28).

We next sought to assess the effects of SDHA lysine acetylation on SDHA catalytic function. For these studies, we determined the impact of a site-directed lysine acetylation-mimetic (K to Q) mutation on SDHA activity. The mutagenesis studies focused on the K179 residue of SDHA, given that it is hyperacetylated in human HF (Figure 3). In addition, K179 is an established SIRT3 substrate and is located in a conserved FAD^+-binding region (32, 36). Enzyme activity studies were conducted on

mitochondria isolated from HEK293 cells in which WT SDHA or the acetyl-mimetic mutant (K179Q) was overexpressed. The K179Q mutant exhibited a significantly increased K_m (Figure 5B). These results suggest that K179 acetylation affects substrate or cofactor (FAD^+) binding to SDHA. To further assess the impact of the K179 hyperacetylation on SDHA activity in the cellular context as it relates to complex II function, effects on mitochondrial respiration were measured. Complex II–driven respiration in cells overexpressing K179Q was significantly lower compared to SDHA overexpression controls (Figure 5, C and D). This effect was also observed under both basal and ADP-stimulated conditions. Collectively, these results provide evidence that increased acetylation of SDHA at specific lysine residues, as observed in the failing heart, reduces its function in the TCA cycle and as a component of complex II. It is likely that hyperacetylation of other mitochondrial proteins also confers a functional impact in the failing heart.

Figure 5. Evidence for acetylation effects on succinate dehydrogenase A function relevant to heart failure.

(A) Mitochondrial complex II respiration rates determined on cardiac muscle strips isolated from heart failure (HF) and sham-operated control mice using succinate (5 mM) as a substrate in the presence of rotenone (10 μM) to inhibit complex I flux. Basal, state 3 (ADP-stimulated), and post-oligomycin VO2 rates are shown normalized to mg dry tissue weight (mg dw). RC, respiratory control ratio (state 3/state 4). Bars represent mean respiration rates ± SEM (n = 5–11). *P < 0.05 compared to sham based on Student's t test. (B) Succinate dehydrogenase A (SDHA) activity was measured in mitochondria isolated from HEK293 cells expressing WT SDHA (WT) or the acetyl-mimetic mutant (K179Q). Km was derived from measurements of initial velocity generated from a range of substrate concentrations using nonlinear regression. Bars represent mean values ± SEM (3 separate experiments each with n = 3/condition). *P < 0.05 compared to WT based on Student's t test. (C) Oxygen consumption rates (OCRs) were measured in permeabilized NIH-3T3 cells transfected with either a vector encoding WT SDHA (pCS6-SDHA) or K179Q (pCS6-K179Q). The OCR was normalized to the total amount of SDHA in each sample, as quantified by Western blot. The graph shown is representative of 3 separate experiments, each with n = 10. Data points represent mean values ± SEM. *P < 0.05 compared to SDHA-K179Q based on Student's t test. (D) Area under the curve (AUC) was calculated from the combination of all 3 individual experiments for basal and succinate-driven respiration (n = 30). Bars represent mean values ± SEM. *P < 0.05 compared to WT based on Student's t test.

Discussion

We used unbiased quantitative proteomics to detect posttranslational changes in mitochondrial proteins during the transition from compensated cardiac hypertrophy to HF in mice. This approach was spawned by the results of our recent study demonstrating that reduced mitochondrial fuel catabolic flux in the failing heart cannot be fully explained by alterations at the level of gene transcription (28). In addition, we and others have recently found that a subset of myocardial short-chain carbon pools, including acetyl-CoA levels, are increased in the failing mouse heart (28), setting the stage for posttranslational modifications of myocyte proteins during the development of HF. The results herein demonstrate striking alterations in the cardiac mitochondrial protein acetylome during the development of HF in well-defined mouse models and in end-stage HF in humans.

The basis for increased mitochondrial protein acetylation in the failing heart is unclear, but several lines of evidence suggest that it is driven, at least in part, by changes in the mitochondrial matrix environment. Emerging data suggest that the degree of lysine acetylation of proteins is controlled by both enzymatic and nonenzymatic mechanisms. Mitochondrial proteins may be particularly susceptible to nonenzymatic lysine acetylation due to the alkaline pH and relatively high concentrations of acetyl-CoA within the matrix (38). We recently found that levels of C2-carnitine, which reflect changes in the mitochondrial pool of acetyl-CoA, were increased in mouse HF but not CH samples (28). In addition, very recent work has shown that acetyl-CoA levels are increased in the myocardium of humans with end-stage HF (29).

The basis for the increased levels of acetyl-CoA in the early-stage failing heart is unknown, but several possible mechanisms could be at play. First, an increase in mitochondrial short-chain carbon pools could reflect shifts in myocardial fuel oxidative flux, leading to metabolite “bottlenecks.” We recently found that the hypertrophied and failing mouse heart shifts to ketone bodies as a fuel source in the context of reduced capacity for utilization of fatty acids (39). Chronic utilization of ketones by the cardiomyocyte increases levels of several intermediates, including C2-carnitine. It is possible that the concentration of acetyl-CoA generated by ketone oxidation exceeds capacity for entry into the TCA cycle, increasing the mitochondrion acetyl-CoA pool size. Second, impaired export of mitochondrial acetyl-CoA may contribute to an expansion of the mitochondrial acetyl-CoA pool. In support of this notion, we found that carnitine acetyltransferase (CRAT) is hyperacetylated in the CH and HF samples (Supplemental Tables 2 and 4). CRAT exports acetyl units from the mitochondrion by converting acetyl-CoA to the membrane-permeant carnitine conjugate, C2-carnitine. Progressive reduction in CRAT activity in the context of increased mitochondrial acetyl-CoA levels could set the stage for increased mitochondrial protein acetylation. Third, altered NAD^+ homeostasis could contribute to the increased mitochondrial protein acetylation observed in the failing heart by diminishing the activity of SIRT3 (40), a key mitochondrial deacetylase. Notably, SIRT3-null mice exhibit increased mitochondrial protein acetylation and are more susceptible to stress-induced mitochondrial dysfunction (32, 36, 37). Cardiac SIRT3 expression was not reduced in the CH or HF groups (data not shown). However, we found that NAD^+ levels were significantly

reduced in the mouse and human HF samples, likely resulting in reduced sirtuin activity (Figure 4, A and B). Interestingly, our comprehensive profiling of metabolites involved in NAD^+ metabolism (Figure 4B) indicated that the basis for reduced NAD^+ levels could involve multiple mechanisms, including alterations in both the biosynthesis and salvage pathways (Figure 4C), given that NMN levels are increased in the context of reduced NAD^+. Taken together, we propose that both increased mitochondrial acetyl-CoA levels and reduced SIRT3 activity due to derangements in NAD^+ metabolism conspire to drive increased lysine acetylation of mitochondrial proteins in the failing heart.

The results described herein provide evidence that increased acetylation of selected mitochondrial proteins impairs mitochondrial fuel oxidation and ATP synthesis in the failing heart. Increased lysine acetylation has been shown to reduce the enzymatic activity of mitochondrial proteins involved in FAO, glucose oxidation, the TCA cycle, and ETC (41–45). In this study, we identified hyperacetylated lysine residues of proteins within the FAO, TCA, and ETC/OXPHOS pathways in the HF samples. The functional studies described here focused on SDHA, a key component of both the TCA cycle and respiratory complex II. SDHA was found to be hyperacetylated at multiple lysine residues in both mouse and human samples. Complex II–driven respiration was reduced in cardiac strips prepared from the HF samples, consistent with reduced activity of SDHA. In addition, levels of succinate, the substrate for the TCA cycle reaction catalyzed by SDHA, are increased in the mouse HF samples (28). We found that an acetyl-mimetic point mutation in SDHA altered enzymatic function and succinate-driven respiration via complex II. Notably, human complex II deficiency has

been reported to cause HF (46). As K179 lies within the conserved FAD^+-binding domain, we speculate that acetylation of this residue directly affects FAD^+ binding to SDHA. The observed increased K_m in the SDHA K179Q mutant is consistent with this notion. Interestingly, mitochondrial complex I deficiency in mice results in a phenotype of protein hyperacetylation and HF, suggesting that reduced ETC flux and ATP synthesis could further contribute to mitochondrial protein acetylation, resulting in a vicious cycle (47). It should be noted that current methodology does not allow us to determine the precise acetylation stoichiometry of SDHA and other mitochondrial proteins in the HF samples. Future studies aimed at defining precise lysine acetylation stoichiometry, together with pathway flux analyses, will provide key information on whether the results shown here for alterations in SDHA represent a broader paradigm in HF and other diseases.

Our collective results suggest a model in which progressive mitochondrial protein lysine acetylation, driven by an expansion of the acetyl-CoA pool and reduced NAD^+levels, leads to reduced fuel oxidative flux and diminished ATP synthesis (Figure 6). Our results raise the question as to whether strategies aimed at diminishing mitochondrial protein hyperacetylation by targeting nodal points in this pathogenic scheme could have therapeutic utility for HF. A few studies have shown that activation of SIRT1 improves cardiac function in HF and ischemia-reperfusion models, possibly via activation of AMP-activated protein kinase (48–50). However, the impact of specifically activating mitochondrial SIRT3 on the development of HF has not been reported to our knowledge. In addition, as described above, it is likely that a significant subset of the

hyperacetylated proteins identified herein are not SIRT3 targets. Accordingly, proof-of-concept experimental strategies aimed at maintaining mitochondrial acetyl carbon homeostasis or NAD^+ metabolism should also be considered.

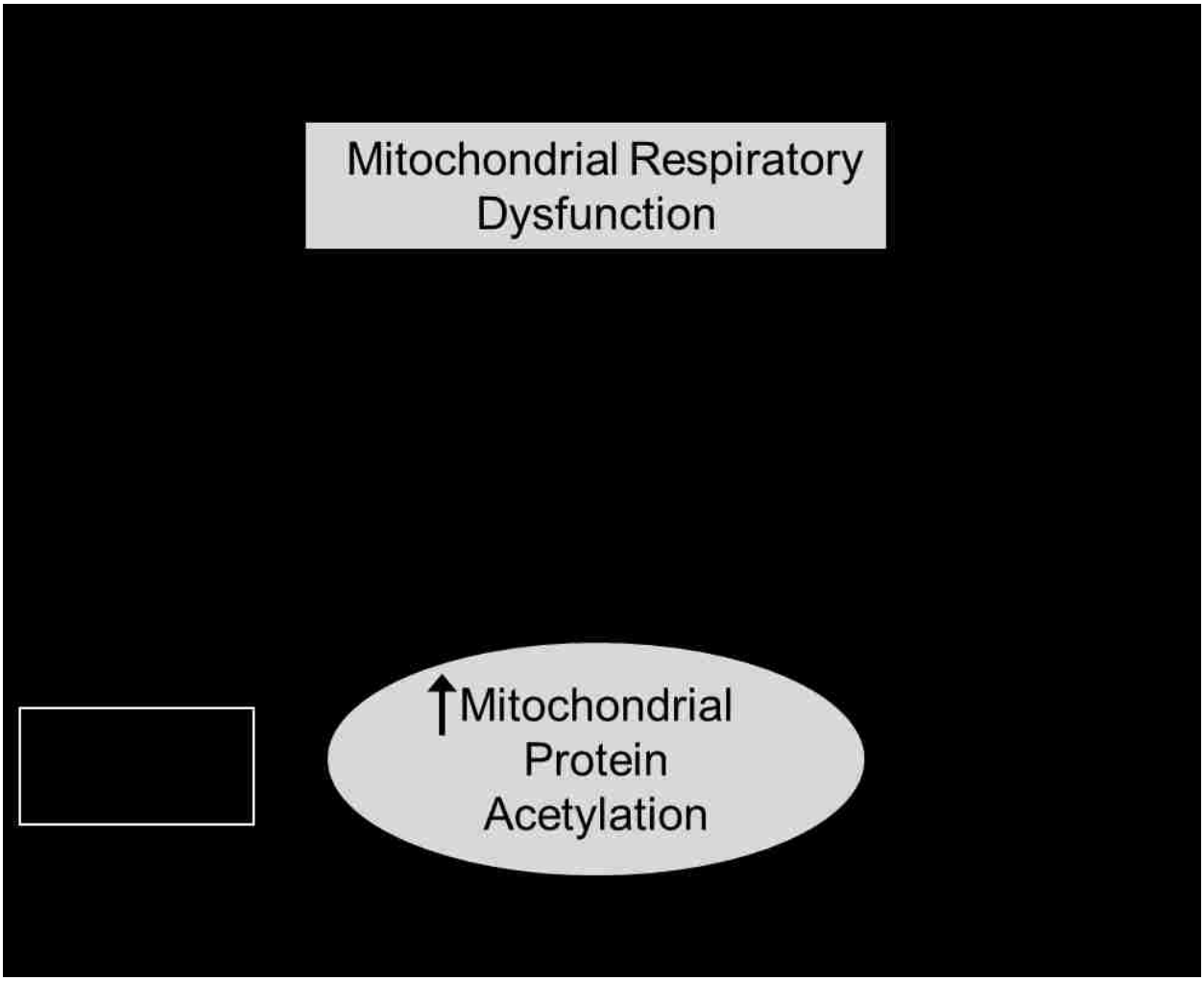

Figure 6. Schematic depicting a conceptual model for the impact of mitochondrial protein lysine acetylation as a driver of the progressive decline in capacity for mitochondrial oxidative flux and ATP synthesis known to occur during the development of heart failure.

Methods

Animal Studies

Animal studies were performed on female C57BL/6J mice (purchased from JAX labs), 7 to 12 weeks of age, on standard chow (16.4% protein, 4.0% fat, and 48.5% carbohydrates; Harlan Teklad, 2016). The TAC and HF (combination of TAC and small apical MI) surgeries were performed on 8-week-old female C57BL/6J mice (purchased from JAX labs) as described previously (28, 34, 35).

Human Studies

Explant dilated nonischemic failing human hearts were procured at the time of orthotopic heart transplantation, and NF hearts were obtained at the time of organ donation from brain-dead donors. In all cases, warm ischemia was prevented by arresting the heart in situ with 1 liter of ice-cold cardioplegia solution, transportation to the laboratory on wet ice, and flash freezing of biopsies in liquid nitrogen within 4 hours of cardiectomy. All samples were full-thickness biopsies obtained from the free wall of the left ventricle. A total of 10 subjects, 5 organ donors, and 5 patients with DCM provided heart tissue for this research. In each group, there were 2 females and 3 males, the ages were comparable (NF 50 ± 3 years vs. DCM 58 ± 5 years), and all but one DCM subject were of mixed European descent. Body mass index was also comparable (NF 31 ± 4 vs. DCM 26 ± 3). Based on heart weight at explant (NF 394 ± 31 grams vs. DCM 531 ± 50 grams, $P < 0.05$) and LVEF determined by echocardiography

(NF 62% ± 8% vs. DCM 10% ± 0%, $P < 0.005$), the DCM hearts had significant pathological hypertrophy and severe contractile dysfunction.

Western Blotting

Western immunoblotting was performed with total cellular lysate. In brief, cells were harvested with RIPA buffer (1% NP40, 0.1% SDS, 100 mM phenylmethylsulfonyl fluoride, cOmplete Protease Inhibitors [Roche catalog 11697498001]) on ice. DNA was sheered by passing the sample through a 21-gauge needle. The lysate was incubated on ice for 30 minutes and subsequently centrifuged at 4°C at 20,000 *g* for 20 minutes. The supernatant was collected, and total protein was quantified using the Micro BCA Protein Assay Kit (Thermo Fisher Scientific catalog 23235). Protein samples were run on 12% SDS-PAGE and transferred to nitrocellulose membrane. The membranes were blocked with Odyssey Blocking Buffer (LI-COR Biosciences catalog 927-50000) for 1 hour at room temperature and then probed with primary antibody complex II Fp subunit (Invitrogen catalog 459200) at 1:5,000 in 1:1 Odyssey Blocking Buffer and 0.1% Tween in Tris-buffered saline (TBS-T) overnight at 4°C. The membranes were rinsed for 10 minutes 3 times with TBS-T at room temperature. Secondary antibody IRDye 800CW donkey anti-mouse IgG (H + L) (LI-COR Biosciences catalog 926-32212) was applied to the blot at 1:7,500 dilution in 1:1 Odyssey Blocking Buffer and TBS-T and incubated for 1 hour at room temperature. Western blot image detection and quantification were performed using the LI-COR Odyssey. Protein quantification was performed using the Odyssey Image Studio software (LI-COR Biosciences).

Metabolomic Analysis of NAD^+ Metabolites

For the NAD^+ metabolite measurements, pulverized frozen mouse heart samples (~50 mg per sample) or pulverized frozen human heart (derived from left ventricle; ~50 mg per sample) were homogenized via hand-held rotary homogenizer in 500 µl of either 0.5 M perchloric acid (for NMN, NAD^+, and $NADP^+$ determination) or 50:50 methanol/0.1 M NaOH (for NADH determination). The resulting heart homogenates were aliquoted and stored at –80°C. For NMN, NAD^+, and $NADP^+$ extraction, a 100-µl aliquot of heart homogenate was spiked with a 10-µl aliquot of heavy isotope-labeled internal standards ($^{18}O_2$-labeled NMN and NAD^+; synthesized by the Sanford Burnham Prebys [SBP] Medicinal Chemistry Core). This was followed by the addition of 100 µl of 1 M ammonium formate to adjust the homogenate pH to approximately 4. Samples were vortexed thoroughly and centrifuged at 18,000 *g* for 5 minutes at 10°C. The clarified homogenates were passed through an AcroPrep Advance 3K Omega Filter Plate (Pall Corporation) prior to liquid chromatography–tandem mass spectrometry (LC/MS/MS) analysis.

For NADH extraction, a 100-µl aliquot of heart homogenate was spiked with a 10-µl aliquot of heavy isotope-labeled internal standard ($^{18}O_2$-labeled NADH; synthesized by the SBP Medicinal Chemistry Core). Samples were vortexed thoroughly and centrifuged at 18,000 *g* for 5 minutes at 10°C. The clarified homogenates were passed through an AcroPrep Advance 3K Omega Filter Plate (Pall Corporation) prior to LC/MS/MS analysis. All pyridine nucleotides were separated on a 2.1 × 50 mm, 3-µm Thermo Hypercarb column (T = 30°C) using a 5.8-min linear gradient with 10 mM ammonium

acetate, pH 9.5, and acetonitrile at a flow rate of 0.5 ml/min. Quantitation of pyridine nucleotides was achieved using multiple reaction monitoring on an Dionex UltiMate 3000 HPLC/Thermo Scientific Quantiva triple quadrupole mass spectrometer (Thermo Scientific). For NMN, NAD^+, and $NADP^+$ determination, a standard calibration curve (0.25–200 μM for NAD^+, 0.025–20 μM for $NADP^+$, and 0.0025–2 μM for NMN) was prepared by spiking 10-μl aliquots of pyridine nucleotides (Sigma-Aldrich) and internal standards (synthesized by the SBP Medicinal Chemistry Core) into 100-μl aliquots of 0.5 M perchloric acid. Calibration samples were extracted similarly as pyridine nucleotides in heart homogenate. For NADH determination, a standard calibration curve (0.25–200 μM for both species) was prepared by spiking 10-μl aliquots of pyridine nucleotides (Sigma-Aldrich) and internal standards (synthesized by the SBP Medicinal Chemistry Core) into 200 μl of 50:50 methanol/0.1 M NaOH. Calibration samples were extracted similarly as pyridine nucleotides in mouse liver homogenate. Data from heart samples were normalized to the mass of lyophilized heart powder (mouse) or heart tissue homogenate (human) provided.

Acetylproteomics

Purified mitochondria (mouse samples) or pulverized tissue (human samples) were subjected to quantitative proteomics/acetylproteomics using recently developed methods (36, 51). The mass spectrometry mouse acetylproteomics data have been deposited into the Proteome Xchange Consortium (http://www.ebi.ac.uk/pride/archive/login) via the PRIDE partner repository with the data

set identifier PXD001652. The human acetylproteomics data are available at Chorus (https://chorusproject.org/pages/index.html) under the project title heartFailure_acetylation (ID 965).

Chemicals and Supplies

The Tandem Mass Tag (TMT) reagents were purchased from Thermo Scientific. The BCA assay Protein Assay Kit was purchased from Pierce Biotechnology and Trypsin Gold was purchased from Promega. Sep-Pak tC18 cartridges were purchased from Waters Corporation. A polysulfoethyl A column (9.4 mm × 200 mm, 5 mm, 200Å) was purchased from PolyLC Inc. Bridged Ethylene Hybrid (BEH) C18 resin (1.7-m diameter particles, 130 Å pore size) was purchased from Waters Corporation. Fused-silica capillary tubing was purchased from Polymicro Technologies. Formic acid and trifluoroacetic acid ampoules were purchased from Thermo Scientific. Pan-acetyl lysine antibody agarose conjugate was purchased from ImmuneChem. Protease (cOmplete mini ETDA-free) and phosphatase (PhosSTOP) inhibitors were purchased from Roche. All other chemicals were purchased from Sigma-Aldrich.

Mitochondrial Preparation

For the mouse studies, mitochondria were isolated by differential centrifugation by methods previously reported (52). All steps were performed at 4°C. Tissue was suspended in isolation buffer (220 mM mannitol, 70 mM sucrose, 5 mM HEPES KOH, pH 7.4, 1 mM EGTA) supplemented with 10 mg/ml bovine serum albumin (BSA),

protease inhibitor cocktail (Roche cOmplete tablets, 1 tablet per 50 ml buffer), phosphatase inhibitor cocktail (Roche PhosSTOP), and deacetylase inhibitors (10 mM nicotinamide, 10 μM TSA, 5 μM MS257, 10 mM sodium butyrate, 2 μM SAHA). Heart tissue was suspended to 0.1 g/ml in isolation buffer and homogenized with 4 strokes of a power-driven Potter-Elvehjem glass/Teflon homogenizer. The homogenate was decanted and spun at 800 *g* for 10 minutes. Any lipids were removed from the top of the supernatant by aspiration. The supernatant containing mitochondria was removed and transferred to a Beckman Ultra-clear centrifuge tube and spun at 8,000 g for 10 minutes. The supernatant was discarded, and the pellet was resuspended in 1 ml of isolation buffer. The crude mitochondria were transferred to a 1.5-ml microfuge tube and spun at 8,000 *g* for 10 minutes in a bench-top centrifuge. The supernatant was removed, and the pellet was washed with resuspension buffer. (Note, resuspension buffer is equivalent to isolation buffer but lacks BSA). The mitochondria were pelleted by centrifugation at 8,000 *g* for 10 minutes in a bench-top centrifuge. The supernatant was aspirated, and the pellet was frozen immediately in liquid nitrogen.

Sample Preparation

Either purified mitochondria (mouse samples) or pulverized frozen human heart samples were suspended in 8 M urea, 40 mM Tris, pH 8.0, 30 mM NaCl, 1 mM $CaCl_2$, 1× protease inhibitor tablet, 1× phosphatase inhibitor tablet, and 1× deacetylase inhibitors. Protein was extracted by sonication with a probe sonicator on ice and quantified by BCA assay. Protein from each sample (180 μg for mouse samples, 1 mg

for human samples) was reduced with 5 mM dithiothreitol for 45 minutes at 58°C and then alkylated with 15 mM iodoacetamide for 45 minutes at ambient temperature in the dark. The alkylation was quenched with 5 mM dithiothreitol. Following dilution to 1.5 M urea with 50 mM Tris, pH 8.0, the samples were digested with trypsin (50:1 protein/enzyme) overnight. Additional trypsin (50:1 protein/enzyme) was spiked into the sample the following morning, digestions were quenched by TFA acidification 2 hours later, and samples were desalted with a tC18 sep-Pak. Desalted material was resuspended in 200 mM TEAB pH 8.5 and labeled with 8-plex TMT. Labeled peptides were combined and desalted. Labeling efficiency was evaluated by analyzing a test mixture by LC/MS/MS for each experiment. Labeling efficiency was >95%, calculated by the number of N-terminal–labeled peptides divided by the total number of peptide identifications.

Fractionation and Enrichment

Labeled peptides were fractionated by strong cation exchange on a polysulfoethyl A column (0.4 mm × 200 mm) with mobile phases A (5 mM KH_2PO_4, pH 2.7, and 30% acetonitrile); B (5 mM KH_2PO_4, pH 2.7, 350 mM KCl, and 30% acetonitrile); C (5 mM KH_2PO_4, pH 6.5, 500 mM KCL, and 20% acetonitrile); and D (water). Peptides were eluted over the following gradient on a Surveyor LC quaternary pump (Thermo Scientific) at 3 ml/min: 0–2 minutes, 100% A; 2–5 minutes, 0%–10% B; 5–35 minutes, 10%–60% B; 35–41 minutes, 60%–100% B; this gradient was followed by washes with C and D prior to reequilibration with mobile phase A. Sixteen fractions were collected

and desalted. A small portion, 5%, of each was retained for protein analysis, while the remaining material was pooled into 6 fractions for acetyl lysine enrichment.

These pooled fractions were dissolved in 50 mM HEPES, pH 7.6, 100 mM NaCl, and each fraction was combined with approximately 50 µl pan-acetyl lysine antibody agarose conjugate. The samples were rotated overnight at 4°C and then rinsed 8 times with cold 50 mM HEPES, pH 7.6, and 100 mM NaCl. Rinses were followed by elution with 0.1% TFA, and eluted peptides were desalted prior to analysis.

LC/MS/MS

Mouse samples were analyzed by reverse-phase liquid chromatography on a nanoAcquity (Waters Corporation) coupled to an Orbitrap Elite (Thermo Scientific). Samples were loaded onto a 75-µm-inner diameter analytical column made in-house, packed with 1.7-m-diameter, 130-Å-pore-size, BEH C18 particles (Waters Corporation) to a final length of 30 cm. The column was heated to 62°C for all runs. The elution portion of the gradient was 5% to 30% B (A: water/0.2% formic acid; B: acetonitrile/0.2% formic acid) over 80 minutes for both acetyl enriched fraction and protein fractions.

Instrument methods for mass spectrometry all started with one mass spectrometry survey scan (resolution = 60,000; 300 Th to 1,500 Th) followed by data-dependent mass spectrometry fragmentation and analysis (resolution = 30,000) of the 15 most intense precursors by beam-type CAD (HCD; normalized collision energy = 35%, target value = 5e4). Only those precursors with charge state of +2 or higher were

sampled for mass spectrometry. The dynamic exclusion duration was set to 40 seconds, with a 10-ppm tolerance around the selected precursor and its isotopes, and monoisotopic precursor selection was turned on.

Human samples were analyzed by reverse-phase liquid chromatography on a nanoAcquity (Waters Corporation) coupled to an Orbitrap Fusion (Thermo Scientific). Samples were loaded onto a 75-µm-inner diameter analytical column made in-house, packed with 1.7-m-diameter, 130-Å-pore-size, BEH C18 particles (Waters Corporation) to a final length of 35 cm. The column was heated to 65°C for all runs. Mobile-phase buffer A was composed of water, 0.2% formic acid, and 5% dimethyl sulfoxide (DMSO). Mobile-phase B was composed of acetonitrile, 0.2% formic acid, and 5% DMSO. Samples were loaded onto the column for 12 minutes at 0.35 µl/min. Mobile-phase B increases to 4% in the first 0.1 minutes and then to 30% B over 80 minutes, followed by a 5-minute wash at 70% B and a reequilibration at 0% B.

Instrumental methods for mass spectrometry all started with one mass spectrometry survey scan (resolution = 60,000 at 200 *m*/*z*; target value = 5e5; 350 Th to 1,400 Th) followed by data-dependent mass spectrometry fragmentation and analysis in the Orbitrap (resolution = 60,000 at 200 *m*/*z*) of the most intense precursors by beam-type CAD (HCD; normalized collision energy = 37%, target value = 5e4) over a 5-second cycle. Only those precursors with charge state of +2 or higher were sampled for mass spectrometry. The dynamic exclusion duration was set to 30 seconds, with a 10

ppm tolerance around the selected precursor and its isotopes, and monoisotopic precursor selection was turned on.

Database Search, FDR filtering, and Acetylation Analysis

Spectra were converted to searchable text files using a DTA generator. Generated text files were searched for fully tryptic peptides with up to 3 missed cleavages against a UniProt target-decoy database populated with mouse canonical plus isoforms (downloaded August 7, 2013) or human canonical plus isoforms (downloaded July 20, 2012) using the Open Mass Spectrometry Search Algorithm v.2.1.8 (53). Mass tolerance was set to ± 2.5 Da for precursors and ± 0.015 Da for fragment ions. Carbamidomethylation of cysteine, isobaric labeling of lysine, and isobaric labeling of the peptide N-terminus were searched as fixed modifications for all samples. Enriched fractions were additionally searched for variable acetylation modifications, in which the acetylation mass shift was set to the difference between an acetyl group and an isobaric label (-187.1523 Da) to allow the isobaric label on lysine to remain a fixed modification even for acetylated peptides. Search results were filtered to 1% FDR at the unique peptide level using the COMPASS software suite (54). TMT quantitation of identified peptides was performed within COMPASS, as previously reported (55). Peptides were grouped into proteins according to previously reported rules, and protein identifications were further filtered to 1% FDR (56). Protein quantitation was performed by summing all reporter ion intensities within each channel for each protein.

Acetylation events were localized to specific residues using previously described probabilistic methods (57). An acetylation event was considered localized if the calculated localization confidence was 95% or greater based on comparisons to theoretically possible acetyl isoforms. If localized acetylated peptides shared identical modification sites, those peptides were grouped together and their reporter ion intensities were summed; peptides with C-terminal acetylation were excluded from quantitation.

Protein Normalization

All reporter ion intensities were $\log_2$ transformed and mean normalized for every acetyl isoform and protein. To account for protein abundance differences, the acetyl isoforms were normalized by subtracting the quantitative value of the reporter ion channel for the corresponding protein from the value for each acetyl isoform reporter ion channel. This resulted in a protein-normalized acetylation mean value that was then used to investigate fold changes between conditions. Fold change calculations were made by averaging the protein-normalized values for each condition and then calculating the difference of averages.

Mitochondrial Assignment

Proteins were identified as mitochondrial or nonmitochondrial based on inclusion or exclusion from the MitoCarta compendium of mitochondrial mouse proteins (58). MitoCarta EntrezID identifiers were converted to Uniprot identifiers with the Uniprot ID

mapping function. Our list was limited to contain only proteins that were in the canonical database used for searching. Additional mitochondrial proteins identified by Database for Annotation, Visualization and Integrated Discovery were also included.

Mitochondrial Respiration

Mitochondrial respiration rates were determined on saponin-permeabilized LV muscle strips with succinate (5 mM)/rotenone (10 μM) as substrate as described previously (28, 59).

Vector Construction

An MGC premier Expression-Ready cDNA clone for SDHA-BC031849 (pCS6-BC031849) (Transomic Technologies catalog TCM1304) was used for the WT SDHA vector construct (pCS6-SDHA). Site-directed mutagenesis was performed using a modification to the QuikChange (Stratagene catalog 200518-5) protocol to create the SDHA K179Q in the pCS6-SDHA vector as described previously (60). The following primers were used for the site-directed mutagenesis: CCTCCAGTTTGGGAAAGGCGGGCAGG (forward) and CCCAAACTGGAGGCTCTGTCCACCAAATGCAC (reverse).

Cellular Oxygen Consumption Rates

Oxygen consumption rates were measured using the Seahorse Bioscience XF 96 analyzer as described previously (61). Briefly, NIH3T3 (ATCC) cells were transfected with Lipofectamine 3000 (Thermo Scientific catalog L3000-015) using the

manufacturer's instructions with expression constructs for WT or K179Q SDHA (pCS6-SDHA or pCS6-K179Q). In the Seahorse assay, two measurements were taken at basal conditions and after each reagent injection. The cells were first injected with 10 mM succinate, 1.5 nM rPFO (Seahorse Bioscience catalog 102504-100), and 4 μM rotenone. ADP was added at a final concentration of 4 mM. The final concentration of antimycin A was 1 μM. The oxygen consumption rate was then normalized to total amount of SDHA present, as determined by Western blot of cells transfected with indicated expression construct.

SDHA Activity

HEK293 cells were transfected with pCS6-SDHA or pCS6-K179Q constructs. Mitochondria were isolated and SDHA-specific activity was measured as described previously (62–64). In brief, a coupled enzymatic colorimetric assay utilizing 2 redox dyes, 2,6-dichlorophenolindophenol sodium salt hydrate (DCPIP) and phenazine methosulfate (PMS), was used to measure the oxidation of succinate to fumarate by SDHA. Succinate (21.7 mM) was added to the isolated mitochondria and preincubated to remove oxaloacetate, which is an inhibitor of SDHA succinate oxidation. The reaction solution (2.17 μM antimycin A, 5.4 μM rotenone, 54 μM DCPIP, PMS between 0 mM and 1.07 mM) was then added, and absorbance was measured at 600 nm. The K_m was derived by fitting a curve made from measurements of initial velocity at various substrate concentrations using nonlinear regression analysis in GraphPad Prism 6 after

measuring the total amount of SDHA present via Western blot. The replicates test confirmed the adequacy of the fit to the Michaelis-Menten model.

Statistics

All statistical analyses were performed with 2-tailed Student's *t* test as indicated. The level of significance was set at $P < 0.05$ in all cases.

Study Approval

All animal experiments and euthanasia protocols were approved by the Institutional Animal Care and Use Committee at SBP at Lake Nona. Procurement of human myocardial tissue was performed under protocols approved by Institutional Review Boards at the University of Pennsylvania, and consent for research use of explanted tissues was prospectively obtained in all cases.

Author Contributions

JLH, OJM, RBV, DJP, JJC, DMM, and DPK conceived the study. JLH, LL, NMR, ALR, and JJC devised experimental methodology. JLH, OJM, LL, NMR, and ALR performed experiments. TCL, RBV, NMR, and ALR curated data. KCB and KBM provided resources. JLH, OJM, LL, NMR, and ALR provided formal analysis. JLH, OJM, RBV, and DPK wrote the original draft. JLH, LL, NMR, ALR, JJC, DMM, TCL, RBV, and DPK reviewed and edited the manuscript. DPK, DJP, JJC, DMM, and KBM acquired funding. JJC and DPK provided supervision.

Acknowledgements

We wish to thank Gregory Aubert for expert scientific discussion at the onset of this project and Lorenzo Thomas for assistance with the preparation of the manuscript. We would like to acknowledge the following Core Facilities at SBP at Lake Nona: Cardiometabolic Phenotyping, Metabolomics, and Medicinal Chemistry. We wish to thank Jeff Culver, Christopher Petucci, and Stephen Gardell for development and assistance with the nicotinamide metabolite measurements. We also thank Lauren Ashley Gabriel and Caron Stonebrook for assistance with the animal studies. This work was supported by NIH grants R01 HL58493 (to D.P. Kelly), R01 HL101189 (to D.P. Kelly and D.M. Muoio), R01 DK098672 (to D.J. Pagliarini), R01 GM080148 (to J.J. Coon), and R01 HL105993 (to K.B. Margulies). N.M. Riley gratefully acknowledges support from a National Science Foundation Graduate Research Fellowship (DGE-1256259). A.L. Richards gratefully acknowledges support from the American Chemical Society Division of Analytical Chemistry and from the Society of Analytical Chemists of Pittsburgh.

Footnotes

Conflict of Interest:

D.P. Kelly is a scientific consultant for Pfizer Inc. and receives research support from Takeda Pharmaceuticals and Acorda Therapeutics. R.B. Vega and D.M. Muoio receive research support from Pfizer Inc. J.J. Coon is a consultant for Thermo Fisher Scientific.

Reference Information:

JCI Insight. 2016;1(2):e84897. doi:10.1172/jci.insight.84897.

References

1. Bing RJ. The metabolism of the heart. Harvey Lect. 1954;50:27–70.

2. Bing RJ, Siegel A, Ungar I, Gilbert M. Metabolism of the human heart. II. Studies on fat, ketone and amino acid metabolism. Am J Med. 1954;16(4):504–515. doi: 10.1016/0002-9343(54)90365-4.

3. Wisneski JA, Gertz EW, Neese RA, Mayr M. Myocardial metabolism of free fatty acids. Studies with 14C-labeled substrates in humans. J Clin Invest. 1987;79(2):359–366. doi: 10.1172/JCI112820.

4. Lopaschuk GD, Belke DD, Gamble J, Itoi T, Schonekess BO. Regulation of fatty acid oxidation in the mammalian heart in health and disease. Biochim Biophys Acta. 1994;1213(3):263–276. doi: 10.1016/0005-2760(94)00082-4.

5. van der Vusse GJ, van Bilsen M, Glatz JF. Cardiac fatty acid uptake and transport in health and disease. Cardiovasc Res. 2000;45(2):279–293. doi: 10.1016/S0008-6363(99)00263-1.

6. Kelly DP, Strauss AW. Inherited cardiomyopathies. N Engl J Med. 1994;330(13):913–919. doi: 10.1056/NEJM199403313301308.

7. Bishop SP, Altschuld RA. Increased glycolytic metabolism in cardiac hypertrophy and congestive failure. Am J Physiol. 1970;218(1):153–159.

8. Taegtmeyer H, Overturf ML. Effects of moderate hypertension on cardiac function and metabolism in the rabbit. Hypertension. 1988;11(5):416–426. doi: 10.1161/01.HYP.11.5.416.

9. Allard MF, Schonekess BO, Henning SL, English DR, Lopaschuk GD. Contribution of oxidative metabolism and glycolysis to ATP production in hypertrophied hearts. Am J Physiol. 1994;267(2 pt 2):H742–H750.

10. Christe ME, Rodgers RL. Altered glucose and fatty acid oxidation in hearts of the spontaneously hypertensive rat. J Mol Cell Cardiol. 1994;26(10):1371–1375. doi: 10.1006/jmcc.1994.1155.

11. Paolisso G, et al. Total-body and myocardial substrate oxidation in congestive heart failure. Metabolism. 1994;43(2):174–179. doi: 10.1016/0026-0495(94)90241-0.

12. Sambandam N, Lopaschuk GD, Brownsey RW, Allard MF. Energy metabolism in the hypertrophied heart. Heart Fail Rev. 2002;7(2):161–173. doi: 10.1023/A:1015380609464.

13. Chandler MP, et al. Moderate severity heart failure does not involve a downregulation of myocardial fatty acid oxidation. Am J Physiol Heart Circ Physiol. 2004;287(4):H1538–H1543. doi: 10.1152/ajpheart.00281.2004.

14. Wallhaus TR, et al. Myocardial free fatty acid and glucose use after carvedilol treatment in patients with congestive heart failure. Circulation. 2001;103(20):2441–2446. doi: 10.1161/01.CIR.103.20.2441.

15. Davila-Roman VG, et al. Altered myocardial fatty acid and glucose metabolism in idiopathic dilated cardiomyopathy. J Am Coll Cardiol. 2002;40(2):271–277. doi: 10.1016/S0735-1097(02)01967-8.

16. de las Fuentes L, Herrero P, Peterson LR, Kelly DP, Gropler RJ, Davila-Roman VG. Myocardial fatty acid metabolism: independent predictor of left ventricular mass in hypertensive heart disease. Hypertension. 2003;41(1):83–87. doi: 10.1161/01.HYP.0000047668.48494.39.

17. Ingwall JS, et al. The creatine kinase system in normal and diseased human myocardium. New Engl J Med. 1985;313(17):1050–1054. doi: 10.1056/NEJM198510243131704.

18. de Roos A, Doornbos J, Luyten PR, Oosterwaal LJ, van der Wall EE, den Hollander JA. Cardiac metabolism in patients with dilated and hypertrophic cardiomyopathy: assessment with proton-decoupled P-31 MR spectroscopy. J Magn Reson Imaging. 1992;2(6):711–719. doi: 10.1002/jmri.1880020616.

19. Tian R, Nascimben L, Kaddurah-Daouk R, Ingwall JS. Depletion of energy reserve via the creatine kinase reaction during the evolution of heart failure in cardiomyopathic hamsters. J Mol Cell Card. 1996;28(4):755–765. doi: 10.1006/jmcc.1996.0070.

20. Ingwall JS, Weiss RG. Is the failing heart energy starved? On using chemical energy to support cardiac function. Circ Res. 2004;95(2):135–145. doi: 10.1161/01.RES.0000137170.41939.d9.

21. Carley AN, Taegtmeyer H, Lewandowski ED. Matrix revisited: mechanisms linking energy substrate metabolism to the function of the heart. Circ Res. 2014;114(4):717–729. doi: 10.1161/CIRCRESAHA.114.301863.

22. Neubauer S, et al. Myocardial phosphocreatine-to-ATP ratio is a predictor of mortality in patients with dilated cardiomyopathy. Circulation. 1997;96(7):2190–2196. doi: 10.1161/01.CIR.96.7.2190.

23. Neubauer S. The failing heart--an engine out of fuel. New Engl J Med. 2007;356(11):1140–1151. doi: 10.1056/NEJMra063052.

24. Razeghi P, Young ME, Alcorn JL, Moravec CS, Frazier OH, Taegtmeyer H. Metabolic gene expression in fetal and failing human heart. Circulation. 2001;104(24):2923–2931. doi: 10.1161/hc4901.100526.

25. Huss JM, Kelly DP. Mitochondrial energy metabolism in heart failure: a question of balance. J Clin Invest. 2005;115(3):547–555. doi: 10.1172/JCI24405.

26. Sack MN, Rader TA, Park S, Bastin J, McCune SA, Kelly DP. Fatty acid oxidation enzyme gene expression is downregulated in the failing heart. Circulation. 1996;94(11):2837–2842. doi: 10.1161/01.CIR.94.11.2837.

27. Chen L, Gong Q, Stice JP, Knowlton AA. Mitochondrial OPA1, apoptosis, and heart failure. Cardiovasc Res. 2009;84(1):91–99. doi: 10.1093/cvr/cvp181.

28. Lai L, et al. Energy metabolic reprogramming in the hypertrophied and early stage failing heart: a multisystems approach. Circ Heart Fail. 2014;7(6):1022–1031. doi: 10.1161/CIRCHEARTFAILURE.114.001469.

29. Bedi KC, Jr, et al. Evidence for intramyocardial disruption of lipid metabolism and increased myocardial ketone utilization in advanced human heart failure. Circulation. doi: 10.1161/CIRCULATIONAHA.1. [published online ahead of print January 27, 2016]. doi: 10.1161/CIRCULATIONAHA.115.017545.

30. Fernandes J, et al. Lysine acetylation activates mitochondrial aconitase in the heart. Biochemistry. 2015;54(25):4008–4018. doi: 10.1021/acs.biochem.5b00375.

31. Baeza J, Smallegan MJ, Denu JM. Site-specific reactivity of nonenzymatic lysine acetylation. ACS Chem Biol. 2015;10(1):122–128. doi: 10.1021/cb500848p.

32. Dittenhafer-Reed KE, et al. SIRT3 mediates multi-tissue coupling for metabolic fuel switching. Cell Metab. 2015;21(4):637–646. doi: 10.1016/j.cmet.2015.03.007.

33. Cimen H, Han MJ, Yang Y, Tong Q, Koc H, Koc EC. Regulation of succinate dehydrogenase activity by SIRT3 in mammalian mitochondria. Biochemistry. 2010;49(2):304–311. doi: 10.1021/bi901627u.

34. Huss JM, et al. The nuclear receptor ERRα is required for the bioenergetic and functional adaptation to cardiac pressure overload. Cell Metab. 2007;6(1):25–37. doi: 10.1016/j.cmet.2007.06.005.

35. Weinheimer CJ, Lai L, Kelly DP, Kovacs A. Novel mouse model of left ventricular pressure overload and infarction causing predictable ventricular remodelling and progression to heart failure. Clin Exp Pharmacol Physiol. 2015;42(1):33–40. doi: 10.1111/1440-1681.12318.

36. Hebert AS, et al. Calorie restriction and SIRT3 trigger global reprogramming of the mitochondrial protein acetylome. Mol Cell. 2013;49(1):186–199. doi: 10.1016/j.molcel.2012.10.024.

37. Hirschey MD, et al. SIRT3 deficiency and mitochondrial protein hyperacetylation accelerate the development of the metabolic syndrome. Mol Cell. 2011;44(2):177–190. doi: 10.1016/j.molcel.2011.07.019.

38. Wagner GR, Payne RM. Widespread and enzyme-independent Nepsilon-acetylation and Nepsilon-succinylation of proteins in the chemical conditions of the mitochondrial matrix. J Biol Chem. 2013;288(40):29036–29045. doi: 10.1074/jbc.M113.486753.

39. Aubert G, et al. The failing heart relies on ketone bodies as a fuel. Circulation. doi: 10.1161/CIRCULATIONAHA.1. [published online ahead of print January 27, 2016]. [PMC free article] [PubMed] [Cross Ref]

40. Peek CB, et al. Circadian clock NAD+ cycle drives mitochondrial oxidative metabolism in mice. Science. 2013;342(6158):e84897 doi: 10.1126/science.1243417.

41. Ahn BH, et al. A role for the mitochondrial deacetylase Sirt3 in regulating energy homeostasis. Proc Natl Acad Sci U S A. 2008;105(38):14447–14452. doi: 10.1073/pnas.0803790105.

42. Anderson KA, Hirschey MD. Mitochondrial protein acetylation regulates metabolism. Essays Biochem. 2012;52:23–35. doi: 10.1042/bse0520023.

43. Choudhary C, Weinert BT, Nishida Y, Verdin E, Mann M. The growing landscape of lysine acetylation links metabolism and cell signalling. Nat Rev Mol Cell Biol. 2014;15(8):536–550.

44. Hirschey MD, et al. SIRT3 regulates mitochondrial fatty-acid oxidation by reversible enzyme deacetylation. Nature. 2010;464(7285):121–125. doi: 10.1038/nature08778.

45. Fan J, et al. Tyr phosphorylation of PDP1 toggles recruitment between ACAT1 and SIRT3 to regulate the pyruvate dehydrogenase complex. Mol Cell. 2014;53(4):534–548. doi: 10.1016/j.molcel.2013.12.026.

46. Jain-Ghai S, et al. Complex II deficiency — a case report and review of the literature. Am J Med Genet A. 2013;161A(2):285–294.

47. Karamanlidis G, et al. Mitochondrial complex I deficiency increases protein acetylation and accelerates heart failure. Cell Metab. 2013;18(2):239–250. doi: 10.1016/j.cmet.2013.07.002.

48. Hsu CP, et al. Silent information regulator 1 protects the heart from ischemia/reperfusion. Circulation. 2010;122(21):2170–2182. doi: 10.1161/CIRCULATIONAHA.110.958033.

49. Yamamoto T, Sadoshima J. Protection of the heart against ischemia/reperfusion by silent information regulator 1. Trends Cardiovasc Med. 2011;21(1):27–32. doi: 10.1016/j.tcm.2012.01.005.

50. Gu XS, et al. Resveratrol, an activator of SIRT1, upregulates AMPK and improves cardiac function in heart failure. Genet Mol Res. 2014;13(1):323–335. doi: 10.4238/2014.January.17.17.

51. Still AJ, et al. Quantification of mitochondrial acetylation dynamics highlights prominent sites of metabolic regulation. J Biol Chem. 2013;288(36):26209–26219. doi: 10.1074/jbc.M113.483396.

52. Grimsrud PA, et al. A quantitative map of the liver mitochondrial phosphoproteome reveals posttranslational control of ketogenesis. Cell Metab. 2012;16(5):672–683. doi: 10.1016/j.cmet.2012.10.004.

53. Geer LY, et al. Open mass spectrometry search algorithm. J Proteome Res. 2004;3(5):958–964. doi: 10.1021/pr0499491.

54. Wenger CD, Phanstiel DH, Lee MV, Bailey DJ, Coon JJ. COMPASS: a suite of pre- and post-search proteomics software tools for OMSSA. Proteomics. 2011;11(6):1064–1074. doi: 10.1002/pmic.201000616.

55. Phanstiel DH, et al. Proteomic and phosphoproteomic comparison of human ES and iPS cells. Nat Methods. 2011;8(10):821–827. doi: 10.1038/nmeth.1699.

56. Nesvizhskii AI, Aebersold R. Interpretation of shotgun proteomic data: the protein inference problem. Mol Cell Proteomics. 2005;4(10):1419–1440. doi: 10.1074/mcp.R500012-MCP200.

57. Kim W, et al. Systematic and quantitative assessment of the ubiquitin-modified proteome. Mol Cell. 2011;44(2):325–340. doi: 10.1016/j.molcel.2011.08.025.

58. Pagliarini DJ, et al. A mitochondrial protein compendium elucidates complex I disease biology. Cell. 2008;134(1):112–123. doi: 10.1016/j.cell.2008.06.016.

59. Saks VA, et al. Permeabilized cell and skinned fiber techniques in studies of mitochondrial function in vivo. Mol Cell Biochem. 1998;184(1–2):81–100.

60. Liu H, Naismith JH. An efficient one-step site-directed deletion, insertion, single and multiple-site plasmid mutagenesis protocol. BMC Biotechnol. 2008;8:e84897

61. Salabei JK, Gibb AA, Hill BG. Comprehensive measurement of respiratory activity in permeabilized cells using extracellular flux analysis. Nat Protoc. 2014;9(2):421–438. doi: 10.1038/nprot.2014.018.

62. Ackrell BA, Kearney EB, Singer TP. Mammalian succinate dehydrogenase. Methods Enzymol. 1978;53:466–483.

63. Birch-Machin MA, Turnbull DM. Assaying mitochondrial respiratory complex activity in mitochondria isolated from human cells and tissues. Methods Cell Biol. 2001;65:97–117. doi: 10.1016/S0091-679X(01)65006-4.

64. Acin-Perez R, et al. ROS-triggered phosphorylation of complex II by Fgr kinase regulates cellular adaptation to fuel use. Cell Metab. 2014;19(6):1020–1033. doi: 10.1016/j.cmet.2014.04.015.

Supplemental Material

Supplemental Table 1. Cardiac mitochondrial acetyl proteoforms in the mouse heart.

Uniprot ID	Gene Symbol	Acetyl Proteoform
Q8BWT1	*Acaa2*	K137
Q8BWT1	*Acaa2*	K171
Q8BWT1	*Acaa2*	K234
Q8BWT1	*Acaa2*	K240
D3Z7X0	*Acad12*	K334
Q8JZN5	*Acad9*	K206
P51174	*Acadl*	K156
P51174	*Acadl*	K419

Uniprot ID	Gene Symbol	Acetyl Proteoform
P50544	*Acadvl*	K240
P50544	*Acadvl*	K279
P50544	*Acadvl*	K52
Q8QZT1	*Acat1*	K171
Q8QZT1	*Acat1*	K187
Q8QZT1	*Acat1*	K220
Q8QZT1	*Acat1*	K242
Q8QZT1	*Acat1*	K248
Q8QZT1	*Acat1*	K304
Q8QZT1	*Acat1*	K335
Q8QZT1	*Acat1*	K340
Q8QZT1	*Acat1*	K80
Q99KI0	*Aco2*	K50
Q99KI0	*Aco2*	K517
Q99KI0	*Aco2*	K517|K520
Q99KI0	*Aco2*	K521
Q99KI0	*Aco2*	K523
Q99KI0	*Aco2*	K689
Q99KI0	*Aco2*	K723
Q99KI0	*Aco2*	K736
Q99KI0	*Aco2*	K739
Q9CQR4	*Acot13*	K127
Q9CQR4	*Acot13*	K27
Q9CQR4	*Acot13*	K37
Q9CQR4	*Acot13*	K43
Q9WTP7	*Ak3*	K29
Q8CG76	*Akr7a2*	K123
Q8CHT0	*Aldh4a1*	K54
Q8CHT0	*Aldh4a1*	K92
Q9EQ20	*Aldh6a1*	K117
Q9EQ20	*Aldh6a1*	K47
Q925I1	*Atad3*	K494
Q03265	*Atp5a1*	K126
Q03265	*Atp5a1*	K239
Q03265	*Atp5a1*	K498
Q03265	*Atp5a1*	K531
Q03265	*Atp5a1*	K539
P56480	*Atp5b*	K133
P56480	*Atp5b*	K485
P56480	*Atp5b*	K522
Q9DCX2	*Atp5h*	K117
Q9DCX2	*Atp5h*	K48
Q9DCX2	*Atp5h*	K63
Q9DCX2	*Atp5h*	K63|K72

Uniprot ID	Gene Symbol	Acetyl Proteoform
Q9DCX2	*Atp5h*	K78
Q9DCX2	*Atp5h*	K85
Q9DCX2	*Atp5h*	K95
Q06185	*Atp5i*	K34
Q06185	*Atp5i*	K48
P97450	*Atp5j*	K105
P97450	*Atp5j*	K41
P97450	*Atp5j*	K46
P97450	*Atp5j*	K99
Q9DB20	*Atp5o*	K162
Q9DB20	*Atp5o*	K192
Q9DB20	*Atp5o*	K53
Q9DB20	*Atp5o*	K60
Q9DB20	*Atp5o*	K70
Q9DB20	*Atp5o*	K84
Q9JLZ3	*Auh*	K80
Q91VT4	*Cbr4*	K151
Q91WS0	*Cisd1*	K68
Q6P8J7	*Ckmt2*	K292
Q6P8J7	*Ckmt2*	K344
Q8R4N0	*Clybl*	K55
Q8R4N0	*Clybl*	K80
Q8R4N0	*Clybl*	K90
P19783	*Cox4i1*	K164
P19783	*Cox4i1*	K67
P19783	*Cox4i1*	K78
P12787	*Cox5a*	K109
P56391	*Cox6b1*	K85
P56392	*Cox7a1*	K31
P56393	*Cox7b*	K75
P17665	*Cox7c*	K25
Q9CZU6	*Cs*	K321
Q9CZU6	*Cs*	K327
Q9CZU6	*Cs*	K370
Q9CZU6	*Cs*	K52
Q9D172	*D10Jhu81e*	K162
Q9D172	*D10Jhu81e*	K201
Q9D172	*D10Jhu81e*	K231
Q9CQ62	*Decr1*	K185
Q9CQ62	*Decr1*	K42
Q8BMF4	*Dlat*	K632
O08749	*Dld*	K104
O08749	*Dld*	K143
O08749	*Dld*	K155

Uniprot ID	Gene Symbol	Acetyl Proteoform
O08749	*Dld*	K273
O08749	*Dld*	K410
O08749	*Dld*	K420
O08749	*Dld*	K66
Q9D2G2	*Dlst*	K268
Q9D2G2	*Dlst*	K268|K273
Q9D2G2	*Dlst*	K273
Q9D2G2	*Dlst*	K278
O35459	*Ech1*	K97
Q8BH95	*Echs1*	K101
P42125	*Eci1*	K222
P42125	*Eci1*	K229
P42125	*Eci1*	K76
Q99LC5	*Etfa*	K162
Q99LC5	*Etfa*	K164
Q99LC5	*Etfa*	K69
Q99LC5	*Etfa*	K75
Q9DCW4	*Etfb*	K110
Q9DCW4	*Etfb*	K114
P26443	*Glud1*	K415
P26443	*Glud1*	K503
P26443	*Glud1*	K84
P05202	*Got2*	K122
P05202	*Got2*	K296
P05202	*Got2*	K302
P05202	*Got2*	K309
P05202	*Got2*	K363
P05202	*Got2*	K396
P05202	*Got2*	K404
P05202	*Got2*	K73
P05202	*Got2*	K90
Q61425	*Hadh*	K127
Q61425	*Hadh*	K185
Q61425	*Hadh*	K192
Q61425	*Hadh*	K212
Q61425	*Hadh*	K241
Q61425	*Hadh*	K75
Q61425	*Hadh*	K81
Q61425	*Hadh*	K87
Q8BMS1	*Hadha*	K289
Q8BMS1	*Hadha*	K334
Q8BMS1	*Hadha*	K353
Q8BMS1	*Hadha*	K386
Q8BMS1	*Hadha*	K406

Uniprot ID	Gene Symbol	Acetyl Proteoform
Q8BMS1	*Hadha*	K540
Q8BMS1	*Hadha*	K569
Q8BMS1	*Hadha*	K60
Q8BMS1	*Hadha*	K728
Q99JY0	*Hadhb*	K202
Q99JY0	*Hadhb*	K273
Q99JY0	*Hadhb*	K333
Q99JY0	*Hadhb*	K73
Q99L13	*Hibadh*	K237
Q99L13	*Hibadh*	K94
Q8QZS1	*Hibch*	K352
P38647	*Hspa9*	K135
P38647	*Hspa9*	K288
P38647	*Hspa9*	K300
P38647	*Hspa9*	K612
P38647	*Hspa9*	K76
P63038	*Hspd1*	K125
P63038	*Hspd1*	K130
P63038	*Hspd1*	K202
P63038	*Hspd1*	K455
P63038	*Hspd1*	K87
Q8BIJ6	*Iars2*	K725
Q8CAK1	*Iba57*	K222
P54071	*Idh2*	K106
P54071	*Idh2*	K155
P54071	*Idh2*	K166
P54071	*Idh2*	K180
P54071	*Idh2*	K199
P54071	*Idh2*	K256
P54071	*Idh2*	K272
P54071	*Idh2*	K280
P54071	*Idh2*	K384
P54071	*Idh2*	K400
P54071	*Idh2*	K48
P54071	*Idh2*	K67
Q9D6R2	*Idh3a*	K100
Q9D6R2	*Idh3a*	K336
Q9D6R2	*Idh3a*	K343
Q9D6R2	*Idh3a*	K58
Q9D6R2	*Idh3a*	K77
Q9JHI5	*Ivd*	K76
P14152	*Mdh1*	K107
P14152	*Mdh1*	K164
P08249	*Mdh2*	K165

Uniprot ID	Gene Symbol	Acetyl Proteoform
P08249	*Mdh2*	K239
P08249	*Mdh2*	K296
P08249	*Mdh2*	K301
P08249	*Mdh2*	K307
P08249	*Mdh2*	K328|K329
Q9CQ75	*Ndufa2*	K64
Q62425	*Ndufa4*	K56
Q9CPP6	*Ndufa5*	K36
Q9CPP6	*Ndufa5*	K40
Q9CPP6	*Ndufa5*	K60
Q9CPP6	*Ndufa5*	K66
Q9DC69	*Ndufa9*	K189
Q9DC69	*Ndufa9*	K254
Q9D6J5	*Ndufb8*	K176
Q9CQJ8	*Ndufb9*	K121
Q9DCT2	*Ndufs3*	K259
P52503	*Ndufs6*	K41
Q9D6J6	*Ndufv2*	K60
Q60597	*Ogdh*	K897
Q91ZA3	*Pcca*	K146
Q91ZA3	*Pcca*	K61
P35486	*Pdha1*	K244
P35486	*Pdha1*	K267
P35486	*Pdha1*	K321
P35486	*Pdha1*	K63
P35486	*Pdha1*	K83
Q8BKZ9	*Pdhx*	K321
P20108	*Prdx3*	K254
P20108	*Prdx3*	K92
Q8K2B3	*Sdha*	K179
Q8K2B3	*Sdha*	K480
Q8K2B3	*Sdha*	K485
Q8K2B3	*Sdha*	K498
Q8K2B3	*Sdha*	K547
Q8K2B3	*Sdha*	K550
Q8K2B3	*Sdha*	K608
Q9CQA3	*Sdhb*	K269
Q9CQA3	*Sdhb*	K53
Q9CQA3	*Sdhb*	K57
Q8BH59	*Slc25a12*	K578
P51881	*Slc25a5*	K105
P51881	*Slc25a5*	K155
P09671	*Sod2*	K114
P09671	*Sod2*	K122
P09671	*Sod2*	K130

Uniprot ID	Gene Symbol	Acetyl Proteoform
P09671	*Sod2*	K68
Q9WUM5	*Suclg1*	K54
Q8R1I1	*Uqcr10*	K59
Q9DB77	*Uqcrc2*	K92
Q9CR68	*Uqcrfs1*	K172
P99028	*Uqcrh*	K40
P99028	*Uqcrh*	K83
Q78IK2	*Usmg5*	K16

All identified mitochondrial acetylproteoforms are listed. Mitochondrial proteins were defined based on GOCC annotation in DAVID and MITOCARTA.

Supplemental Table 2. Mitochondrial protein acetylation sites regulated in HF mice.

Uniprot ID	Gene Symbol	Acetyl Proteoform	HF/Sham (FC)	SIRT3 Target	Regulated in CH
Q8BWT1	*Acaa2*	K137	1.56	No	Yes
D3Z7X0	*Acad12*	K334	2.08	No	No
P50544	*Acadvl*	K52	1.91	No	No
P50544	*Acadvl*	K240	1.75	Yes	No
Q8QZT1	*Acat1*	K187	1.67	No	No
Q99KI0	*Aco2*	K50	1.50	No	No
Q32MW3|Q9R0X4	*Acot10|Acot9*	K102	1.69	Yes	Yes
Q9CQR4	*Acot13*	K27	2.72	No	No
Q9Z0X1| B1AU25	*Aifm1*	K592	-1.66	No	Yes
Q8CG76	*Akr7a2*	K123	1.63	No	No
P47738|Q3U9J7| Q3U6I3|Q3UJW1| Q3TVM2	*Aldh2*	K370	1.53	Yes	Yes
P56480	*Atp5b*	K133	1.60	Yes	Yes
Q9D3D9|Q9DCZ0| Q9D0J2	*Atp5d*	K165	-1.55	No	Yes
Q8R4N0	*Clybl*	K80	1.56	Yes	No
Q8R4N0	*Clybl*	K55	1.56	Yes	No
P19783	*Cox4i1*	K67	1.77	No	No
P47934|H7BX88	*Crat*	K270	1.70	No	Yes
Q9D172	*D10Jhu81e*	K231	1.79	Yes	No
Q9D172	*D10Jhu81e*	K201	1.62	Yes	No
Q9CQ62	*Decr1*	K42	2.07	Yes	No
Q8BH95	*Echs1*	K101	1.55	Yes	No
P21550	*Eno3*	K28	-2.43	No	No
Q9DCW4	*Etfb*	K114	1.77	No	No
Q921G7|Q6PF96	*Etfdh*	K133	1.72	No	No
Q61425	*Hadh*	K87	1.60	Yes	No
Q8BMS1	*Hadha*	K406	1.68	Yes	No
Q99JY0	*Hadhb*	K73	1.92	Yes	Yes
P38647	*Hspa9*	K300	2.26	No	No
P63038	*Hspd1*	K455	2.66	No	Yes
P63038	*Hspd1*	K130	1.52	Yes	No
P63038	*Hspd1*	K125	1.51	Yes	No
Q8CAK1	*Iba57*	K222	-2.87	No	No
P54071	*Idh2*	K67	2.78	No	No
P54071	*Idh2*	K272	1.56	No	No
P54071	*Idh2*	K106	1.56	No	No
P08249	*Mdh2*	K165	1.69	No	No
P03930|A3R404| Q5GA80	*Mtatp8|mt-Atp8|ATP8*	K48	1.69	Yes	No

Uniprot ID	Gene Symbol	Acetyl Proteoform	HF/Sham (FC)	SIRT3 Target	Regulated in CH
P09541|Q9CZ19|A2A6Q8	*Myl4*	K140	1.66	No	No
Q3UIU2|A2AP32	*Ndufb6*	K24	1.67	No	No
Q9D6J5	*Ndufb8*	K176	-1.88	No	No
P52503	*Ndufs6*	K41	2.11	No	Yes
Q8K2B3	*Sdha*	K608	1.98	No	Yes

A fold-change cut-off of ±1.5 was used for this analysis.

Supplemental Table 3. Pathway analysis of mitochondrial proteins with regulated acetylation sites in murine HF.

Ingenuity Canonical Pathways	# of genes regulated	# of genes in pathway	p-value	Acetylated Proteins
Oxidative Phosphorylation/Electron Transport Chain	**7**	**100**	7.943E-10	**SDHA,ATP5B,ATP5D,NDUFS6, NDUFB6,NDUFB8,COX4I1**
Fatty Acid β-oxidation I	**5**	**30**	2.754E-09	**HADHB,ECHS1,ACAA2,HADHA, HADH**
Glutaryl-CoA Degradation	4	11	3.802E-09	HADHB,ACAT1,HADHA,HADH
Isoleucine Degradation I	4	14	1.148E-08	HADHB,ECHS1,ACAT1,HADHA
Tryptophan Degradation III (Eukaryotic)	4	20	5.623E-08	HADHB,ACAT1,HADHA,HADH
Ketolysis	3	8	3.715E-07	HADHB,ACAT1,HADHA
Ketogenesis	3	10	7.943E-07	HADHB,ACAT1,HADHA
Mevalonate Pathway I	3	12	1.445E-06	HADHB,ACAT1,HADHA
Superpathway of Geranylgeranyldiphosphate Biosynthesis I (via Mevalonate)	3	12	3.631E-06	HADHB,ACAT1,HADHA
Valine Degradation I	3	18	5.370E-06	HADHB,ECHS1,HADHA
TCA Cycle II (Eukaryotic)	**3**	**22**	8.710E-06	**SDHA,ACO2,MDH2**
Superpathway of Cholesterol Biosynthesis	3	27	1.905E-05	HADHB,ACAT1,HADHA
Gluconeogenesis I	2	24	8.318E-04	ENO3,MDH2
Phenylethylamine Degradation I	1	4	7.762E-03	ALDH2
Aspartate Degradation II	1	7	1.148E-02	MDH2
LXR/RXR Activation	2	110	1.950E-02	ECHS1,HADH
Phenylalanine Degradation IV (Mammalian, via Side Chain)	1	14	2.512E-02	ALDH2
Histamine Degradation	1	12	2.512E-02	ALDH2
Methylglyoxal Degradation III	1	14	2.692E-02	AKR7A2
Putrescine Degradation III	1	16	3.090E-02	ALDH2
Fatty Acid α-oxidation	1	15	3.090E-02	ALDH2
Oxidative Ethanol Degradation III	1	15	3.090E-02	ALDH2
Tryptophan Degradation X (Mammalian, via Tryptamine)	1	17	3.236E-02	ALDH2
Aldosterone Signaling in Epithelial Cells	2	148	3.311E-02	HSPA9,HSPD1
Ethanol Degradation IV	1	17	3.467E-02	ALDH2
Dopamine Degradation	1	20	3.802E-02	ALDH2
Glycolysis I	1	23	4.169E-02	ENO3
Tumoricidal Function of Hepatic Natural Killer Cells	1	22	4.365E-02	AIFM1

All significantly regulated pathways as identified by Ingenuity Pathway Analysis are listed. Major energy transduction pathways are shown in bold.

Supplemental Table 4. Mitochondrial protein acetylation sites regulated in CH mice.

Uniprot ID	Gene Symbol	Acetyl Proteoform	CH/Sham (FC)	SIRT3 Target	Regulated in HF
Q8BWT1	*Acaa2*	K137	1.59	No	Yes
Q8QZT1	*Acat1*	K80	-1.50	No	No
Q8QZT1	*Acat1*	K171	-1.65	No	No
Q99KI0	*Aco2*	K739	-1.60	Yes	No
Q32MW3|Q9R0X4	*Acot10|Acot9*	K102	1.50	Yes	Yes
Q9Z0X1|B1AU25	*Aifm1*	K592	-2.08	No	Yes
P47738|Q3U9J7| Q3U6I3|Q3UJW1| Q3TVM2	*Aldh2*	K370	1.61	Yes	Yes
Q03265	*Atp5a1*	K126	-1.54	Yes	No
P56480	*Atp5b*	K133	1.96	Yes	Yes
Q9D3D9|Q9DCZ0| Q9D0J2	*Atp5d*	K165	1.75	No	Yes
Q9DCX2	*Atp5h*	K48	1.77	No	No
P97450	*Atp5j*	K99	-1.64	No	No
P97450	*Atp5j*	K41	-1.66	No	No
Q6P8J7	*Ckmt2*	K292	1.63	No	No
P19536|Q9D881	*Cox5b*	K74	1.67	No	No
P19536|Q9D881	*Cox5b*	K121	1.64	No	No
P56393	*Cox7b*	K75	1.85	No	No
P47934|H7BX88	*Crat*	K270	2.04	No	Yes
Q9D0M3|Q9D0M3-2	*Cyc1*	K177	-1.98	No	No
O08749	*Dld*	K420	1.79	No	No
Q9D2G2	*Dlst*	K278	-1.63	No	No
O35459	*Ech1*	K97	1.69	No	No
P42125	*Eci1*	K222	-2.12	No	No
Q9WUR2|Q9WUR2-2| Q3TCD4	*Eci2*	K138	3.39	No	No
Q99LC5	*Etfa*	K164	1.54	No	No
P26443	*Glud1*	K415	2.35	No	No
P26443	*Glud1*	K84	-1.82	No	No
P05202	*Got2*	K122	1.74	No	No
Q61425	*Hadh*	K127	1.52	No	No
Q8BMS1	*Hadha*	K334	1.58	Yes	No
Q8BMS1	*Hadha*	K519	1.54	No	No
Q99JY0	*Hadhb*	K73	-1.64	Yes	Yes
P63038	*Hspd1*	K455	2.46	No	Yes
P54071	*Idh2*	K400	2.32	No	No
Q9D6R2	*Idh3a*	K336	-1.57	No	No
E9Q800|Q3TEY5	*Immt*	K596	1.80	No	No
P08249	*Mdh2*	K239	1.53	Yes	No
P51667	*Myl2*	K165	1.64	No	No

Uniprot ID	Gene Symbol	Acetyl Proteoform	CH/Sham (FC)	SIRT3 Target	Regulated in HF
Q9CPP6	*Ndufa5*	K36	1.51	No	No
Q91VD9|Q3TIU7	*Ndufs1*	K98	1.62	No	No
P52503	*Ndufs6*	K41	1.58	No	Yes
Q9JHW2	*Nit2*	K68	-2.80	No	No
Q60597	*Ogdh*	K897	-1.52	No	No
P35486	*Pdha1*	K321	1.76	No	No
P35486	*Pdha1*	K63	1.65	No	No
Q8K1R3|Q8K1R3-2|Q3TST0|Q3UNL5|Q3TN29	*Pnpt1*	K285	1.64	No	No
Q8K2B3	*Sdha*	K608	2.07	No	Yes
Q8VEM8|G5E902|Q3THU8	*Slc25a3*	K230	2.41	No	No
P51881	*Slc25a5*	K155	1.57	No	No
Q9D855|Q9CQB4	*Uqcrb*	K110	1.59	No	No
Q9D855|Q9CQB4	*Uqcrb*	K83	-1.99	No	No

A fold-change cut-off of ±1.5 was used for this analysis.

Supplemental Table 5. Mitochondrial protein acetylation sites regulated in human failing hearts.

Uniprot ID	Gene Symbol	Acetyl Proteoform	DCM/NF (FC)	p-value
Q9UKU7	*ACAD8*	K144	2.22	0.055
P16219	*ACADS*	K343	2.04	0.059
A2A274	*ACO2*	K50	1.35	0.021
A2A274	*ACO2*	K138	2.03	0.022
B7Z452	*ACSL1*	K561	1.83	0.059
P30038	*ALDH4A1*	K531	2.01	0.013
P30038	*ALDH4A1*	K119	1.99	0.042
P30038	*ALDH4A1*	K93	1.52	0.169
Q8NCW5	*APOA1BP*	K148	1.62	0.030
Q6UXV4	*APOOL*	K105	2.46	0.033
P25705	*ATP5A1*	K252	2.55	0.004
P25705	*ATP5A1*	K498	-1.62	0.007
P25705	*ATP5A1*	K316	1.53	0.010
P25705	*ATP5A1*	K194	1.82	0.038
P25705	*ATP5A1*	K506	1.45	0.040
P25705	*ATP5A1*	K531	-1.62	0.186
P25705	*ATP5A1*	K230	2.09	0.074
O75947	*ATP5H*	K58	1.59	0.110
P18859	*ATP5J*	K94	1.85	0.095
Q9UII2	*ATPIF1*	K82	1.79	0.045
Q02338	*BDH1*	K97	1.88	0.045
Q02338	*BDH1*	K212	1.62	0.060
P04040	*CAT*	K237	2.29	0.023
Q03135	*CAV1*	K47	1.85	0.064
Q9NZ45	*CISD1*	K68	2.05	0.001
P12277	*CKB*	K307	3.76	0.002
P12277	*CKB*	K298	1.67	0.088
P17540	*CKMT2*	K230	1.67	0.001
Q14061	*COX17*	K40	2.45	0.003
P13073	*COX4I1*	K159	1.97	0.040
Q92523	*CPT1B*	K40	2.01	0.022
P07339	*CTSD*	K341	2.01	0.063
Q9UHQ9	*CYB5R1*	K167	-1.23	0.018
P11182	*DBT*	K295	1.60	0.255
P11182	*DBT*	K243	2.01	0.071
P11182	*DBT*	K257	2.03	0.153
P36957	*DLST*	K267/K272	1.54	0.255
P15924	*DSP*	K916	1.41	0.003
P15924	*DSP*	K1687	2.04	0.012
P15924	*DSP*	K485	1.91	0.039
P15924	*DSP*	K1099	1.84	0.126
P15924	*DSP*	K2393	1.84	0.095
P30084	*ECHS1*	K115	1.70	0.056
P13804	*ETFA*	K69	1.94	0.075
Q16134	*ETFDH*	K96	1.60	0.025
P00505	*GOT2*	K279	2.55	0.016
P00505	*GOT2*	K94	2.19	0.024

Uniprot ID	Gene Symbol	Acetyl Proteoform	DCM/NF (FC)	p-value
P40939	*HADHA*	K406	-2.49	0.008
P40939	*HADHA*	K353	-1.67	0.135
P40939	*HADHA*	K411	-1.63	0.072
P40939	*HADHA*	K326/K334	1.54	0.409
P40939	*HADHA*	K605	2.45	0.064
P49590	*HARS2*	K52	1.92	0.020
P31937	*HIBADH*	K56	1.89	0.103
O75874	*IDH1*	K81	2.28	0.018
P50213	*IDH3A*	K223	-1.82	0.008
O43837	*IDH3B*	K199	3.74	0.002
P83111	*LACTB*	K225	1.60	0.187
P42704	*LRPPRC*	K66	2.37	0.038
Q9BQ69	*MACROD1*	K117	1.53	0.007
P21397	*MAOA*	K469	2.36	0.058
P23368	*ME2*	K24	-2.33	0.020
P82909	*MRPS36*	K78	2.13	0.015
Q9Y3D2	*MSRB2*	K176	2.38	0.038
Q9UI09	*NDUFA12*	K114	1.70	0.005
Q9UI09	*NDUFA12*	K47	1.72	0.169
Q9P0J0	*NDUFA13*	K22	2.05	0.288
Q9P0J0	*NDUFA13*	K7	2.80	0.105
P56556	*NDUFA6*	K44	1.60	0.575
P51970	*NDUFA8*	K106	3.13	0.005
P51970	*NDUFA8*	K38	1.60	0.148
Q16795	*NDUFA9*	K163	2.17	0.006
O96000	*NDUFB10*	K121	1.86	0.078
O95298	*NDUFC2*	K114	1.59	0.002
O75489	*NDUFS3*	K109	1.84	0.000
O43920	*NDUFS5*	K38	1.63	0.008
O43920	*NDUFS5*	K101	1.32	0.012
O00217	*NDUFS8*	K88	2.00	0.037
Q13423	*NNT*	K100	2.10	0.007
Q13423	*NNT*	K331	1.58	0.009
Q13423	*NNT*	K462	1.75	0.020
Q13423	*NNT*	K453	2.32	0.030
Q13423	*NNT*	K403	1.69	0.178
E9PCR7	*OGDH*	K363	2.53	0.006
E9PCR7	*OGDH*	K402	1.58	0.033
E9PCR7	*OGDH*	K416	-1.64	0.093
E9PCR7	*OGDH*	K252	2.37	0.053
P55809	*OXCT1*	K41	2.46	0.037
P55809	*OXCT1*	K296	1.51	0.333
P30405	*PPIF*	K73	-1.81	0.018
P30405	*PPIF*	K167	1.95	0.040
P47897	*QARS*	K230	2.17	0.036
Q9Y512	*SAMM50*	K227	1.34	0.012
D6RFM5	*SDHA*	K361	1.64	0.018
E9PEF8	*SDHA*	K396	1.52	0.020
D6RFM5	*SDHA*	K179	1.84	0.130

Uniprot ID	Gene Symbol	Acetyl Proteoform	DCM/NF (FC)	p-value
P12235	*SLC25A4*	K163	1.67	0.003
P12235	*SLC25A4*	K33	1.81	0.013
P12235	*SLC25A4*	K96	1.53	0.051
P53597	*SUCLG1*	K54	1.88	0.012
P21980	*TGM2*	K672	2.51	0.001
P49411	*TUFM*	K297	2.13	0.015
P49411	*TUFM*	K55	1.78	0.101
P31930	*UQCRC1*	K447	1.60	0.032
P22695	*UQCRC2*	K159	1.35	0.043
P07919	*UQCRH*	K85	1.85	0.002
O14949	*UQCRQ*	K33	1.90	0.040
P21796	*VDAC1*	K224	1.20	0.018
P21796	*VDAC1*	K109	1.23	0.019
P21796	*VDAC1*	K252	1.74	0.022

A fold-change cut-off of ±1.5 or $p < 0.05$ was used for this analysis.

CHAPTER FOUR:
THE FAILING HEART RELIES ON KETONE BODIES AS A FUEL[2]

[2]This is a non-final version of an article published in its final form as: GA Aubert, OJ Martin, JL Horton, L Lai, RB Vega, TC Leone, T Koves, SJ Gardell, M Kruger, CL Hoppel, ED Lewandowski, PA Crawford, DM Muoio, and DP Kelly. The Failing Heart Relies on Ketone Bodies as a Fuel. *Circulation.* 2016;133(8):698-705

Abstract

Background

Significant evidence indicates that the failing heart is “energy-starved”. During the development of heart failure, the capacity of the heart to utilize fatty acids, the chief fuel, is diminished. Identification of alternate pathways for myocardial fuel oxidation could unveil novel strategies to treat heart failure.

Methods and Results

Quantitative mitochondrial proteomics was used to identify energy metabolic derangements that occur during the development of cardiac hypertrophy and heart failure in well-defined mouse models. As expected, amounts of proteins involved in fatty acid utilization were downregulated in myocardial samples from the failing heart. Conversely, expression of β-hydroxybutyrate dehydrogenase 1 (BDH1), a key enzyme in the ketone oxidation pathway, was increased in the heart failure samples.

Studies of relative oxidation studies in an isolated heart preparation using ex vivo NMR combined with targeted quantitative myocardial metabolomic profiling using mass spectrometry revealed that the hypertrophied and failing heart shifts to oxidizing ketone

bodies as a fuel source in the context of reduced capacity to oxidize fatty acids. Distinct myocardial metabolomic signatures of ketone oxidation were identified.

Conclusions

These results indicate that the hypertrophied and failing heart shifts to ketone bodies as a significant fuel source for oxidative ATP production. Specific metabolite biosignatures of in vivo cardiac ketone utilization were identified. Future studies aimed at determining whether this fuel shift is adaptive or maladaptive could unveil new therapeutic strategies for heart failure.

Keywords:

heart failure, hypertrophy, metabolism, molecular biology, fatty acid

Introduction

Growing evidence indicates that derangements in myocardial fuel metabolism and bioenergetics contribute to the development of heart failure, a global health problem. The adult mammalian heart requires enormous amounts of energy to sustain contractile function. Given that cardiac myocyte energy reserves are limited, ATP must be continually generated by oxidation of carbon fuels (1–5). Over 95% of the ATP produced in the healthy adult mammalian heart comes from mitochondrial oxidative phosphorylation, with the remainder being derived from glycolysis (2–5). Genetic studies have provided evidence that alterations in mitochondrial ATP production is casually linked to the development of heart failure. Specifically, human genetic defects

in mitochondrial fatty acid oxidation (FAO) and oxidative phosphorylation (OXPHOS) cause cardiomyopathy.

Studies in humans with common acquired forms of heart failure have also provided evidence that derangements in fuel and energy metabolism contribute to heart failure. Cardiac magnetic resonance spectroscopy studies have shown that myocardial “high-energy” phosphate (phosphocreatine or PCr) stores are reduced in humans with pathological ventricular hypertrophy, with further decline during the transition to heart failure (6–10). Notably, the [PCr]/[ATP] ratio correlates with heart failure severity and is a strong predictor of cardiovascular mortality (11,12). In addition, studies conducted in animal models have consistently revealed re-programming of myocardial fuel utilization in the hypertrophied and failing heart; a shift from the chief fuel metabolic pathway, fatty acid oxidation (FAO), to increased reliance on glycolysis (13–20). Cardiac positron emission tomography studies in humans with hypertensive cardiac hypertrophy or idiopathic cardiomyopathy have largely corroborated this fuel shift (21–23). The mechanisms through which the failing heart compensates for this reduced capacity for oxidizing its chief energy substrate are unknown. Delineation of such alternate fuel utilization pathways, if they exist, could unveil new therapeutic strategies for heart failure.

In this study, we undertook an unbiased proteomic approach to probe mitochondrial fuel and energy metabolic abnormalities that occur during the development of heart failure in well-defined models of compensated and de-compensated pressure overload-induced cardiac hypertrophy in mice. Our results

confirmed that contents of proteins involved in fatty acid utilization are reduced in the hypertrophied and failing heart. The proteomic dataset also demonstrated that the β-hydroxybutyrate dehydrogenase 1 (BDH1), a key enzyme in the ketone oxidation pathway, is upregulated in the hypertrophied and failing heart. Metabolite profiling and labeled substrate utilization studies supported the conclusion that the hypertrophied and failing heart shifts to ketone bodies as an alternate fuel.

Methods

Animal Studies

All animal experiments and euthanasia protocols were approved by the Institutional Animal Care and Use Committee at Sanford Burnham Prebys Medical Discovery Institute at Lake Nona. Studies were performed on female C57BL/6J mice 7–12 weeks of age on either standard chow (16.4% protein, 4.0% fat and 48.5% carbohydrates; Harlan Teklad, #2016) or ketogenic diet (8.6% protein, 75.1% fat and 3.2% carbohydrates; BioServ Co, AIN-76A). Animals were fed the ketogenic diet starting at 7–8 weeks of age.

8 week old female C57BL/6J mice in the following groups were utilized: compensated hypertrophy (CH) vs sham controls; heart failure (HF) vs sham controls. CH was achieved by transverse aortic constriction (TAC). HF was achieved by TAC plus a small apical myocardial infarction as described (24–26). Mice were harvested 1 month following each procedure.

Proteomics using Stable Labeling by Amino Acids (SILAC)

Mass spectrometry-based quantitative proteomics was conducted on mitochondrial enriched fractions (27) prepared from cardiac tissue of CH, HF, and sham control non-labeled (light) mice, spiked with Lys6 labeled mitochondria prepared from cardiac tissue of Lys6 (^{13}C6-Lysine, Silantes) labeled (heavy) non-surgery mice, (28) as described in the Data Supplement. The proteomics data have been deposited into the Proteome Xchange Consortium (http://proteomecentral.proteomexchange.org) via the PRIDE partner repository with the dataset identifier PXD001820.

Substrate Oxidation Measurements

Langendorff heart perfusions were performed as previously described (29,30). Briefly, mice received 100 units of heparin by intraperitoneal injection and 10 min later were anesthetized with an intraperitoneal injection of 390 mg/kg sodium pentobarbital.

Excised hearts were perfused with a modified Krebs-Henseliet buffer (118 mM NaCl, 25 mM $NaHCO_3$, 4.7 mM KCl, 0.4 mM KH_2PO_4, 2.5 mM $CaCl_2$, pH 7.4) supplemented with 5 mM glucose and either i) 0.6 mM [2, 4,6,8,10,12,14,16-^{13}C8] palmitate complexed (3:1 ratio) to a 3% fatty acid free bovine serum albumin (BSA) plus unlabeled 1 mM βOHB or unlabeled 0.6 mM palmitate/BSA plus 1 mM [2, 4-^{13}C2] βOHB, with 1 mU/ml insulin (rDNA origin; Lilly) and continuous equilibration to a 95% O2/5% CO_2 gas mixture. Following each perfusion, hearts were snap frozen in LN_2 cooled tongs.

In vitro NMR spectroscopy was performed on reconstituted (D2O) lyophilized samples of neutralized, acid extracts of frozen myocardium, as previously described using either direct detect proton-decoupled ^{13}C NMR or ^{13}C-edited, 1H-observed NMR (30,31). The relative contribution of each substrate was calculated as previously described (29,31). Briefly, glutamate enrichment was used as a reporter of carbon entry into the TCA cycle. The fractional enrichment of acetyl-coenzyme A (Fc) entering the TCA cycle and the contribution of anaplerosis relative to citrate synthase activity (Y) were determined by isotopomer analysis of the glutamate 3- and 4-carbon ^{13}C resonance.

RNA Analyses

Total RNA was isolated from mouse bi-ventricle using the RNAzol method (Tel-Test). qRT-PCR was performed as described previously (32) and in the Data Supplement.

Western Blot

Western blotting was performed with lysates from bi-ventricle as previously described (33) using the following antibodies: VDAC/porin, (Abcam #ab15895); and BDH1 (Abcam #ab93931). Detection was performed by measuring the chemiluminescent signal as assayed by SuperSignal Dura (Pierce).

Metabolomic Analysis of Organic Acids and Acylcarnitines

Measurements of succinate, C4OH-carnitine, and acetylcarnitine (C2-carnitine) in mouse heart were conducted as described (25,34) and in the Data Supplement.

Plasma Biochemistry Measurements

Ketone bodies (total and β-hydroxybutyrate) were measured in blood serum using assays from Wako (Wako Diagnostics) according to the manufacturer's instructions or on a Beckman-Coulter UniCel DxC 600 Analyzer. Plasma glucose and free fatty acids were measured using assays from Cayman (Cayman Chemical). Plasma triglyceride levels were determined using the Stanbio (Stanbio Laboratory) assay. The assays were conducted according to the manufacturer's instructions.

Statistical Analyses

All data were analyzed with a 2-tailed Mann-Whitney or Student's T-test (GraphPad Prism 6), where noted. The level of significance was set at $p < 0.05$ in all cases. The Pearson's correlation coefficient was used to define the relationship between the amounts of CH and HF proteins.

Results

Mitochondrial Proteomic Profiling Reveals Evidence for Altered Fuel Utilization in the Hypertrophied and Early Stage Failing Mouse Heart

As an initial step towards defining energy metabolic alterations in the hypertrophied and early stage failing heart, quantitative mitochondrial proteomics was conducted on two well-defined mouse surgical models that exhibit distinct cardiac functional manifestations over a 4 week period: i) Left ventricular (LV) hypertrophy with preserved ventricular function (compensated hypertrophy or CH) achieved via surgically-placed transverse aortic constriction (TAC); (24) and ii) decompensated cardiac hypertrophy

(heart failure or HF) caused by combining TAC with a small apical myocardial infarction (TAC/MI) leading to reduced LV systolic function and global chamber dilatation (25,26). To identify regulated proteins, mitochondrial-enriched samples prepared from cardiac ventricles of CH and HF mice, and corresponding sham-operated control mice were subjected to quantitative proteomics using Stable Isotope Labeling by Amino Acids (SILAC) in mouse. Heavy isotope-tagged mitochondrial-enriched proteins were prepared from the hearts of control mice fed a diet containing ^{13}C6-Lysine (Lys6) for 3 generations (35) (Figure 7A). 516 mitochondrial proteins were identified in all samples (Table 1 in the Data Supplement). The levels of 55 of these protein were determined to be regulated in CH (23), HF (10) or both (22) groups compared to corresponding controls, using a cutoff of < −1.25 or > 1.5-fold change (Figure 7B, and in the Data Supplement Table 7). Notably, the majority of dysregulated proteins in the HF group were similarly impacted in the CH group. In addition, changes in protein amounts in CH and HF are significantly correlated (Pearson correlation coefficient r=0.82; Figure 7C).

Rather surprisingly, the proteomic data revealed that few proteins involved in the electron transport chain (ETC) or mitochondrial OXPHOS were downregulated in CH or HF mice, in contrast to the results from other studies using models of chronic heart failure (36–39). These results are consistent, however, with the results of our previous transcriptomic profiling of the same samples demonstrating that very few genes involved in ETC/OXPHOS were regulated in CH or HF samples (25). Many of the regulated proteins detected in our study were involved in myocyte fuel metabolism.

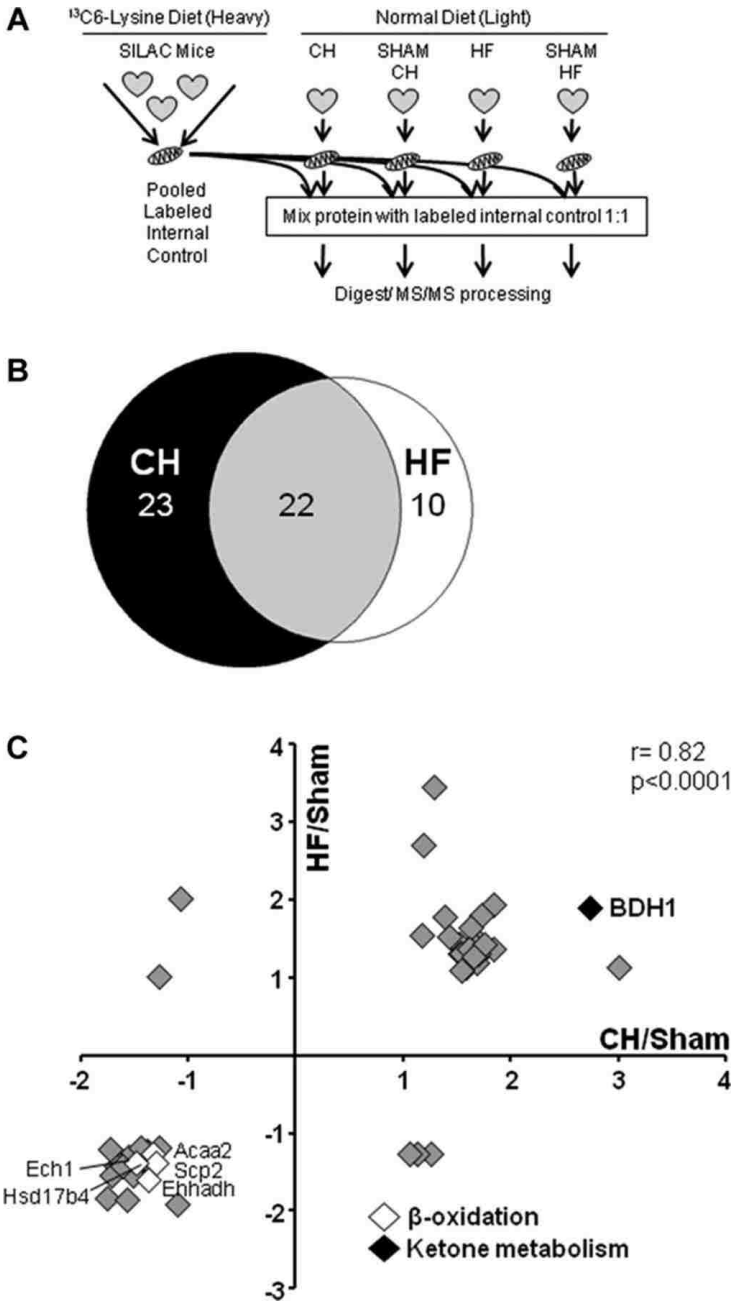

Figure 7. Mitochondrial proteomic profiling in the hypertrophied and failing mouse heart.

(A) Schematic of the experimental design for quantitative proteomic analysis using stable isotope labeling by amino acids (SILAC), in mitochondrial-enriched fractions, from the ventricles of sham-operated, compensated hypertrophy (CH), and heart failure (HF) animals. **(B)** Venn diagram displaying the number of regulated proteins identified in the CH, HF, or both groups using a cutoff of –1.25- or >1.5-fold change (FC) in comparison with sham-operated controls (n=2 per group). **(C)** The graph denotes fold change in levels of proteins that meet the defined cutoffs: HF/sham (ordinate) and CH/sham (abscissa). The key denotes regulated proteins involved in 2 fuel utilization pathways of interest as described in the text: fatty acid β-oxidation (white) and ketone catabolism (black). Spearman correlation coefficient (r) was calculated to determine the relationship between the CH and HF protein changes. BDH1 indicates β-hydroxybutyrate dehydrogenase 1

First, proteins needed for cellular fatty acid utilization were reduced in both the CH and HF groups [enoyl-CoA, hydratase/3-hydroxyacyl CoA dehydrogenase (EHHADH), enoyl CoA hydratase 1 (ECH1), acetyl-CoA acyltransferase 2 (ACAA2), and hydroxysteroid (17-beta) dehydrogenase 4 (HSD17B4), non-specific lipid transfer protein (SCP2); Figure 7C]. These results are concordant with many published studies showing that expression of genes involved in FAO are downregulated in the hypertrophied and failing hearts (15,16,20,40–42). Secondly, BDH1, an enzyme involved in ketone body metabolism, was increased in both CH and HF samples (2.8 and 1.9 fold, respectively; Figure 7C, and in the Data Supplement Table 7). The induction of BDH1 protein expression was among the highest in the dataset. Quantitative real-time PCR (qRT-PCR) and immunoblotting confirmed a significant increase in Bdh1 mRNA and protein expression in CH and HF hearts harvested under both fed and fasted conditions (Figures 8A, B).

The Hypertrophied Heart Re-programs to Utilize Ketone Bodies as an Alternate Fuel Source

We next conducted studies to determine whether the hypertrophied heart shifts to using ketone bodies as suggested by the results of the proteomic profiling. ^{13}C-NMR studies were performed to measure the relative contribution of fatty acids and ketone bodies tricarboxylic acid (TCA) cycle flux. For these studies, hearts isolated from CH or sham-operated control groups were perfused in the Langendorff mode with ^{13}C-labeled palmitate in the presence of unlabeled R-β-hydroxybutyrate (R-βOHB), or ^{13}C-labeled R-βOHB in the presence of unlabeled palmitate. Consistent with findings described in

numerous published studies (15,16,18,31,41,43,44), the contribution of ^{13}C-labeled palmitate to oxidative intermediary metabolism was decreased by approximately 40% in the CH hearts (Figure 1 in the Data Supplement).

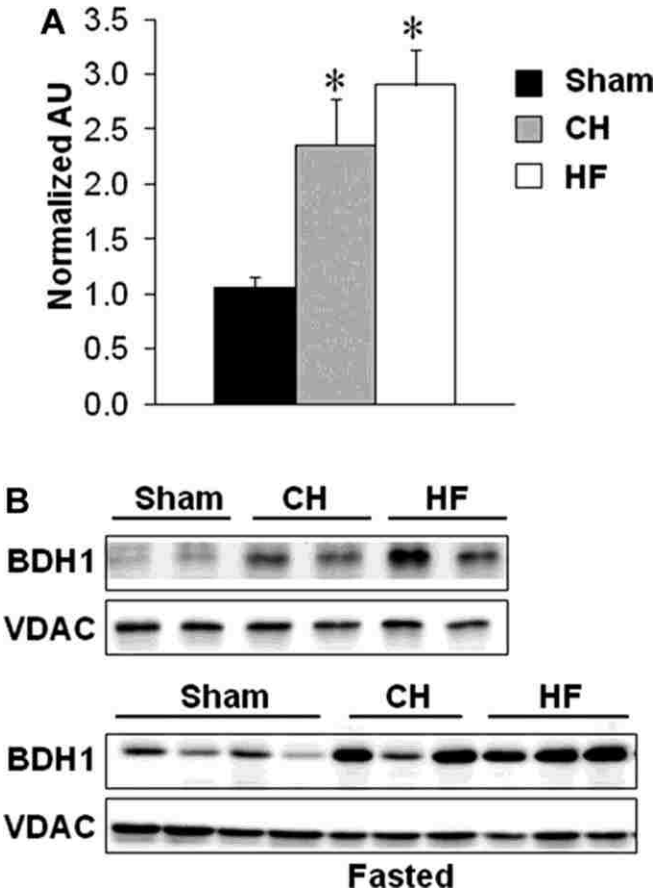

Figure 8. *Bdh1* expression is induced in the hypertrophied and failing mouse heart.

(A) *Bdh1* mRNA levels in cardiac ventricular tissue from mice 4 weeks after sham, TAC (CH), or TAC/MI (HF) surgeries. Expression is normalized to *Rplp0* (36B4). Bars represent mean±SEM values (n=9–11 per group). *P<0.05. **(B)** Representative immunoblot analyses performed using protein extracts prepared from mouse cardiac ventricular tissue homogenates 4 weeks postsham, post-CH, or post-HF surgeries collected in the fed state (4 hours after feeding) or following a 24-hour fast. Antibodies used are shown on the left. Anti-VDAC was used as a mitochondrial protein-loading control. AU indicates arbitrary unit; BDH1, β-hydroxybutyrate dehydrogenase 1; CH, compensated hypertrophy; HF, heart failure; MI, myocardial infarction; SEM, standard error of the mean; TAC, transverse aortic constriction; and VDAC, voltage-dependent anion channel.

Conversely, the contribution of βOHB to carbon entry into the oxidative pathway of the TCA cycle increased significantly in hearts from CH mice compared to control mice (Figure 9, left). These data indicate a 25% increase in the contribution of βOHB to oxidative production of ATP from carbon flux through the TCA cycle. In addition, the entry of anaplerotic carbon flux into the TCA cycle was increased in the CH heart, consistent with previous reports (31,43,45) (Figure 9, right).

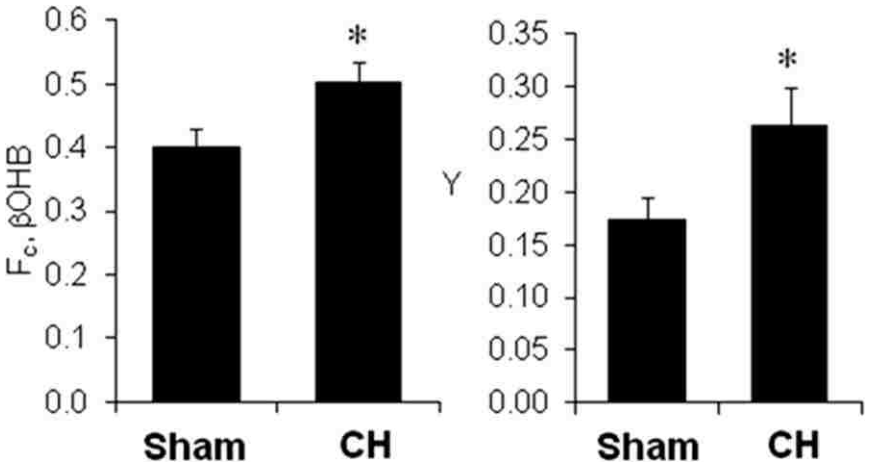

Figure 9. Increased βOHB oxidation in the hypertrophied heart.

Left, The fraction of ^{13}C-enriched acetyl-CoA entering the TCA cycle from ^{13}C-labeled βOHB (Fc, βOHB) is shown. **Right**, The fraction of carbon entering the TCA cycle via anaplerosis relative to that entering via citrate synthase (Y) is shown for CH and sham-operated controls. Data are shown as mean±SEM (n=10, sham; and n=11, CH). *P<0.05. CH indicates compensated hypertrophy; CoA, coenzyme A; βOHB, β-hydroxybutyrate; SEM, standard error of the mean; and TCA, tricarboxylic acid.

Identification of Metabolite Signatures of Ketone Utilization in the Myocardium of the Failing Heart

We next sought to determine whether cardiac ketone utilization was increased in vivo in the failing heart. To this end, we measured myocardial levels of metabolites that reflect ketone body oxidation. Targeted quantitative metabolomic datasets generated previously from heart samples of the CH and HF groups and corresponding controls

(25) were analyzed for changes in metabolites that can be produced during ketone body metabolism including hydroxybutyrylcarnitine (C4OH-carnitine), acetylcarnitine (C2-carnitine), and succinate (Figure 10A). Levels of C4OH-carnitine and C2-carnitine have been shown to rise in the context of increased ketone body utilization in human and mouse skeletal muscle, and in human subcutaneous interstitial fluid (46–48)

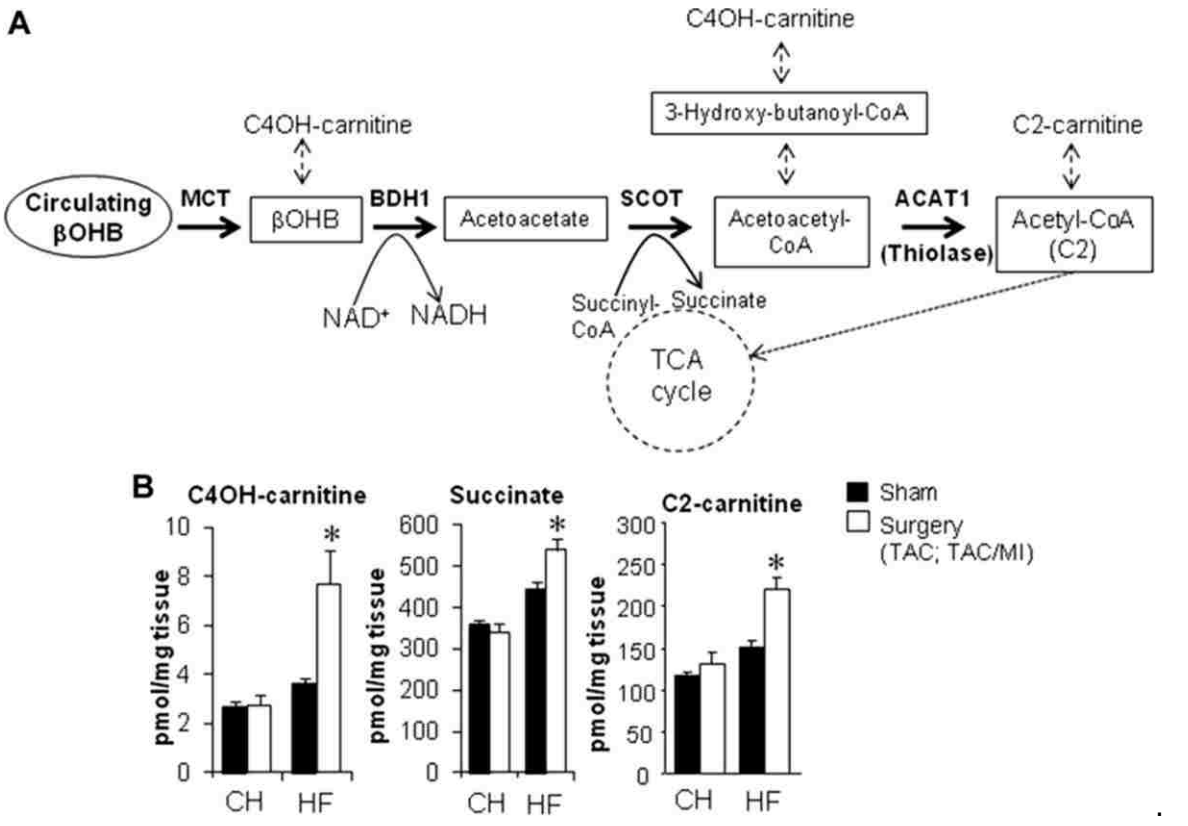

Figure 10. The myocardial metabolite profile of the failing heart is indicative of increased ketone utilization in the failing heart.

(A) Schematic of the ketone metabolism pathway indicating relevant intermediary metabolite derivatives (dashed arrows). **(B)** Levels of ketone utilization pathway metabolite derivatives (C4OH-carnitine, succinate, C2-carnitine) in cardiac biventricular tissue from CH or HF mice and corresponding sham-operated controls 4 weeks postsurgery as measured previously by using mass spectrometry–based quantitative metabolomics (25). Data are shown as mean±SEM (n=6 per group). *P<0.05. ACAT1 indicates acetyl-CoA acetyltransferase 1; BDH1, β-hydroxybutyrate dehydrogenase 1; C2-carnitine, acetylcarnitine; C4OH-carnitine, hydroxybutyrylcarnitine; CH, compensated hypertrophy; CoA, coenzyme A; HF, heart failure; MCT, monocarboxylate transporters; MI, myocardial infarction; βOHB, β-hydroxybutyrate; SCOT, succinyl-CoA:3-oxoacid-CoA transferase; SEM, standard error of the mean; TAC, transverse aortic constriction; and TCA, tricarboxylic acid

Concentrations of C4OH-carnitine, C2-carnitine, and succinate were increased in hearts of the HF group, but not the CH samples, compared to corresponding controls (Figure 10B), consistent with increased flux through the reaction catalyzed by BDH1The relevance of the distinct HF metabolite signatures to myocardial ketone body metabolism was further assessed by comparison with profiles obtained from hearts of wild-type C57BL/6J mice fed a ketogenic diet for 4 weeks to increase myocardial ketone body delivery and utilization (29,49–51). As expected, the ketogenic diet resulted in a dramatic increase in concentration of plasma ketone bodies compared to controls fed a standard chow (Figure 2 in the Data Supplement). Notably, this dietary intervention had no effect on ventricular function in this timeframe (echocardiographic data not shown). Importantly, the pattern of myocardial metabolite alterations observed in the mice fed a ketogenic diet was strikingly similar to that observed for the HF mice on a standard chow diet, including elevated amounts of both the R and S enantiomers of C4OH-carnitine (Figure 11A). An increase in both C4OH-carnitine enantiomers is consistent with an increase in uptake and oxidation of ketone bodies. In addition, rat ventricular myocytes cultured in fatty-acid free, ketone body-rich media also showed an elevated content of C4OH-carnitine compared to cells in control (ketone body-free) media (Figure 11B). Notably, the amount of Coenzyme A (CoASH) was not different between HF and control groups (data not shown).

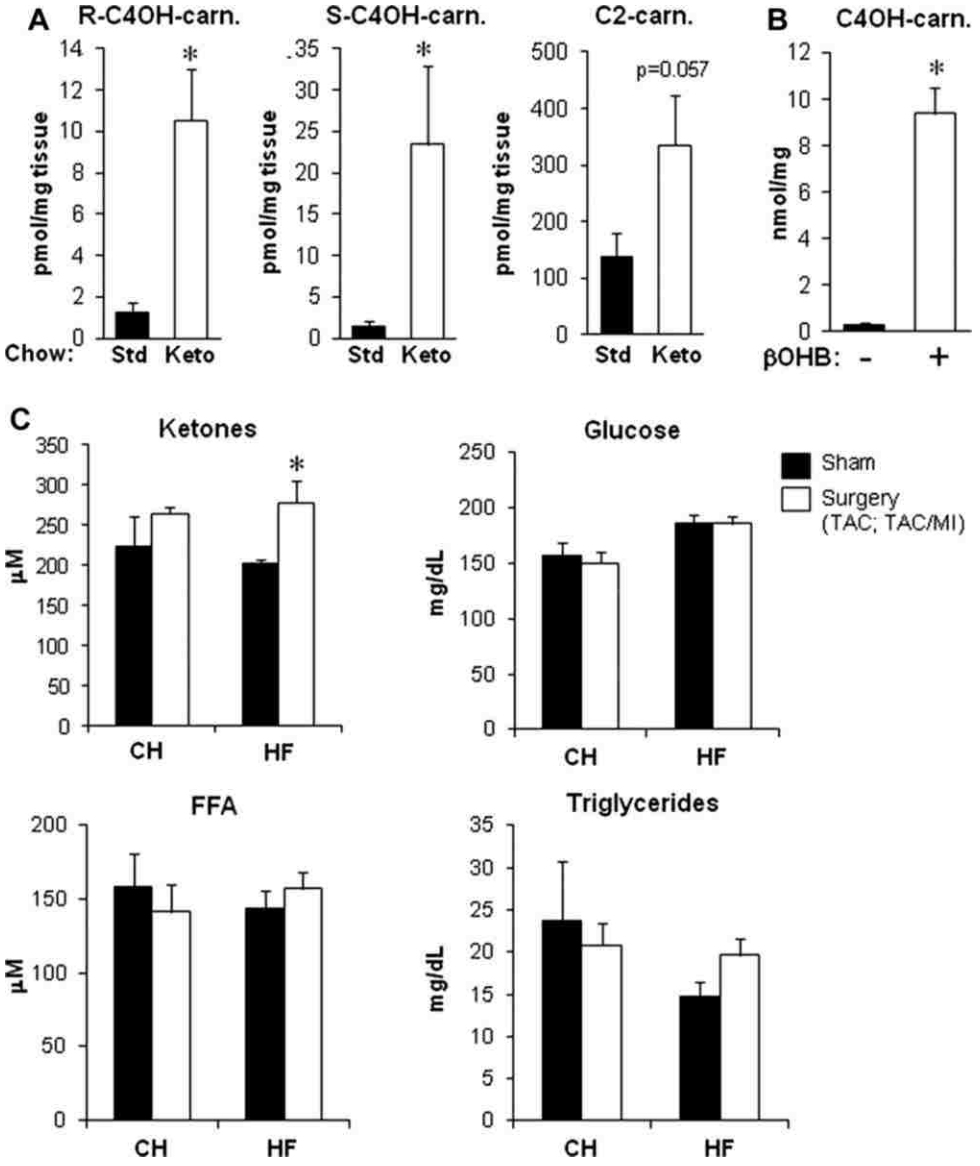

Figure 11. Myocardial metabolite profile on a ketogenic diet is similar to that observed for the HF mice on a standard chow diet.

A, Levels of R-C4OH-carnitine, S-C4OH-carnitine, and C2-carnitine in cardiac ventricular tissue from wild-type C57BL/6J mice fed a ketogenic (Keto) diet or standard (Std) chow diet for 4 weeks (n=5 per group). Values were determined by using mass spectrometry. *P<0.05. B, Total C4OH-carnitine levels in extracts prepared from neonatal rat ventricular myocytes (NRVMs) cultured in media ± 8 mmol/L ketone, R-βOHB, in the presence of 1g/L glucose and 1 mmol/L carnitine, for 24 hours (n=3 per group, *P<0.05 by the Student t test). C, Total plasma ketones (acetoacetate+βOHB), glucose, free fatty acids (FFA), and triglycerides in CH, HF, and sham-operated control mice in the fed state (after a 4-hour morning fast; n=5–11 per group). Bars represent mean±SEM for all panels.*P<0.05. C2-carnitine indicates acetylcarnitine; CH, compensated hypertrophy; C4OH-carnitine, hydroxybutyrylcarnitine; HF, heart failure; MI, myocardial infarction; βOHB, β-hydroxybutyrate; SEM, standard error of the mean; and TAC, transverse aortic constriction.

Lastly, to assess ketone delivery to the heart in the CH and HF groups, plasma substrate concentrations were measured. Plasma ketone body levels were modestly but significantly increased in HF but not CH, compared to corresponding controls (Figure 11C). Plasma glucose, free fatty acid levels, and triglycerides were unchanged in CH or HF groups (Figure 11C). The expression of the genes encoding the putative cellular ketone body transporters [*Slc16a1* (MCT1) and *Slc16a7* (MCT2)] were also assessed as an indirect measure of transport capacity given that Bdh1 expression was increased in CH and HF. Analysis of our published gene expression profiles (25) did not reveal any differences in CH or HF compared with control myocardium following a 4h fast. However, after a 24h fast, when circulating ketone bodies are increased, we found that *Slc16a7* mRNA levels were significantly increased in both CH and HF samples, compared to corresponding sham-operated controls (Figure 3 in the Data Supplement). Taken together, these results provide evidence that myocardial ketone body utilization is increased in the HF mice through several potential mechanisms including increased delivery of ketone bodies and gene regulatory re-programming of ketone uptake and oxidation.

Discussion

The results of this study yielded several new findings including: 1) the amounts of relatively few mitochondrial proteins involved in energy transduction and ATP production are regulated in the early stages of cardiac hypertrophy (CH) and heart failure (HF) in the mouse models studied here. Within the subset of regulated proteins in

the CH and HF samples, a significant number were involved in fatty acid utilization, providing proteomic confirmation that the failing heart has reduced capacity for oxidizing fatty acids as a fuel; 2) the hypertrophied and failing rodent heart oxidizes ketone bodies as an alternate fuel for oxidative ATP production; and 3) metabolite signatures of myocardial ketone oxidation have been identified and suggest that a subset of mitochondrial ketone oxidation intermediate pools accumulate in the failing heart.

Our data support the conclusion that the shift to ketone oxidation in the failing heart occurs through several complementary mechanisms. First, ketone bodies are competitive with other substrates for heart, particularly fatty acids. The observed shift to ketone body oxidation in the hypertrophied and failing heart occurs in the context of reduced oxidation of fatty acids, the chief substrate for the normal adult heart. Downregulation of FAO gene expression is a well-characterized response in the hypertrophied and failing heart, driven at least in part, by reduced PPARα-mediated transcriptional control of genes involved in fatty acid utilization (20,52–54). Second, the delivery of ketone bodies is increased in the failing heart (increased plasma concentration). Indeed, previous studies have shown that the mammalian heart is capable of avid ketone body uptake and oxidation (55–57). We also cannot rule out the possibility that ketone body synthesis is activated in the cardiac myocyte although our gene expression data do not support this notion. Third, our results indicate that the hypertrophied and failing heart undergo gene regulatory re-programming to increase capacity for uptake and oxidation of ketone bodies. Specifically, the expression of Bdh1 and the transporter *Slc16a1* were increased in CH and HF.

Our work has identified metabolite signatures of myocardial ketone utilization in the failing and normal heart (C4OH-carnitine and C2-carnitine). The metabolites were selected based on known derivatives of ketone utilization pathway intermediates (Figure 10A), and published work by others focused on tissues known to oxidize ketones (46–48). It should be noted that this set of metabolites are not unique to ketone utilization pathways, given that other metabolic pathways can generate the intermediates. However, our results demonstrate that this metabolite profile is elevated in both HF samples and normal mice fed a ketogenic diet, providing additional support for our conclusion. In addition, we found that C4OH content is increased in rat neonatal cardiac myocytes exposed to βOHB. Interestingly, the increase in C4OH-carnitine and C2-carnitine was observed in HF but not CH samples. The reason for this latter specificity is unknown, but could reflect higher ketone oxidation rates related to increased ketone body delivery (elevated plasma levels) in HF. Alternatively, capacity for flux through downstream pathways such as the TCA cycle, ETC, and OXPHOS may become reduced with progression to HF creating a mismatch with high flux rates through the ketone oxidation pathway. This latter conclusion is supported by our observation that most TCA cycle organic acid intermediates (with the exception of succinate) are reduced in HF samples, (25) consistent with a “bottleneck” downstream of ketone and other fuel inputs to the TCA cycle. It will be of significant interest to explore this metabolomic signature in other experimental heart failure models, and in humans, to determine whether activation of ketone utilization is a broad paradigm relevant to energy metabolic reprogramming of the failing heart.

We speculate that the shift toward ketone body utilization in the hypertrophied heart is an early adaptive response to maintain adequate fuel supplies for oxidative ATP production in the context of reduced FAO. Consistent with this notion, a recent study demonstrated that targeted disruption of succinyl-CoA:3-oxoacid-CoA transferase (SCOT), a key enzyme in the ketone body metabolic pathway, resulted in a heart failure phenotype in mice in the context of pressure overload (30). However, it is possible that over the longer term, high rates of ketone utilization lead to maladaptive consequences. Others have shown that ketone oxidation may lead to reduced anaplerotic input in an isolated heart preparation (58). In addition, as noted above, the pools of several metabolite intermediates including succinate and C2-carnitine are expanded in the myocardial samples from the HF group. Increased availability of short-chain carbon moieties and succinate could set the stage for post-translational modifications of mitochondrial enzymes and proteins reducing oxidative flux or ATP generation.

The findings described herein raise the obvious question of relevance to human heart failure. Little is known about ketone body metabolism in the failing human heart, although studies have shown increased concentrations of ketone metabolites in urine and breath samples of patients with heart failure (59–62). In addition, increased concentrations of serum βOHB have been described in patients with severe heart failure (63).

Conclusions

In summary, our findings indicate that during the development of pathologic cardiac remodeling in mouse models of heart failure, the myocardium increasingly relies on ketone bodies as a fuel. We propose that this fuel metabolic shift is triggered by reduced capacity for oxidizing fatty acids, the chief fuel for the normal adult mammalian heart. Future studies aimed at determining the relevance of these findings to human heart failure, and delineation of the impact of chronic ketone utilization on cardiac metabolism and function will be important to determine whether this response represents a new therapeutic target for the metabolic modulation of heart failure.

Clinical Perspective

Significant evidence, based on results of pre-clinical studies and observations in humans, indicates that energy metabolic derangements contribute to the development of heart failure. A prototypical fuel shift occurs in the hypertrophied and failing heart, in which the capacity for oxidizing fatty acids, the chief substrate for the normal adult heart, becomes reduced along with an increase in reliance on glucose. It is generally believed that reduced capacity for oxidation of fatty acids leads to an “energy-starved” heart. Therefore, identification of alternate fuel utilization pathways that may compensate for this fuel shift could lead to new therapeutic strategies aimed at heart failure. In this study, using well-defined mouse models of cardiac hypertrophy and heart failure, we demonstrate that the heart begins to utilize ketone bodies en route to the development of heart failure. This shift to reliance on ketone bodies as a fuel is likely

driven by multiple mechanisms, including elevation in plasma ketones, a reduction in competition with fatty acids, and gene regulatory re-programming of the heart. These findings set the stage for future studies aimed at determining whether the shift to oxidizing ketone bodies in the failing heart is adaptive or maladaptive. This fuel utilization pathway could prove to be a new candidate target for metabolic modulatory therapies aimed at early stages of heart failure.

Acknowledgments

We wish to thank Lorenzo Thomas for assistance with preparation of the manuscript and acknowledge the following Core Facilities at Sanford Burnham Prebys Medical Discovery Institute at Lake Nona: Cardiometabolic Phenotyping and Metabolomics. We wish to thank Olga Ilkayeva and the Duke University School of Medicine's Proteomics and Metabolomics Shared Resource for metabolomics data; and Lauren Ashley Gabriel and Caron Stonebrook for assistance with the animal studies.

Funding Sources: This work was supported by NIH grants R01 HL058493 (D.P.K.), R01 HL101189 (D.P.K. and D.M.M.), R01 DK091538 (P.A.C.), R01 HL062702 (E.D.L.) and R01HL49244 (E.D.L.). G.A was supported by the Swiss National Science Foundation.

References

1. Bing RJ. The metabolism of the heart. Harvey Lect. 1954;50:27–70.

2. Bing RJ, Siegel A, Ungar I, Gilbert M. Metabolism of the human heart. II. Studies on fat ketone and amino acid metabolism. Am J Med. 1954;16:504–515.

3. Wisneski JA, Gertz EW, Neese RA, Mayr M. Myocardial metabolism of free fatty acids. Studies with 14C-labeled substrates in humans. J Clin Invest. 1987;79:359–366.]

4. Lopaschuk GD, Belke DD, Gamble J, Itoi T, Schonekess BO. Regulation of fatty acid oxidation in the mammalian heart in health and disease. Biochim Biophys Acta. 1994;1213:263–276.

5. van der Vusse GJ, van Bilsen M, Glatz JF. Cardiac fatty acid uptake and transport in health and disease. Cardiovasc Res. 2000;45:279–293.

6. Ingwall JS, Kramer MF, Fifer MA, Lorell BH, Shemin R, Grossman W, Allen PD. The creatine kinase system in normal and diseased human myocardium. N Engl J Med. 1985;313:1050–1054.

7. de Roos A, Doornbos J, Luyten PR, Oosterwaal LJ, van der Wall EE, den Hollander JA. Cardiac metabolism in patients with dilated and hypertrophic cardiomyopathy: assessment with proton-decoupled P-31 MR spectroscopy. J Magn Reson Imaging. 1992;2:711–719.

8. Tian R, Nascimben L, Kaddurah-Daouk R, Ingwall JS. Depletion of energy reserve via the creatine kinase reaction during the evolution of heart failure in cardiomyopathic hamsters. J Mol Cell Card. 1996;28:755–765.

9. Ingwall JS, Weiss RG. Is the failing heart energy starved? On using chemical energy to support cardiac function. Circ Res. 2004;95:135–145.

10. Carley AN, Taegtmeyer H, Lewandowski ED. Matrix revisited: mechanisms linking energy substrate metabolism to the function of the heart. Circ Res. 2014;114:717–729.

11. Neubauer S, Horn M, Cramer M, Harre K, Newell JB, Peters W, Pabst T, Ertl G, Hahn D, Ingwall JS, Kochsiek K. Myocardial phosphocreatine-to-ATP ratio is a predictor of mortality in patients with dilated cardiomyopathy. Circulation. 1997;96:2190–2196.

12. Neubauer S. The failing heart--an engine out of fuel. N Engl J Med. 2007;356:1140–1151.

13. Bishop SP, Altschuld RA. Increased glycolytic metabolism in cardiac hypertrophy and congestive failure. Am J Physiol. 1970;218:153–159.

14. Taegtmeyer H, Overturf ML. Effects of moderate hypertension on cardiac function and metabolism in the rabbit. Hypertension. 1988;11:416–426.

15. Allard MF, Schonekess BO, Henning SL, English DR, Lopaschuk GD. Contribution of oxidative metabolism and glycolysis to ATP production in hypertrophied hearts. Am J Physiol. 1994;267:H742–H750.

16. Christe ME, Rodgers RL. Altered glucose and fatty acid oxidation in hearts of the spontaneously hypertensive rat. J Mol Cell Cardiol. 1994;26:1371–1375.

17. Paolisso G, Gambardella A, Galzerano D, D'Amore A, Rubino P, Verza M, Teasuro P, Varricchio M, D'Onofrio F. Total-body and myocardial substrate oxidation in congestive heart failure. Metabolism. 1994;43:174–179.

18. Sambandam N, Lopaschuk GD, Brownsey RW, Allard MF. Energy metabolism in the hypertrophied heart. Heart Fail Rev. 2002;7:161–173.

19. Chandler MP, Kerner J, Huang H, Vazquez E, Reszko A, Martini WZ, Hoppel CL, Imai M, Rastogi S, Sabbah HN, Stanley WC. Moderate severity heart failure does not involve a downregulation of myocardial fatty acid oxidation. Am J Physiol Heart Circ Physiol. 2004;287:H1538–H1543.

20. Sack MN, Rader TA, Park S, Bastin J, McCune SA, Kelly DP. Fatty acid oxidation enzyme gene expression is downregulated in the failing heart. Circulation. 1996;94:2837–2842.

21. Wallhaus TR, Taylor M, DeGrado TR, Russell DC, Stanko P, Nickles RJ, Stone CK. Myocardial free fatty acid and glucose use after carvedilol treatment in patients with congestive heart failure. Circulation. 2001;103:2441–2446.

22. Davila-Roman VG, Vedala G, Herrero P, de las Fuentes L, Rogers JG, Kelly DP, Gropler RJ. Altered myocardial fatty acid and glucose metabolism in idiopathic dilated cardiomyopathy. J Am Coll Cardiol. 2002;40:271–277.

23. de las Fuentes L, Herrero P, Peterson LR, Kelly DP, Gropler RJ, Davila-Roman VG. Myocardial fatty acid metabolism: independent predictor of left ventricular mass in hypertensive heart disease. Hypertension. 2003;41:83–87.

24. Huss JM, Imahashi K, Dufour CR, Weinheimer CJ, Courtois M, Kovacs A, Giguere V, Murphy E, Kelly DP. The nuclear receptor ERRalpha is required for the bioenergetic and functional adaptation to cardiac pressure overload. Cell Metab. 2007;6:25–37.]

25. Lai L, Leone TC, Keller MP, Martin OJ, Broman AT, Nigro J, Kapoor K, Koves TR, Stevens R, Ilkayeva OR, Vega RB, Attie AD, Muoio DM, Kelly DP. Energy metabolic reprogramming in the hypertrophied and early stage failing heart: a multisystems approach. Circ Heart Fail. 2014;7:1022–1031.

26. Weinheimer CJ, Lai L, Kelly DP, Kovacs A. Novel mouse model of left ventricular pressure overload and infarction causing predictable ventricular remodelling and progression to heart failure. Clin Exp Pharmacol Physiol. 2015;42:33–40.

27. Pagliarini DJ, Calvo SE, Chang B, Sheth SA, Vafai SB, Ong SE, Walford GA, Sugiana C, Boneh A, Chen WK, Hill DE, Vidal M, Evans JG, Thorburn DR, Carr SA, Mootha VK. A mitochondrial protein compendium elucidates complex I disease biology. Cell. 2008;134:112–123.

28. Kruger M, Moser M, Ussar S, Thievessen I, Luber CA, Forner F, Schmidt S, Zanivan S, Fassler R, Mann M. SILAC mouse for quantitative proteomics uncovers kindlin-3 as an essential factor for red blood cell function. Cell. 2008;134:353–364.

29. Wentz AE, d'Avignon DA, Weber ML, Cotter DG, Doherty JM, Kerns R, Nagarajan R, Reddy N, Sambandam N, Crawford PA. Adaptation of myocardial substrate metabolism to a ketogenic nutrient environment. J Biol Chem. 2010;285:24447–24456.

30. Schugar RC, Moll AR, Andre d'Avignon D, Weinheimer CJ, Kovacs A, Crawford PA. Cardiomyocyte-specific deficiency of ketone body metabolism promotes accelerated pathological remodeling. Mol Metab. 2014;3:754–769.

31. Pound KM, Sorokina N, Ballal K, Berkich DA, Fasano M, Lanoue KF, Taegtmeyer H, O'Donnell JM, Lewandowski ED. Substrate-enzyme competition attenuates upregulated anaplerotic flux through malic enzyme in hypertrophied rat heart and restores triacylglyceride content: attenuating upregulated anaplerosis in hypertrophy. Circ Res. 2009;104:805–812.

32. Huss JM, Kelly DP. Nuclear receptor signaling and cardiac energetics. Circ Res. 2004;95:568–578.

33. Cresci S, Wright LD, Spratt JA, Briggs FN, Kelly DP. Activation of a novel metabolic gene regulatory pathway by chronic stimulation of skeletal muscle. Am J Physiol. 1996;270:C1413–C1420.

34. Minkler PE, Stoll MS, Ingalls ST, Kerner J, Hoppel CL. Validated Method for the Quantification of Free and Total Carnitine, Butyrobetaine, and Acylcarnitines in Biological Samples. Anal Chem. 2015;87:8994–9001.

35. Konzer A, Ruhs A, Braun T, Kruger M. Global protein quantification of mouse heart tissue based on the SILAC mouse. Methods Mol Biol. 2013;1005:39–52.

36. Gao Z, Xu H, DiSilvestre D, Halperin VL, Tunin R, Tian Y, Yu W, Winslow RL, Tomaselli GF. Transcriptomic profiling of the canine tachycardia-induced heart failure model: global comparison to human and murine heart failure. J Mol Cell Cardiol. 2006;40:76–86.

37. Bugger H, Schwarzer M, Chen D, Schrepper A, Amorim PA, Schoepe M, Nguyen TD, Mohr FW, Khalimonchuk O, Weimer BC, Doenst T. Proteomic remodelling of mitochondrial oxidative pathways in pressure overload-induced heart failure. Cardiovasc Res. 2010;85:376–384.

38. Barth AS, Kumordzie A, Frangakis C, Margulies KB, Cappola TP, Tomaselli GF. Reciprocal transcriptional regulation of metabolic and signaling pathways correlates with disease severity in heart failure. Circ Cardiovasc Genet. 2011;4:475–483.

39. Xu J, Nie HG, Zhang XD, Tian Y, Yu B. Down-regulated energy metabolism genes associated with mitochondria oxidative phosphorylation and fatty acid metabolism in viral cardiomyopathy mouse heart. Mol Biol Rep. 2011;38:4007–4013.

40. Taegtmeyer H, Golfman L, Sharma S, Razeghi P, van Arsdall M. Linking gene expression to function: metabolic flexibility in the normal and diseased heart. Ann N Y Acad Sci. 2004;1015:202–213.

41. Akki A, Smith K, Seymour AM. Compensated cardiac hypertrophy is characterised by a decline in palmitate oxidation. Mol Cell Biochem. 2008;311:215–224.

42. Ardehali H, Sabbah HN, Burke MA, Sarma S, Liu PP, Cleland JG, Maggioni A, Fonarow GC, Abel ED, Campia U, Gheorghiade M. Targeting myocardial substrate metabolism in heart failure: potential for new therapies. Eur J Heart Fail. 2012;14:120–129.

43. Kolwicz SC, Jr, Olson DP, Marney LC, Garcia-Menendez L, Synovec RE, Tian R. Cardiac-specific deletion of acetyl CoA carboxylase 2 prevents metabolic remodeling during pressure-overload hypertrophy. Circ Res. 2012;111:728–738.

44. Lewandowski ED, Fischer SK, Fasano M, Banke NH, Walker LA, Huqi A, Wang X, Lopaschuk GD, O'Donnell JM. Acute liver carnitine palmitoyltransferase I overexpression recapitulates reduced palmitate oxidation of cardiac hypertrophy. Circ Res. 2013;112:57–65.

45. Sorokina N, O'Donnell JM, McKinney RD, Pound KM, Woldegiorgis G, LaNoue KF, Ballal K, Taegtmeyer H, Buttrick PM, Lewandowski ED. Recruitment of compensatory pathways to sustain oxidative flux with reduced carnitine palmitoyltransferase I activity characterizes inefficiency in energy metabolism in hypertrophied hearts. Circulation. 2007;115:2033–2041.

46. Hack A, Busch V, Pascher B, Busch R, Bieger I, Gempel K, Baumeister FA. Monitoring of ketogenic diet for carnitine metabolites by subcutaneous microdialysis. Pediatr Res. 2006;60:93–96.

47. Soeters MR, Serlie MJ, Sauerwein HP, Duran M, Ruiter JP, Kulik W, Ackermans MT, Minkler PE, Hoppel CL, Wanders RJ, Houten SM. Characterization of D-3-hydroxybutyrylcarnitine (ketocarnitine): an identified ketosis-induced metabolite. Metabolism. 2012;61:966–973.

48. DeBalsi KL, Wong KE, Koves TR, Slentz DH, Seiler SE, Wittmann AH, Ilkayeva OR, Stevens RD, Perry CG, Lark DS, Hui ST, Szweda L, Neufer PD, Muoio DM. Targeted metabolomics connects thioredoxin-interacting protein (TXNIP) to mitochondrial fuel selection and regulation of specific oxidoreductase enzymes in skeletal muscle. J Biol Chem. 2014;289:8106–8120.

49. Hasselbaink DM, Glatz JF, Luiken JJ, Roemen TH, Van der Vusse GJ. Ketone bodies disturb fatty acid handling in isolated cardiomyocytes derived from control and diabetic rats. Biochem J. 2003;371:753–760.

50. Stanley WC, Meadows SR, Kivilo KM, Roth BA, Lopaschuk GD. beta-Hydroxybutyrate inhibits myocardial fatty acid oxidation in vivo independent of changes in malonyl-CoA content. Am J Physiol Heart Circ Physiol. 2003;285:H1626–H1631.

51. Veech RL. The therapeutic implications of ketone bodies: the effects of ketone bodies in pathological conditions: ketosis, ketogenic diet, redox states, insulin resistance, and mitochondrial metabolism. Prostaglandins Leukot Essent Fatty Acids. 2004;70:309–319.

52. Tian Q, Barger PM. Deranged energy substrate metabolism in the failing heart. Curr Hypertens Rep. 2006;8:465–471.

53. Barger PM, Brandt JM, Leone TC, Weinheimer CJ, Kelly DP. Deactivation of peroxisome proliferator-activated receptor-alpha during cardiac hypertrophic growth. J Clin Invest. 2000;105:1723–1730.

54. Lahey R, Wang X, Carley AN, Lewandowski ED. Dietary fat supply to failing hearts determines dynamic lipid signaling for nuclear receptor activation and oxidation of stored triglyceride. Circulation. 2014;130:1790–1799.

55. Rudolph W, Maas D, Richter J, Hasinger F, Hofmann H, Dohrn P. [on the Significance of Acetoacetate and Beta-Hydroxybutyrate in Human Myocardial Metabolism] Klin Wochenschr. 1965;43:445–451.

56. Jeffrey FM, Diczku V, Sherry AD, Malloy CR. Substrate selection in the isolated working rat heart: effects of reperfusion, afterload, and concentration. Basic Res Cardiol. 1995;90:388–396.

57. Bartelds B, van der Leij FR, Kuipers JR. Role of ketone bodies in perinatal myocardial energy metabolism. Biochem Soc Trans. 2001;29:325–330.

58. Russell RR, 3rd, Taegtmeyer H. Changes in citric acid cycle flux and anaplerosis antedate the functional decline in isolated rat hearts utilizing acetoacetate. J Clin Invest. 1991;87:384–390.

59. Kupari M, Lommi J, Ventila M, Karjalainen U. Breath acetone in congestive heart failure. Am J Cardiol. 1995;76:1076–1078.

60. Chung JH, Kim JS, Kim OY, Kang SM, Hwang GS, Shin MJ. Urinary ketone is associated with the heart failure severity. Clin Biochem. 2012;45:1697–1699.

61. Marcondes-Braga FG, Gutz IG, Batista GL, Saldiva PH, Ayub-Ferreira SM, Issa VS, Mangini S, Bocchi EA, Bacal F. Exhaled acetone as a new biomaker of heart failure severity. Chest. 2012;142:457–466.

62. Samara MA, Tang WH, Cikach F, Jr, Gul Z, Tranchito L, Paschke KM, Viterna J, Wu Y, Laskowski D, Dweik RA. Single exhaled breath metabolomic analysis identifies unique breathprint in patients with acute decompensated heart failure. J Am Coll Cardiol. 2013;61:1463–1464.

63. Lommi J, Kupari M, Koskinen P, Naveri H, Leinonen H, Pulkki K, Harkonen M. Blood ketone bodies in congestive heart failure. J Am Coll Cardiol. 1996;28:665–672.

Data Supplement

Supplemental Methods

RNA analyses Total RNA was isolated and reverse transcribed with AffinityScript QPCR cDNA Synthesis Kit (Agilent Technologies). PCR reactions were performed in triplicate in a 96-well format using the MX3005P (Stratagene). The primer sets (SYBR green) used to detect specific gene expression are as follows: mBDH1 fwd-TCTCGGACTGCCTGCGCTAT, revACCGCTGTTGCAGTAGGTTT; m36B4 fwd-TGGAAGTCCAACTACTTCCTCAA m36B4 rev-ATCTGCTGCATCTGCTTGGAG; mMCT1 fwdTGCAACGACCAGTGAAGTATC, rev-GACAACCACCAGCGATCATTA;

mMCT2 fwdATACTTGCAGGTCCTCTCATTC, rev-GGAAGAGGCAGACAACGATAA. 36B4 primer set was included in a separate well (in triplicate) and used to normalize the gene expression data. Proteomics using Stable Isotope Labeling by Amino Acids (SILAC) Crude mitochondrial fractions were prepared from cardiac tissue of Lys6 (13C6-Lysine, Silantes) labeled (heavy) and non-labeled (light) mice. Mitochondrial fractions were prepared as previously described (1) Briefly, immediately following euthanasia, the mouse ventricles were dissected, washed and placed in ice-cold isolation buffer (220 mM mannitol, 70 mM sucrose, 5mM HEPES-KOH, pH 7.4, 1mM EGTA, 1mg/ml BSA and protease inhibitor cocktail). The tissue was then minced and homogenized using a Potter-Elvehjem glass/Teflon homogenizer. A crude mitochondrial fraction was extracted from the homogenate using differential centrifugation and resuspended in small amount of the isolation buffer (300 µl). A 1:1 mixture of heavy and light heart mitochondrial fractions were then separated by gel electrophoresis on precast 4–12% NuPAGE gradient gels (Invitrogen) and stained with the 1 Colloidal Blue Staining Kit (Invitrogen). Evenly sized gel pieces were excised and processed for mass spectrometry. The gel pieces were subjected to in-gel reduction and alkylation, followed by LysC (Wako) digestion as described previously (2) In brief, trypsin digested gel pieces were washed twice with 50% 50 mM NH4HCO3 eluent additive for LC-MS (Sigma-Aldrich) / 50% ethanol for 20 min, and dehydrated with 100% ethanol for 10 min, and then vacuum centrifuged. Gel pieces were reduced with 10 mM DTT for 45 min at 56°C and alkylated with 55 mM iodoacetamide for 30 min at RT in the dark. After two cycles of washing and dehydration, samples were dehydrated twice with 100% ethanol

for 15 min and vacuum centrifuged. Gel pieces were digested overnight at 37°C in 50 µl of digestion buffer containing 12.5 ng/µl of LysC (Wako). Released peptides were extracted once with 30% acetonitrile/ 3% trifluoracetic acid (TFA), twice with 70% acetonitrile, followed by two final extractions with 100% acetonitrile. Extracts were vacuum centrifuged to remove acetonitrile and subsequently acidified with 0.5% TFA. Peptides were desalted and concentrated with homemade "STAGE" tips (Stop and Go extraction tips) filled with C-18 (C18 Empore Disks, 3M) as described.(3) Mass spectrometric experiments were performed on a nano-flow HPLC system (Agilent) connected to a LTQ-Orbitrap XL instrument (Thermo Scientific) equipped with a nanoelectrospray source (Proxeon). The mass spectrometer was operated in the data dependent mode to monitor MS and MS/MS spectra. Survey full-scan MS spectra (from m/z 300–2000) were acquired in the Orbitrap with a resolution of R=60,000 at m/z 400 after accumulation of 1,000,000 ions. The five most intense ions from the preview survey scan delivered by the Orbitrap were sequenced by collision-induced dissociation (CID) in the LTQ. Mass spectra were analyzed using MaxQuant software (Version 1.0.14.10)(4) and all tandem mass spectra were 2 searched against the mouse International Protein Index protein sequence database (IPI version 3.54) and concatenated with reversed copies of all sequences. The required false positive rate was set to 1% at the protein and peptide level. Maximum allowed mass deviation was set to 7 ppm in MS mode and 0.5 Da for MS/MS peaks. The parameter settings were: LysC as digesting enzyme, a maximum of two missed cleavages, a minimum of six amino acids, carbamidomethylation at cysteine residues as fixed and oxidation at

methionine residues as variable modifications. Metabolomic analysis of organic acids and acylcarnitines Immediately following deep anesthesia by intraperitoneal injection of pentobarbital (100 mg/kg body weight), bi-ventricle was excised and frozen. Specimens of powdered bi-ventricle tissue were diluted 20-fold (mass:volume) in 50% acetonitrile supplemented with 0.3% formate (acylcarnitines, amino acids, and organic acids). Samples were homogenized in a TissueLyser II (Qiagen). Tissue extracts were derivatized and analyzed as previously described.(5) Levels of succinate, C4OH-carnitine, and C2-carnitine were determined using stable isotope dilution techniques. The data were acquired using a Waters AcquityTM UPLC system equipped with a TQ (triple quadrupole) detector and a data system controlled by MassLynx 4.1 operating system (Waters Corporation). Metabolites were quantified using methods described previously.

Supplemental Table 6. Mitochondrial proteins identified by proteomic profiling in compensated hypertrophy (CH) and/or heart failure (HF) samples.

ID	Gene Name
IPI00387379	2,4-dienoyl CoA reductase 1, mitochondrial
IPI00379604, IPI00127625	3-hydroxy-3-methylglutaryl-Coenzyme A lyase
IPI00330754, IPI00890322, IPI00857778	3-hydroxybutyrate dehydrogenase, type 1
IPI00885424, IPI00154047	3-hydroxyisobutyryl-Coenzyme A hydrolase
IPI00132653, IPI00856651, IPI00858156	3-oxoacid CoA transferase 1
IPI00606168, IPI00856229, IPI00227445, IPI00407499	4-aminobutyrate aminotransferase
IPI00648312	5'-nucleotidase domain containing 3
IPI00648235, IPI00187512	5'-nucleotidase, cytosolic III
IPI00230589, IPI00230591, IPI00230590, IPI00894854, IPI00890007, IPI00230593, IPI00115506, IPI00230592	A kinase (PRKA) anchor protein 1
IPI00323406	ATP synthase mitochondrial F1 complex assembly factor 1
IPI00036348	ATP synthase mitochondrial F1 complex assembly factor 2; similar to ATP synthase mitochondrial F1 complex assembly factor 2
IPI00468181	ATP synthase, H+ transporting mitochondrial F1 complex, beta subunit
IPI00856424, IPI00125460	ATP synthase, H+ transporting, mitochondrial F0 complex, subunit F pseudogene; similar to ATP synthase coupling factor 6, mitochondrial precursor (ATPase subunit F6); ATP synthase, H+ transporting, mitochondrial F0 complex, subunit F
IPI00341282	ATP synthase, H+ transporting, mitochondrial F0 complex, subunit b, isoform 1; predicted gene 12231
IPI00857439, IPI00130280	ATP synthase, H+ transporting, mitochondrial F1 complex, alpha subunit, isoform 1
IPI00750074, IPI00313475, IPI00775853, IPI00776084, IPI00776275, IPI00751391, IPI00776312	ATP synthase, H+ transporting, mitochondrial F1 complex, gamma polypeptide 1
IPI00761646, IPI00872663, IPI00816848	ATP-binding cassette, sub-family B (MDR/TAP), member 7
IPI00856267, IPI00856425, IPI00123422, IPI00459383	ATP-binding cassette, sub-family B (MDR/TAP), member 8
IPI00115646, IPI00553576	ATP-binding cassette, sub-family D (ALD), member 3
IPI00108410	ATPase family, AAA domain containing 1
IPI00126913, IPI00464208	ATPase family, AAA domain containing 3A
IPI00127598, IPI00331463	ATPase inhibitory factor 1
IPI00880712, IPI00880589, IPI00880341, IPI00357510, IPI00357511, IPI00124900	AU RNA binding protein/enoyl-coenzyme A hydratase
IPI00606647, IPI00321499	BCL2-like 13 (apoptosis facilitator)
IPI00128346	CDGSH iron sulfur domain 1
IPI00345740, IPI00649328, IPI00649725	CDGSH iron sulfur domain 3
IPI00222203, IPI00874655, IPI00267596	COX15 homolog, cytochrome c oxidase assembly protein (yeast)
IPI00830383, IPI00830273, IPI00467840, IPI00830443	ClpB caseinolytic peptidase B homolog (E. coli)
IPI00128261	Cytochrome b
IPI00130376, IPI00355248	Cytochrome c oxidase subunit 1
IPI00116896	Cytochrome c oxidase subunit 5; ATP synthase subunit e; ATP synthase protein 8
IPI00347634, IPI00120414, IPI00279858	Dnal (Hsp40) homolog, subfamily A, member 3
IPI00648191, IPI00226466, IPI00828649	Dnal (Hsp40) homolog, subfamily C, member 11
IPI00624902, IPI00468992, IPI00111111, IPI00881254	Dnal (Hsp40) homolog, subfamily C, member 15
IPI00137424	ECSIT homolog (Drosophila)
IPI00828369, IPI00474134, IPI00153350	FAD-dependent oxidoreductase domain containing 1
IPI00267299, IPI00466703	FAST kinase domains 2
IPI00881994, IPI00230283	G elongation factor, mitochondrial 1
IPI00334876, IPI00269240	G elongation factor, mitochondrial 2
IPI00622170, IPI00225294, IPI00336569	GUF1 GTPase homolog (S. cerevisiae)
IPI00117085	GrpE-like 1, mitochondrial
IPI00115598, IPI00230550	H2-K region expressed gene 6
IPI00331517	HIG1 domain family, member 1A
IPI00170051, IPI00881059	HscB iron-sulfur cluster co-chaperone homolog (E. coli)
IPI00110578, IPI00856218, IPI00856829	IscU iron-sulfur cluster scaffold homolog (E. coli); similar to nitrogen fixation cluster-like
IPI00130331	L-2-hydroxyglutarate dehydrogenase; predicted gene 7842
IPI00471097	LYR motif containing 5
IPI00117832, IPI00918067	LYR motif containing 7
IPI00122740	MACRO domain containing 1
IPI00122276	MOCO sulphurase C-terminal domain containing 2
IPI00222753	MTERF domain containing 3
IPI00116748	NADH dehydrogenase (ubiquinone) 1 alpha subcomplex 10
IPI00318645	NADH dehydrogenase (ubiquinone) 1 alpha subcomplex 11
IPI00344004	NADH dehydrogenase (ubiquinone) 1 alpha subcomplex, 12
IPI00230715	NADH dehydrogenase (ubiquinone) 1 alpha subcomplex, 13
IPI00115302	NADH dehydrogenase (ubiquinone) 1 alpha subcomplex, 2
IPI00858238, IPI00132216	NADH dehydrogenase (ubiquinone) 1 alpha subcomplex, 3
IPI00125929	NADH dehydrogenase (ubiquinone) 1 alpha subcomplex, 4
IPI00880753, IPI00331332	NADH dehydrogenase (ubiquinone) 1 alpha subcomplex, 5
IPI00113399	NADH dehydrogenase (ubiquinone) 1 alpha subcomplex, 6 (B14)
IPI00130322	NADH dehydrogenase (ubiquinone) 1 alpha subcomplex, 7 (B14.5a)

IP100120984	NADH dehydrogenase (ubiquinone) 1 alpha subcomplex, 8
IP100120212	NADH dehydrogenase (ubiquinone) 1 alpha subcomplex, 9
IP100226687	NADH dehydrogenase (ubiquinone) 1 alpha subcomplex, assembly factor 1
IP100330551	NADH dehydrogenase (ubiquinone) 1 alpha subcomplex, assembly factor 2
IP100648625, IP100133744	NADH dehydrogenase (ubiquinone) 1 alpha subcomplex, assembly factor 4
IP100133403	NADH dehydrogenase (ubiquinone) 1 beta subcomplex 3; predicted gene 3192
IP100132390	NADH dehydrogenase (ubiquinone) 1 beta subcomplex 4; predicted gene 3473; predicted gene 3244
IP100387430	NADH dehydrogenase (ubiquinone) 1 beta subcomplex 8
IP100880613, IP100121288	NADH dehydrogenase (ubiquinone) 1 beta subcomplex, 10
IP100881846, IP100881750, IP100882364, IP100112531, IP100882043	NADH dehydrogenase (ubiquinone) 1 beta subcomplex, 5
IP100648743, IP100341322	NADH dehydrogenase (ubiquinone) 1 beta subcomplex, 6
IP100133215	NADH dehydrogenase (ubiquinone) 1 beta subcomplex, 7
IP100132621	NADH dehydrogenase (ubiquinone) 1 beta subcomplex, 9
IP100133006, IP100918301, IP100918079	NADH dehydrogenase (ubiquinone) 1, alpha/beta subcomplex, 1; predicted gene 4459
IP100132050, IP100160825	NADH dehydrogenase (ubiquinone) 1, subcomplex unknown, 2; similar to NADH dehydrogenase (ubiquinone) 1, subcomplex unknown, 2
IP100308882	NADH dehydrogenase (ubiquinone) Fe-S protein 1
IP100830766, IP100128023, IP100830872	NADH dehydrogenase (ubiquinone) Fe-S protein 2
IP100229008	NADH dehydrogenase (ubiquinone) Fe-S protein 4
IP100649019, IP100117300	NADH dehydrogenase (ubiquinone) Fe-S protein 5; cDNA sequence BC002163
IP100120232	NADH dehydrogenase (ubiquinone) Fe-S protein 7
IP100120093	NADH dehydrogenase (ubiquinone) Fe-S protein 8
IP100130460	NADH dehydrogenase (ubiquinone) flavoprotein 1
IP100169925, IP100845716	NADH dehydrogenase (ubiquinone) flavoprotein 2
IP100128285	NADH dehydrogenase (ubiquinone) flavoprotein 3
IP100341550	NADH-ubiquinone oxidoreductase chain 1
IP100116843	NADH-ubiquinone oxidoreductase chain 4L; NADH-ubiquinone oxidoreductase chain 4
IP100881776	NFU1 iron-sulfur cluster scaffold homolog (S. cerevisiae); predicted gene 7855
IP100265701	NLR family member X1
IP100407938, IP100133608	OCIA domain containing 1
IP100111512	OMA1 homolog, zinc metallopeptidase (S. cerevisiae)
IP100857491, IP100857001, IP100457976	PET112-like (yeast)
IP100650052, IP100649794, IP100895414, IP100117264, IP100894710, IP100894598, IP100649406, IP100895518, IP100648764, IP100894789	Parkinson disease (autosomal recessive, early onset) 7
IP100133706	RAB1B, member RAS oncogene family
IP100850133, IP100900458, IP100762463	RIKEN cDNA 1300010F03 gene
IP100108431, IP100785241, IP100918883	RIKEN cDNA 1500001M20 gene
IP100132478	RIKEN cDNA 1700021F05 gene
IP100133080	RIKEN cDNA 1700034H14 gene
IP100459357	RIKEN cDNA 1700034J23 gene; predicted gene 10731
IP100654397, IP100133220, IP100458085, IP100109286, IP100170212	RIKEN cDNA 1810020G14 gene; synaptojanin 2 binding protein; predicted gene 4116
IP100113143	RIKEN cDNA 2010107E04 gene
IP100110460, IP100869373	RIKEN cDNA 2310003L22 gene
IP100750687, IP100222284	RIKEN cDNA 2310005E10 gene
IP100270788	RIKEN cDNA 2310028O11 gene
IP100153792	RIKEN cDNA 2430015M20 gene
IP100880887, IP100173167	RIKEN cDNA 2610001C18 gene
IP100895415, IP100453792	RIKEN cDNA 4930402E16 gene
IP100221782	RIKEN cDNA 4933403F05 gene
IP100308195, IP100416621, IP100856408, IP100857151	RIKEN cDNA 9030617O03 gene
IP100856512, IP100267983	RIKEN cDNA 9330129D05 gene
IP100221850	RIKEN cDNA 9430016H08 gene
IP100228106	RIKEN cDNA A230051G13 gene
IP100471368	RNA (guanine-9-) methyltransferase domain containing 1
IP100761950, IP100515530	SCO cytochrome oxidase deficient homolog 1 (yeast)
IP100132762	TNF receptor-associated protein 1
IP100113052, IP100885494	Tu translation elongation factor, mitochondrial
IP100156555	YME1-like 1 (S. cerevisiae)
IP100132696, IP100788370	aarF domain containing kinase 1
IP100226414, IP100886271, IP100404935	abhydrolase domain containing 10
IP100858299, IP100170213	abhydrolase domain containing 11
IP100154054	acetyl-Coenzyme A acetyltransferase 1
IP100226430, IP100653158	acetyl-Coenzyme A acyltransferase 2 (mitochondrial 3-oxoacyl-Coenzyme A thiolase
IP100624175	acid phosphatase 6, lysophosphatidic
IP100116074	aconitase 2, mitochondrial
IP100122631	acyl-CoA synthetase family member 2
IP100634091, IP100762636	acyl-CoA synthetase family member 3

IP00856216, IP00112549, IP00857822, IP00556840, IP00856996, IP00857226	acyl-CoA synthetase long-chain family member 1
IP00915057, IP00651798, IP00169772	acyl-CoA synthetase long-chain family member 3
IP00469942	acyl-CoA synthetase short-chain family member 1
IP00115871	acyl-CoA thioesterase 1
IP00127260	acyl-CoA thioesterase 10
IP00132958	acyl-CoA thioesterase 13
IP00653566, IP00136683	acyl-CoA thioesterase 2
IP00314069	acyl-CoA thioesterase 9
IP00170013	acyl-Coenzyme A dehydrogenase family, member 10
IP00274222	acyl-Coenzyme A dehydrogenase family, member 8
IP00759881, IP00531710, IP00857619	acyl-Coenzyme A dehydrogenase family, member 9
IP00119114, IP00894588	acyl-Coenzyme A dehydrogenase, long-chain
IP00895545, IP00134961, IP00894719	acyl-Coenzyme A dehydrogenase, medium chain
IP00885762, IP00116591, IP00331251	acyl-Coenzyme A dehydrogenase, short chain
IP00880948, IP00119842	acyl-Coenzyme A dehydrogenase, short/branched chain
IP00119203, IP00649885	acyl-Coenzyme A dehydrogenase, very long chain
IP00409360, IP00404355, IP00828479, IP00127558	acyl-Coenzyme A oxidase 1, palmitoyl
IP00128209, IP00750258, IP00752998	adenylate kinase 1
IP00221769, IP00918523	adenylate kinase 3
IP00227186, IP00889240	alcohol dehydrogenase, iron containing, 1
IP00114073	aldehyde dehydrogenase 1 family, member B1
IP00169472, IP00858223	aldehyde dehydrogenase 1 family, member L2
IP00111218, IP00858077	aldehyde dehydrogenase 2, mitochondrial
IP00405699	aldehyde dehydrogenase 4 family, member A1
IP00124372	aldehyde dehydrogenase 9, subfamily A1
IP00461964	aldehyde dehydrogenase family 6, subfamily A1
IP00220084, IP00890092	aldehyde dehydrogenase family 7, member A1
IP00273161	aldehyde dehydrogenase family 8, subfamily A1
IP00224181	aldo-keto reductase family 1, member B7
IP00119458	aldolase C, fructose-bisphosphate
IP00756601, IP00223818	alkylglycerone phosphate synthase
IP00697025, IP00114331	alpha-methylacyl-CoA racemase
IP00874359, IP00121287, IP00918663	aminolevulinic acid synthase 1
IP00170307	apolipoprotein A-I binding protein
IP00112493, IP00874378, IP00828758	apolipoprotein O-like
IP00776047, IP00129577	apoptosis-inducing factor, mitochondrion-associated 1
IP00648997, IP00323177	arginyl-tRNA synthetase 2, mitochondrial
IP00857459, IP00312759	asparaginyl-tRNA synthetase 2 (mitochondrial)(putative)
IP00895398, IP00273767	aspartyl-tRNA synthetase 2 (mitochondrial)
IP00627838, IP00320462, IP00458522	biphenyl hydrolase-like (serine hydrolase, breast epithelial mucin-associated antigen
IP00131896	brain protein 44; similar to brain protein 44; predicted gene 3982
IP00886333, IP00122442, IP00886399, IP00885905	branched chain aminotransferase 2, mitochondrial
IP00331555	branched chain ketoacid dehydrogenase E1, alpha polypeptide
IP00661358, IP00115302, IP00653144	branched chain ketoacid dehydrogenase E1, beta polypeptide; similar to 3-methyl-2-oxobutanoate dehydrogenas
IP00849134	cDNA sequence AK157302
IP00128642, IP00648012	carbonyl reductase 2
IP00127227, IP00895535	carbonyl reductase 4
IP00856889, IP00757912, IP00875497, IP00113347, IP00856855	carnitine acetyltransferase
IP00330894	carnitine palmitoyltransferase 1a, liver
IP00136563	carnitine palmitoyltransferase 1b, muscle
IP00881401, IP00649655, IP00649159, IP00643887, IP00131424	carnitine palmitoyltransferase 2
IP00788396, IP00119808	caseinolytic peptidase X (E.coli)
IP00333270	caseinolytic peptidase, ATP-dependent, proteolytic subunit homolog (E. coli)
IP00869393, IP00312658, IP00755311	catalase
IP00115517	cathepsin B
IP00404551, IP00111013, IP00881091	cathepsin D
IP00856199, IP00857970, IP00760870, IP00117825	caveolin 1, caveolae protein
IP00322554	chaperone, ABC1 activity of bc1 complex like (S. pombe)
IP00331174	chaperonin containing TCP1, subunit 7 (eta)
IP00153903, IP00874574, IP00478485	citrate lyase beta like
IP00113141	citrate synthase
IP00118825	citrate synthase like
IP00649850, IP00169916, IP00648173	clathrin, heavy polypeptide (Hc)
IP00467124	coenzyme Q3 homolog, methyltransferase (yeast
IP00379695, IP00886214	coenzyme Q5 homolog, methyltransferase (yeast
IP00857727, IP00222526, IP00856308, IP00869087	coenzyme Q6 homolog (yeast)
IP00169862	coenzyme Q9 homolog (yeast)
IP00655156, IP00353887	coiled-coil domain containing 109A

IPI00137601	coiled-coil domain containing 44
IPI00153794	coiled-coil domain containing 58
IPI00854928, IPI00110180, IPI00854953	coiled-coil domain containing 90B
IPI00754739, IPI00133562, IPI00757033	coiled-coil-helix-coiled-coil-helix domain containing 3; similar to coiled-coil-helix-coiled-coil-helix domain containing
IPI00124389	coiled-coil-helix-coiled-coil-helix domain containing 4
IPI00775783, IPI00132799	complement component 1, q subcomponent binding protein
IPI00480301	coproporphyrinogen oxidase
IPI00128296	creatine kinase, mitochondrial 1, ubiquitous
IPI00120076	creatine kinase, mitochondrial 2
IPI00857487, IPI00454201, IPI00845690	cysteine conjugate-beta lyase 2
IPI00896595	cysteinyl-tRNA synthetase 2 (mitochondrial)(putative)
IPI00119685	cytochrome P450, family 27, subfamily a, polypeptide 1
IPI00119131, IPI00127437	cytochrome b5 reductase 1
IPI00759904, IPI00121079	cytochrome b5 reductase 3
IPI00117978	cytochrome c oxidase subunit IV isoform 1
IPI00120136	cytochrome c oxidase subunit VIIa polypeptide 2-like; predicted gene 6969
IPI00120238	cytochrome c oxidase, subunit VI a, polypeptide 2
IPI00113196	cytochrome c oxidase, subunit VIIa 1
IPI00225590	cytochrome c oxidase, subunit VIb polypeptide 1
IPI00120719	cytochrome c oxidase, subunit Via
IPI00113203	cytochrome c oxidase, subunit XVII assembly protein homolog (yeast)
IPI00230053	cytochrome c, testis
IPI00845772, IPI00132728	cytochrome c-1
IPI00275050, IPI00402997	death associated protein 3
IPI00331549	dehydrogenase/reductase (SDR family) member 1
IPI00118750	dehydrogenase/reductase (SDR family) member 4
IPI00653062, IPI00125592	demethyl-Q 7
IPI00153660	dihydrolipoamide S-acetyltransferase (E2 component of pyruvate dehydrogenase complex
IPI00845858, IPI00134809	dihydrolipoamide S-succinyltransferase (E2 component of 2-oxo-glutarate complex
IPI00890234, IPI00130555	dihydrolipoamide branched chain transacylase E2
IPI00331564, IPI00874436	dihydrolipoamide dehydrogenase
IPI00918852, IPI00919031, IPI00919119, IPI00107713, IPI00919285, IPI00401712	dihydroorotate dehydrogenase
IPI00114416, IPI00331692	dodecenoyl-Coenzyme A delta isomerase (3,2-trans-enoyl-Coenzyme A isomerase
IPI00121322, IPI00882287	electron transferring flavoprotein, dehydrogenase
IPI00118283, IPI00753211	enoyl Coenzyme A hydratase domain containing 3
IPI00886151, IPI00458049, IPI00459020	enoyl Coenzyme A hydratase, short chain, 1, mitochondrial
IPI00130804, IPI00895351	enoyl coenzyme A hydratase 1, peroxisomal
IPI00554834, IPI00127276	enoyl-Coenzyme A, hydratase/3-hydroxyacyl Coenzyme A dehydrogenase
IPI00111386	ethylmalonic encephalopathy 1
IPI00109611	family with sequence similarity 162, member A
IPI00649589, IPI00187249, IPI00875611	family with sequence similarity 82, member B
IPI00452981	ferredoxin reductase
IPI00228343, IPI00608064	ferrochelatase
IPI00856326, IPI00132217, IPI00857192	fission 1 (mitochondrial outer membrane) homolog (yeast)
IPI00136201	frataxin
IPI00129828, IPI00759940	fumarate hydratase 1
IPI00968850, IPI00653743	fumarylacetoacetate hydrolase domain containing 1
IPI00121218	fumarylacetoacetate hydrolase domain containing 2A
IPI00115827, IPI00651782	glioblastoma amplified sequence
IPI00606398, IPI00114209	glutamate dehydrogenase 1; predicted gene 5902
IPI00117312	glutamate oxaloacetate transaminase 2, mitochondrial
IPI00120235, IPI00885605, IPI00788131	glutaryl-Coenzyme A dehydrogenase
IPI00121051	glutathione S-transferase kappa 1
IPI00876504, IPI00126120	glutathione transferase zeta 1 (maleylacetoacetate isomerase)
IPI00135446, IPI00604687, IPI00654090, IPI00224993	glycerol kinase
IPI00123975	glycerol kinase 2
IPI00876082, IPI00131182	glycerol phosphate dehydrogenase 2, mitochondrial
IPI00230185	glycerol-3-phosphate dehydrogenase 1 (soluble)
IPI00112555	glycyl-tRNA synthetase
IPI00831130, IPI00110721, IPI00112630	glyoxalase domain containing 4
IPI00410978	growth factor, erv1 (S. cerevisiae)-like (augmenter of liver regeneration)
IPI00126721	growth hormone inducible transmembrane protein
IPI00263863, IPI00120045	heat shock protein 1 (chaperonin 10); predicted gene, EG628438; heat shock protein 1 (chaperonin 10), related sequence 1, predicted gene 2903
IPI00133208	heat shock protein 1B; heat shock protein 1A; heat shock protein 1-like
IPI00187494, IPI00131546	heat shock protein 2
IPI00880830, IPI00113903	heat shock protein 9
IPI00554929, IPI00229080	heat shock protein 90 alpha (cytosolic), class B member 1
IPI00117281, IPI00660262, IPI00463220, IPI00227783	heterogeneous nuclear ribonucleoprotein L-like; glutathione peroxidase 4

IP000762858, IP000283612, IP000759938, IP000468553, IP000283611	hexokinase 1
IP000114342	hexokinase 2
IP000113034	histidine triad nucleotide binding protein 2
IP000116138	histidyl-tRNA synthetase 2, mitochondrial (putative)
IP000134572, IP000109285	holocytochrome c synthetase
IP000880410, IP000880541, IP000115866, IP000882305	hydroxyacyl glutathione hydrolase
IP000121105	hydroxyacyl-Coenzyme A dehydrogenase
IP000223092	hydroxyacyl-Coenzyme A dehydrogenase/3-ketoacyl-Coenzyme A thiolase/enoyl-Coenzyme A hydratase (trifunctional protein), alpha subunit
IP000220847, IP000830581, IP000626132	hydroxysteroid (17-beta) dehydrogenase 10
IP000331628	hydroxysteroid (17-beta) dehydrogenase 4
IP000649718, IP000117214	hydroxysteroid dehydrogenase like 2
IP000133350, IP000894954, IP000894692	hypothetical protein LOC675054, RIKEN cDNA 2900010M23 gene
IP000555088, IP000581412, IP000228150, IP000581413, IP000554845	inner membrane protein, mitochondrial
IP000119784, IP000828796, IP000407289	insulin degrading enzyme
IP000720014	iron-sulfur cluster assembly 1 homolog (S. cerevisiae
IP000857308, IP000118614, IP000875110	isocitrate dehydrogenase 2 (NADP+), mitochondrial
IP000680978, IP000859225	isocitrate dehydrogenase 3 (NAD+) alpha
IP000126635	isocitrate dehydrogenase 3 (NAD+) beta
IP000109169	isocitrate dehydrogenase 3 (NAD+), gamma
IP000453499, IP000830173, IP000720234	isoleucine-tRNA synthetase 2, mitochondrial; similar to isoleucine-tRNA synthetase 2, mitochondria
IP000471246	isovaleryl coenzyme A dehydrogenase
IP000280156, IP000229510, IP000776197	lactate dehydrogenase B; predicted gene 5514
IP000885799, IP000885728, IP000830170, IP000169752	lactation elevated 1
IP000331436, IP000828469	leucine aminopeptidase 3
IP000131177	leucine zipper-EF-hand containing transmembrane protein 1
IP000875457, IP000420706	leucine-rich PPR-motif containing
IP000123138	leucyl-tRNA synthetase, mitochondrial
IP000761408, IP000319518	lon peptidase 1, mitochondrial
IP000130018, IP000831119, IP000400117, IP000831016	lysophospholipase 1
IP000336324, IP000649895	malate dehydrogenase 1, NAD (soluble)
IP000323592	malate dehydrogenase 2, NAD (mitochondrial)
IP000308976, IP000415361	malic enzyme 3, NADP(+)-dependent, mitochondrial
IP000759857, IP000114866	malonyl-CoA decarboxylase
IP000225254, IP000874889	metaxin 2
IP000475322, IP000331442	methionine sulfoxide reductase A
IP000109655	methionine sulfoxide reductase B2
IP000652521, IP000881206, IP000320850	methylcrotonoyl-Coenzyme A carboxylase 1 (alpha)
IP000134792, IP000553717	methylcrotonoyl-Coenzyme A carboxylase 2 (beta)
IP000122862	methylenetetrahydrofolate dehydrogenase (NADP+ dependent), methenyltetrahydrofolate cyclohydrolase, formyltetrahydrofolate synthase
IP000112720	methylmalonic aciduria (cobalamin deficiency) type F
IP000750681, IP000653086, IP000283203	methylmalonic aciduria (cobalamin deficiency) type B homolog (human
IP000113776	methylmalonyl CoA epimerase
IP000133553, IP000850737	methylmalonyl-Coenzyme A mutase
IP000330688	mitochondrial ribosomal protein S7
IP000122075	mitochondrial antiviral signaling protein
IP000864752, IP000132039, IP000807902, IP000750596	mitochondrial carrier homolog 2 (C. elegans); predicted gene, 100039384, predicted gene, 100039506
IP000222838, IP000750039	mitochondrial intermediate peptidase; similar to Mipep protein
IP000459344	mitochondrial poly(A) polymerase
IP000720216, IP000118237	mitochondrial ribosomal protein L1
IP000132412, IP000648692	mitochondrial ribosomal protein L10
IP000132470	mitochondrial ribosomal protein L11
IP000118963	mitochondrial ribosomal protein L12
IP000134011	mitochondrial ribosomal protein L13
IP000798614, IP000131732	mitochondrial ribosomal protein L15
IP000118230	mitochondrial ribosomal protein L16
IP000271726, IP000919171	mitochondrial ribosomal protein L28
IP000837677, IP000118235, IP000856509	mitochondrial ribosomal protein L3
IP000858168, IP000111406	mitochondrial ribosomal protein L39
IP000881504, IP000326669	mitochondrial ribosomal protein L40
IP000665641, IP000607969	mitochondrial ribosomal protein L44
IP000132895, IP000474272, IP000856299	mitochondrial ribosomal protein L45
IP000111211	mitochondrial ribosomal protein L46
IP000322422	mitochondrial ribosomal protein L47
IP000274131, IP000874379	mitochondrial ribosomal protein L48
IP000131988, IP000271410	mitochondrial ribosomal protein L49; similar to mitochondrial ribosomal protein L49
IP000132170	mitochondrial ribosomal protein L51
IP000654010, IP000284978	mitochondrial ribosomal protein L9

IPI00895548, IPI00895482, IPI00148248, IPI00895361	mitochondrial ribosomal protein S10
IPI00321858	mitochondrial ribosomal protein S15
IPI00320963, IPI00880873, IPI00556725	mitochondrial ribosomal protein S18A
IPI00223360, IPI00118193	mitochondrial ribosomal protein S18B
IPI00110918	mitochondrial ribosomal protein S22
IPI00649272, IPI00882119, IPI00882252, IPI00515295, IPI00754363, IPI00853715, IPI00284934	mitochondrial ribosomal protein S23; similar to Mrps23 protein
IPI00222514, IPI00462763	mitochondrial ribosomal protein S27
IPI00110672	mitochondrial ribosomal protein S28
IPI00132504	mitochondrial ribosomal protein S30
IPI00124828	mitochondrial ribosomal protein S31
IPI00894878, IPI00222558	mitochondrial ribosomal protein S35
IPI00269020	mitochondrial ribosomal protein S6
IPI00461565, IPI00855075, IPI00336292	mitochondrial ribosomal protein S9
IPI00109501	mitochondrial ribosome recycling factor; similar to mitochondrial ribosome recycling factor; predicted gene 6374
IPI00648884, IPI00121276	mitochondrial trans-2-enoyl-CoA reductase
IPI00776049, IPI00649361, IPI00649863, IPI00551118, IPI00649625, IPI00133227	mitochondrial translational initiation factor 2
IPI00649455, IPI00308263, IPI00649724	mitochondrial ubiquitin ligase activator of NFKB 1
IPI00653062, IPI00881102, IPI00881801, IPI00135575	mitoferrin 1
IPI00226140	monoamine oxidase B
IPI00121107	myosin, light chain 10, regulatory
IPI00894940, IPI00407982, IPI00130747	nephrosophthosis 3 (adolescent); acyl-Coenzyme A dehydrogenase family, member 1
IPI00114829, IPI00405682, IPI00874680	neurolysin (metallopeptidase M3 family)
IPI00115459, IPI00858044	nicotinamide nucleotide adenylyltransferase 3
IPI00762127, IPI00874645, IPI00875011, IPI00830812	nicotinamide nucleotide transhydrogenase
IPI00119945	nitrilase family, member 2
IPI00760086, IPI00511072	nitrogen fixation gene 1 (S. cerevisiae); similar to Nitrogen fixation gene 1 (S. cerevisiae
IPI00807996, IPI00110522	nudix (nucleoside diphosphate linked moiety X)-type motif 13
IPI00312507	optic atrophy 3 (human)
IPI00129178	ornithine aminotransferase
IPI00308001	ovalbumin assembly 1-like
IPI00123765, IPI00857222	oxidoreductase NAD-binding domain containing 1
IPI00460118, IPI00719841, IPI00845652, IPI00626237, IPI00420882	oxoglutarate dehydrogenase (lipoamide)
IPI00126857	pentatricopeptide repeat domain 2
IPI00338458	pentatricopeptide repeat domain 3
IPI00750433, IPI00120199	peptidase (mitochondrial processing) alpha
IPI00274656	peptidase (mitochondrial processing) beta
IPI00116228	peptidylprolyl isomerase F (cyclophilin F
IPI00649645, IPI00848536, IPI00648105, IPI00605254, IPI00121788, IPI00648615	peroxiredoxin 1; predicted gene 7204
IPI00116192	peroxiredoxin 3
IPI00828909	peroxiredoxin 4
IPI00475031, IPI00759999, IPI00129517	peroxiredoxin 5
IPI00322931, IPI00877214	peroxisomal delta3, delta2-enoyl-Coenzyme A isomerase
IPI00459332, IPI00720114, IPI00387505	phenylalanine-tRNA synthetase 2 (mitochondrial
IPI00788337, IPI00788353, IPI00170126	pitrilysin metallopeptidase 1
IPI00654405, IPI00117689	polymerase I and transcript release factor
IPI00315808	predicted gene 10078; predicted gene 3544; similar to mitochondrial ribosomal protein S36; mitochondrial ribosomal protein S36; predicted gene 7258; predicted gene 4676
IPI00222419, IPI00265259	predicted gene 10108; cytochrome c, somatic; predicted gene 10053; similar to cytochrome c
IPI00133342, IPI00876323	predicted gene 10221; predicted gene 4602; predicted gene 9391; ATP synthase, H+ transporting, mitochondrial F0 complex, subunit G2, pseudogene; predicted gene 11477; predicted gene 9712; ATP synthase, H+ transporting, mitochondrial F0 complex, subunit g; predicted gene 4045
IPI00136505, IPI00623553, IPI00881799, IPI00219507	predicted gene 10250; hypothetical protein LOC676483; predicted gene 5051; ATP synthase, H+ transporting, mitochondrial F0 complex, subunit d; predicted gene 4953; similar to ATP synthase, H+ transporting, mitochondrial F0 complex, subunit d
IPI00116222	predicted gene 11225; 3-hydroxyisobutyrate dehydrogenase
IPI00110524, IPI00848762, IPI00659536	predicted gene 11945; predicted gene 6258; mitochondrial ribosomal protein L38
IPI00111877, IPI00408243	predicted gene 12115; single-stranded DNA binding protein 1
IPI00308885, IPI00853695, IPI00830313, IPI00845678, IPI00461249	predicted gene 12141; heat shock protein 1 (chaperonin)
IPI00118196, IPI00894830	predicted gene 13128; mitochondrial ribosomal protein S5
IPI00866165, IPI00129035, IPI00648501, IPI00649018, IPI00651879	predicted gene 13639; similar to adenylate kinase 4; adenylate kinase 3-like 1
IPI00858282, IPI00474281, IPI00115607, IPI00850941	predicted gene 13910; similar to Hydroxyacyl-Coenzyme A dehydrogenase/3-ketoacyl-Coenzyme A thiolase/enoyl-Coenzyme A hydratase (trifunctional protein), beta subunit; hydroxyacyl-Coenzyme A dehydrogenase/3-ketoacyl-Coenzyme A thiolase/enoyl-Coenzyme A hydratase (trifunctional protein), beta subunit; predicted gene 9108
IPI00115040, IPI00850545, IPI00677484	predicted gene 14506; BCL2/adenovirus E1B interacting protein 3; predicted gene 6532; similar to E1B 19K/Bcl-2-binding protein homolog

IP00116385	predicted gene 13683; RIKEN cDNA 2310005N01 gene; similar to RIKEN cDNA 2310005N01
IP00116753	predicted gene 2893; electron transferring flavoprotein, alpha polypeptide
IP00112347, IP00555000	predicted gene 2962; ubiquinol-cytochrome c reductase binding protein
IP00111770, IP00875971	predicted gene 2972; ATP synthase, H+ transporting, mitochondrial F1F0 complex, subunit e
IP00453724, IP00536699, IP00755768	predicted gene 3672; similar to Glycine cleavage system H protein, mitochondrial precursor; glycine cleavage system protein H (aminomethyl carrier)
IP00133363	predicted gene 4237; NADH dehydrogenase (ubiquinone) 1, subcomplex unknown, 1
IP00119731, IP00849049, IP00059907, IP00874964, IP00753028, IP00849031, IP00850955, IP00850432, IP00850377, IP00462008, IP00462075, IP00850337, IP00620663, IP00850243, IP00848648, IP00848411, IP00273646, IP00848801, IP00656311, IP00850028, IP00849532, IP00848807, IP00762304, IP00850062, IP00863987, IP00848511, IP00849530, IP00135284, IP00751102, IP00849050, IP00751677, IP00752685, IP00756025, IP00752289, IP00849792, IP00849045, IP00850760, IP00851086, IP00271869, IP00622795, IP00849046, IP00850779, IP00853668, IP00850434	predicted gene 4691; predicted gene 6944; predicted gene 10290; predicted gene 10566; predicted gene 10291; predicted gene 3200; predicted gene 12070; predicted gene 7286; predicted gene 6946; predicted gene 8825; predicted gene 9081; glyceraldehyde-3-phosphate dehydrogenase; predicted gene 10359; predicted gene 10358; predicted gene 7784; predicted gene 12416; predicted gene 14148; predicted gene 11882; predicted gene 4217; predicted gene 7183; predicted gene 10313; predicted gene 2467; predicted gene 5787; predicted gene 2193; predicted gene 13292; predicted gene, 380687; predicted gene 2076; predicted gene 3222; predicted gene 7507; predicted gene 7293; predicted gene 15191; predicted gene, 674324; predicted gene 10284; predicted gene 8055; similar to hL3:19788856; predicted gene 2574; similar to glyceraldehyde-3-phosphate dehydrogenase; predicted gene 7545; predicted gene 12033; predicted gene 3272; predicted gene 3534; predicted gene 2308; predicted gene 3839; predicted gene 9061; predicted gene 3671; predicted gene 8513; predicted gene 4658; predicted gene 12537; predicted gene 4929; predicted gene 3652; predicted gene 9568; predicted gene 8349; predicted gene 2546; predicted gene 7129; similar to Glyceraldehyde-3-phosphate dehydrogenase (GAPDH); predicted gene 8318; glyceraldehyde-3-phosphate dehydrogenase pseudogene; predicted gene 7611; predicted gene 2445; predicted gene 6283; predicted gene 11557; predicted gene 4335; predicted gene 9127; predicted gene 3695; predicted gene 5507; predicted gene 8134; predicted gene 4609; predicted gene 3809; predicted gene 9034; predicted gene 2606; predicted gene 4525; predicted gene 12286; predicted gene 11658; predicted gene 5732; predicted gene 16374; predicted gene 8100; predicted gene 11953; predicted gene, EG545741; predicted gene 2451; predicted gene 14130
IP00118986, IP00919068	predicted gene 5436; similar to ATP synthase, H+ transporting, mitochondrial F1 complex, O subunit; ATP synthase, H+ transporting, mitochondrial F1 complex, O subunit
IP00648759, IP00115117, IP00648577, IP00649191	predicted gene 5626; stomatin (Eph7.2)-like 2
IP00132042	predicted gene 6123; pyruvate dehydrogenase (lipoamide) beta
IP00131771, IP00622837	predicted gene 6265; similar to cytochrome c oxidase, subunit Vlc; cytochrome c oxidase, subunit Vlc
IP00114246	predicted gene 6444; NADH dehydrogenase (ubiquinone) 1 beta subcomplex, 11
IP00407130, IP00645840	predicted gene 6560; predicted gene 2124; predicted gene 6992; pyruvate kinase, muscle; similar to M2-type pyruvate kinase
IP00856384, IP00271986	predicted gene 6835; ATP synthase, H+ transporting, mitochondrial F0 complex, subunit f, isoform 2; predicted gene 6581
IP00225318	predicted gene 6997; mitochondrial ribosomal protein L22
IP00128857, IP00670735, IP00881197	predicted gene 7049; similar to NADP-dependent malic enzyme (NADP-ME) (Malic enzyme 1); malic enzyme 1, NADP(+)-dependent, cytosolic
IP00876341, IP00122548	predicted gene 7591; voltage-dependent anion channel 3
IP00127417, IP00379441	predicted gene 7730; non-metastatic cells 2, protein (NM23B) expressed in; predicted gene 5566; predicted gene 5425; similar to Nucleoside diphosphate kinase B (NDK B) (NDP kinase B) (P18)
IP00119994, IP00751369, IP00754398, IP00756114	predicted gene 7997; lactate dehydrogenase A; predicted gene 5452
IP00798555, IP00113606	predicted gene 8546; acylglycerol kinase
IP00130589, IP00135857	predicted gene 8566; superoxide dismutase 1, soluble; similar to Superoxide dismutase
IP00378520	predicted gene 9481; mitochondrial ribosomal protein L41
IP00625588, IP00460132, IP00274407	predicted gene 9755; Tu translation elongation factor, mitochondrial
IP00133167	predicted gene 9803; mitochondria-associated protein involved in granulocyte-macrophage colony-stimulating factor signal transduction
IP00124015, IP00856157, IP00857160	presenilin associated, rhomboid-like
IP00651865, IP00880977, IP00321718	prohibitin 2
IP00126917, IP00133440, IP00649084	prohibitin; predicted gene 4373; RIKEN cDNA 1700071K01 gene
IP00881014, IP00522760, IP00882128, IP00479037	proline dehydrogenase
IP00719401, IP00720189, IP00131548	proline synthetase co-transcribed
IP00918862, IP00606510, IP00918838, IP00468653	propionyl Coenzyme A carboxylase, beta polypeptide
IP00330523, IP00859257, IP00858124	propionyl-Coenzyme A carboxylase, alpha polypeptide
IP00321190	prosaposin
IP00312174	prostaglandin E synthase 2
IP00226766	protein phosphatase 1K (PP2C domain containing)
IP00672824, IP00850694, IP00857971, IP00849866	protein phosphatase 2C, magnesium dependent, catalytic subunit
IP00408727, IP00881514, IP00881722, IP00881568, IP00127050	pyrophosphatase (inorganic) 2
IP00114710	pyruvate carboxylase
IP00337893	pyruvate dehydrogenase E1 alpha 1
IP00113594	pyruvate dehydrogenase E1 alpha 2
IP00753072, IP00222767, IP00752435	pyruvate dehydrogenase complex, component X; similar to pyruvate dehydrogenase complex, component 3
IP00221407, IP00776169	pyruvate dehydrogenase kinase, isoenzyme 1
IP00122251	pyruvate dehydrogenase kinase, isoenzyme 2
IP00881473, IP00881737, IP00459279	quinoid dihydropteridine reductase; similar to Quinoid dihydropteridine reductase
IP00222930, IP00307931, IP00515349, IP00123188	ras homolog gene family, member T1
IP00875863, IP00474370, IP00473646	ras homolog gene family, member T2
IP00858050, IP00320716	reticulon 4 interacting protein 1

IPI00895515, IPI00229040, IPI00857145	retinol dehydrogenase 13 (all-trans and 9-cis)
IPI00129164	sepiapterin reductase
IPI00318006	serine hydrolase-like
IPI00454008	serine hydroxymethyltransferase 2 (mitochondrial)
IPI00109354	seryl-aminoacyl-tRNA synthetase 2
IPI00170357, IPI00850215	similar to AFG3(ATPase family gene 3)-like 2 (yeast); AFG3(ATPase family gene 3)-like 2 (yeast
IPI00225288, IPI00471436	similar to Coiled-coil domain containing 90B; coiled-coil domain containing 90B
IPI00848492, IPI00121440, IPI00757916	similar to Electron transferring flavoprotein, beta polypeptide; electron transferring flavoprotein, beta polypeptide
IPI00121309, IPI00475158	similar to NADH dehydrogenase (ubiquinone) Fe-S protein 3; NADH dehydrogenase (ubiquinone) Fe-S protein 3; predicted gene 12251
IPI00673568, IPI00886222, IPI00128345, IPI00674389	similar to NADH dehydrogenase (ubiquinone) Fe-S protein 6; NADH dehydrogenase (ubiquinone) Fe-S protein 6; predicted gene 6415
IPI00653905, IPI00757305, IPI00830434, IPI00850402, IPI00153266	similar to Saccharopine dehydrogenase (putative); saccharopine dehydrogenase (putative)
IPI00850430, IPI00124771	similar to Solute carrier family 25 (mitochondrial carrier, phosphate carrier), member 3; solute carrier family 25 (mitochondrial carrier, phosphate carrier), member 3
IPI00553262, IPI00480233	similar to Unknown (protein for IMAGE:4910858); predicted gene 4070
IPI00753287, IPI00122547, IPI00750490	similar to Voltage-dependent anion-selective channel protein 2 (VDAC-2) (mVDAC2) (mVDAC6) (Outer mitochondrial membrane protein porin 2); predicted gene 7832; voltage-dependent anion channel 2
IPI00269076, IPI00648318	similar to adenylate kinase 2; adenylate kinase 2
IPI00848729, IPI00918701, IPI00124292	similar to brain protein 44-like protein; brain protein 44-like; predicted gene 3452; predicted gene 8219
IPI00315794	similar to cytochrome b5 outer mitochondrial membrane precursor; cytochrome b5 type I
IPI00111255, IPI00850715	similar to cytochrome c oxidase, subunit VIIc; predicted gene 3386; cytochrome c oxidase, subunit VIIb
IPI00785410, IPI00116154	similar to cytochrome c oxidase, subunit VIc; predicted gene 11273; cytochrome c oxidase, subunit Vb
IPI00133284	similar to es1 protein; DNA segment, Chr 10, Johns Hopkins University 81 expressed
IPI00109293, IPI00890317	similar to lactamase, beta; lactamase, beta
IPI00469103	similar to lysyl-tRNA synthetase; lysyl-tRNA synthetase
IPI00342938	similar to mitochondrial malonyltransferase isoform b precursor; malonyl CoA:ACP acyltransferase (mitochondrial
IPI00894305, IPI00857674, IPI00312244, IPI00649816, IPI00415517, IPI00816883, IPI00894813	similar to mitofusin 2; mitofusin 2
IPI00855011, IPI00117657, IPI00918906, IPI00918990, IPI00918878, IPI00403336, IPI00919056	similar to optic atrophy 1 (autosomal dominant); optic atrophy 1 homolog (human)
IPI00321923, IPI00556859	similar to polynucleotide phosphorylase-like protein; polyribonucleotide nucleotidyltransferase 1
IPI00169883	sirtuin 5 (silent mating type information regulation 2 homolog) 5 (S. cerevisiae
IPI00137194	solute carrier family 16 (monocarboxylic acid transporters), member 1
IPI00111584	solute carrier family 25 (mitochondrial carnitine/acylcarnitine translocase), member 20
IPI00230754, IPI00648357, IPI00648119	solute carrier family 25 (mitochondrial carrier oxoglutarate carrier), member 11
IPI00308162	solute carrier family 25 (mitochondrial carrier, Aralar), member 12
IPI00125651	solute carrier family 25 (mitochondrial carrier, adenine nucleotide translocator), member 1
IPI00115564	solute carrier family 25 (mitochondrial carrier, adenine nucleotide translocator), member 4
IPI00127841, IPI00858303	solute carrier family 25 (mitochondrial carrier, adenine nucleotide translocator), member 5; similar to ADP/ATP translocase 2 (Adenine nucleotide translocator 2) (ANT 2) (ADP,ATP carrier protein 2) (Solute carrier family 25 member 5); predicted gene 5529; predicted gene 8429; predicted gene 5256
IPI00885254, IPI00278926	solute carrier family 25 (mitochondrial carrier, citrate transporter), member 1
IPI00117074	solute carrier family 25 (mitochondrial carrier, dicarboxylate transporter), member 10
IPI00756073, IPI00754831, IPI00109275, IPI00856458, IPI00754329	solute carrier family 25 (mitochondrial carrier, glutamate), member 22
IPI00849619, IPI00226854	solute carrier family 25, member 40
IPI00320503	solute carrier family 25, member 42
IPI00387392, IPI00653424	solute carrier family 25, member 46
IPI00221608	sorting and assembly machinery component 50 homolog (S. cerevisiae
IPI00830372, IPI00830269, IPI00170128, IPI00830563	spastic paraplegia 7 homolog (human)
IPI00323129	staphylococcal nuclease and tudor domain containing 1
IPI00648476, IPI00648299, IPI00134131, IPI00648007	sterol carrier protein 2, liver
IPI00230351	succinate dehydrogenase complex, subunit A, flavoprotein (Fp)
IPI00338536	succinate dehydrogenase complex, subunit B, iron sulfur (Ip); similar to succinate dehydrogenase Ip subunit
IPI00831418, IPI00319111	succinate dehydrogenase complex, subunit C, integral membrane protein
IPI00806442	succinate-CoA ligase, GDP-forming, alpha subunit
IPI00261627	succinate-Coenzyme A ligase, ADP-forming, beta subunit
IPI00665996, IPI00459487	succinate-Coenzyme A ligase, GDP-forming, beta subunit
IPI00750524, IPI00113998	sulfide quinone reductase-like (yeast)
IPI00153144	sulfite oxidase
IPI00109109	superoxide dismutase 2, mitochondrial
IPI00114919	suppressor of var1, 3-like 1 (S. cerevisiae)
IPI00119022	tRNA 5-methylaminomethyl-2-thiouridylate methyltransferase
IPI00187402, IPI00651932	tRNA nucleotidyl transferase, CCA-adding, 1
IPI00125652, IPI00828588	thioredoxin 2
IPI00471266, IPI00350590, IPI00126699, IPI00271280	thioredoxin reductase 2; similar to thioredoxin reductase 2
IPI00223216, IPI00762128	thiosulfate sulfurtransferase, mitochondrial
IPI00895166, IPI00112822, IPI00895392, IPI00230512	transcription factor A, mitochondrial

IPI00649594, IPI00848390, IPI00453815, IPI00829226, IPI00881341, IPI00648278	transforming growth factor beta regulated gene 4; similar to Transforming growth factor beta regulated gene 4
IPI00126861	transglutaminase 2, C polypeptide
IPI00165902	translocase of inner mitochondrial membrane 10 homolog (yeast
IPI00134484	translocase of inner mitochondrial membrane 13 homolog (yeast
IPI00885780, IPI00315325, IPI00515156	translocase of inner mitochondrial membrane 22 homolog (yeast
IPI00133068, IPI00859924	translocase of inner mitochondrial membrane 44
IPI00111045	translocase of inner mitochondrial membrane 50 homolog (yeast
IPI00125513	translocase of inner mitochondrial membrane 8 homolog (yeast
IPI00474157, IPI00875326	translocase of outer mitochondrial membrane 40 homolog (yeast
IPI00751137, IPI00377728	translocase of outer mitochondrial membrane 70 homolog A (yeast)
IPI00122499, IPI00885696, IPI00830213	transmembrane protein 143
IPI00130061	tripeptidyl peptidase I
IPI00460008, IPI00111613, IPI00307938	tryptophanyl tRNA synthetase 2 (mitochondrial)
IPI00118384, IPI00828266, IPI00883651	tyrosine 3-monooxygenase/tryptophan 5-monooxygenase activation protein, epsilon polypeptide
IPI00119138	ubiquinol cytochrome c reductase core protein 2
IPI00857580, IPI00109603, IPI00857713, IPI00919103, IPI00859246, IPI00858043, IPI00857602, IPI00230305, IPI00749564	ubiquinol-cytochrome c reductase complex chaperone, CBP3 homolog (yeast)
IPI00653598, IPI00111885	ubiquinol-cytochrome c reductase core protein 1
IPI00133240	ubiquinol-cytochrome c reductase, Rieske iron-sulfur polypeptide 1
IPI00648640, IPI00224210	ubiquinol-cytochrome c reductase, complex III subunit VII
IPI00114153	uncoupling protein 3 (mitochondrial, proton carrier)
IPI00624653	upregulated during skeletal muscle growth 5
IPI00222180	valyl-tRNA synthetase 2, mitochondrial (putative); similar to valyl-tRNA synthetase 2-hk
IPI00230540, IPI00122548, IPI00857067	voltage-dependent anion channel 1
IPI00221369	zinc binding alcohol dehydrogenase, domain containing 2

Mitochondrial proteomic profiling in compensated hypertrophy (CH) and heart failure (HF). Quantitative proteomic analysis was done using the Stable Isotope Labeling by Amino ACids (SILAC) method in mitochondria isolated from the ventricles of sham-operated, CH, and HF animals. Mitochondrial proteins identified in all samples are listed. GOCC annotation in DAVID and the Mitocarta were used to define proteins as mitochondrial.

Supplemental Table 7. Proteins regulated in compensated hypertrophy (CH) and heart failure (HF) samples.

Gene Symbol	Protein Names	CH/CTRL	HF/CTRL
Abhd11	Abhydrolase domain-containing protein 11	1.28	3.45
Nfu1	Putative uncharacterized protein	1.19	2.71
Fahd2a	Fumarylacetoacetate hydrolase domain-containing protein 2A	+1.07	2.02
Abat	4-aminobutyrate aminotransferase	1.84	1.95
Bdh1	3-hydroxybutyrate dehydrogenase	2.74	1.89
Hagh	Hydroxyacylglutathione hydrolase	1.73	1.80
Cltc	Clathrin heavy chain	1.38	1.78
Nln	Neurolysin	1.63	1.65
Slc25a10	Mitochondrial dicarboxylate carrier	1.17	1.55
Rars2	Probable arginyl-tRNA synthetase	1.43	1.52
Cbr2	Carbonyl reductase [NADPH] 2	1.68	1.49
Ccdc58	Coiled-coil domain-containing protein 58	1.51	1.44
Hk1	Hexokinase 1	1.65	1.44
Ctsb	Cathepsin B;Cathepsin B I;Cathepsin B light chain;Cathepsin B heavy chain	1.53	1.43
Slc25a1	Solute carrier family 25	1.75	1.43
Cyb5r3	Cytochrome b5 reductase 3	1.84	1.38
Nudt13	Nucleoside diphosphate-linked moiety X motif 13	1.62	1.37
Acot9	Acyl-coenzyme A thioesterase 9	1.67	1.37
Cyb5r1	NADH-cytochrome b5 reductase 1	1.76	1.37
Cpox	Coproporphyrinogen-III oxidase	1.68	1.33
Hk2	Hexokinase-2	1.69	1.32
Ghitm	Growth hormone-inducible transmembrane protein	1.53	1.31
Gyk	Glycerol kinase	1.54	1.31
Tomm70a	Translocase of outer membrane 70 kDa subunit	1.65	1.28
Glrx	FAD-linked sulfhydryl oxidase ALR	1.69	1.20
Acsf2	Acyl-CoA synthetase family member 2	1.59	1.14
Tmem126a	Transmembrane protein 126A	3.00	1.13
Mrps30	28S ribosomal protein S30	1.54	1.10
Tomm22	Mitochondrial import inner membrane translocase subunit	-1.27	1.02
Slc25a42	Solute carrier family 25 member 42	-1.44	-1.18
Acss3	Acetyl-coenzyme A synthetase 2-like	-1.27	-1.19
Agps	Alkylglycerone phosphate synthase	-1.73	-1.19
Cat	Catalase	-1.37	-1.21
Gstk1	Glutathione S-transferase kappa 1	-1.37	-1.25
Opa3	Optic atrophy 3 protein homolog	1.13	-1.26
Tmem143	Transmembrane protein 143	1.06	-1.26
Cisd1	CDGSH iron sulfur domain-containing protein 1	1.22	-1.26
Acaa2	Acetyl-Coenzyme A acyltransferase 2	-1.32	-1.27
9030617O03Rik	Probable 10-formyltetrahydrofolate dehydrogenase	-1.55	-1.29
Slc25a22	Mitochondrial glutamate carrier 1	-1.39	-1.32
Cox6a2	Cytochrome c oxidase subunit 6A2	-1.38	-1.35
Scp2	Non-specific lipid-transfer protein	-1.33	-1.37
Ak1	Adenylate kinase isoenzyme 1	-1.29	-1.38
Hsd17b4	17-beta-hydroxysteroid dehydrogenase 4	-1.46	-1.38
Ech1	Delta(3,5)-Delta(2,4)-dienoyl-CoA isomerase	-1.47	-1.39
Gpd1	Glycerol-3-phosphate dehydrogenase [NAD+]	-1.35	-1.39
Abcd3	ATP-binding cassette, sub-family D (ALD), member 3	-1.64	-1.41
Acad11	Acyl-CoA dehydrogenase family member 11	-1.66	-1.42
Ppm1k	Protein phosphatase 1K	-1.61	-1.42
Acox1	Acyl-Coenzyme A oxidase 1	-1.71	-1.54
Mdh1	Malate dehydrogenase	-1.51	-1.54
Ehhadh	Enoyl-CoA hydratase/3,2-trans-enoyl-CoA isomerase	-1.36	-1.60
Ldhb	L-lactate dehydrogenase B chain	-1.75	-1.83
Ucp3	Mitochondrial uncoupling protein 3	-1.56	-1.84
Pkm2	Pyruvate kinase isozymes M1/M2;Pyruvate kinase muscle isozyme	-1.10	-1.91

Quantitative proteomic analyses was done using the Stable Isotope Labeling by Amino ACids (SILAC) method in mitochondria isolated from the ventricles of sham-operated, CH, and HF animals. Proteins that exhibited a significant difference in the CH and/or HF models vs. corresponding sham-operated controls as determined using mass spectrometry-based quantitative proteomic analysis (MS/MS processing; Thermo Scientific LTQ Orbitrap Velos) are listed. A cut-off of < -1.25 or > 1.5 FC was used to identify regulated proteins.

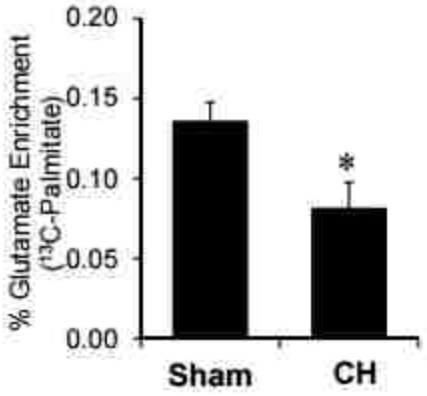

Supplemental Figure 1. Reduced palmitate oxidation in the hypertrophied heart. The relative contribution of palmitate to TCA carbon cycle flux is shown for CH and sham-operated controls. Data are shown as mean ±SEM (n=6, Sham and 7, CH).

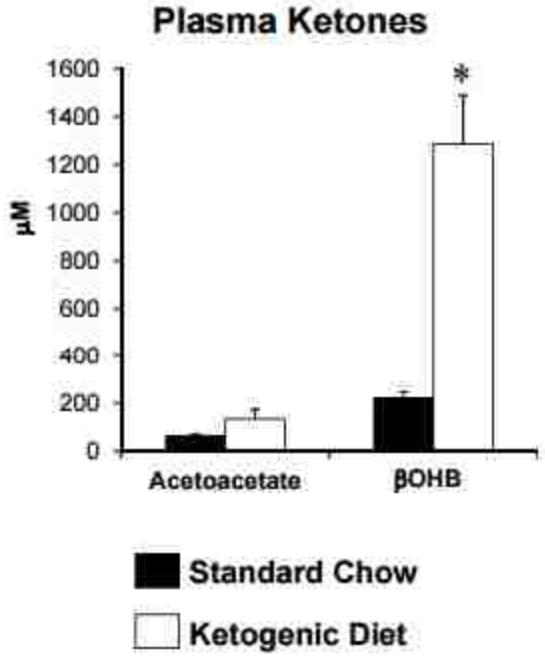

Supplemental Figure 2. Ketogenic diet results in an increase in circulating ketone bodies. Plasma ketone levels measured in wild-type C57BL/6J mice fed a ketogenic diet for 4 weeks compared to control diet fed mice. Bars represent mean ±SEM values (n=6-7 per group) *p<0.05.

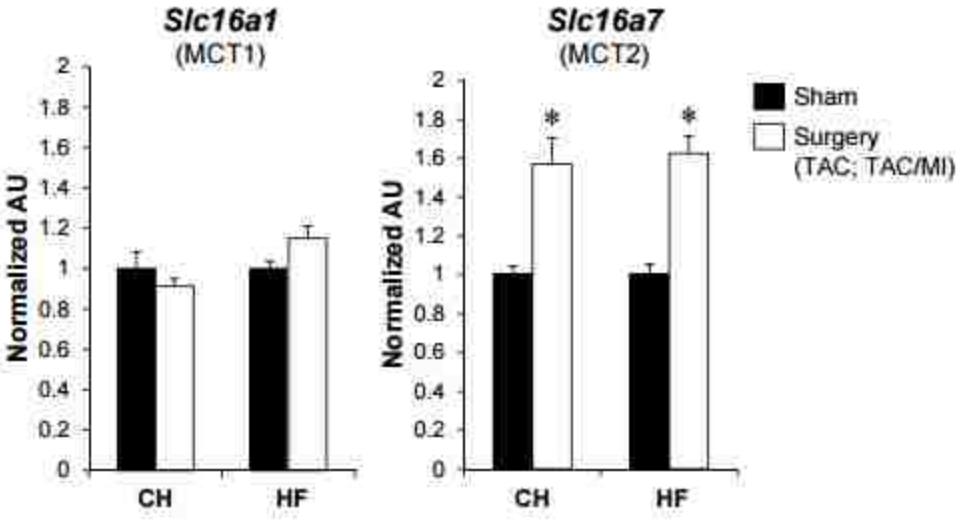

Supplemental Figure 3. *Slc16a1* expression is induced in the hypertrophied and failing mouse heart. *Slc16a1* (MCT1) and *Slc16a7* (MCT2) mRNA levels in cardiac ventricular tissue from mice 4 weeks after sham, TAC (CH), or TAC/MI (HF) surgeries. Samples were taken 24 h (Fasted) after feeding. Expression is normalized to *Rplp0* (36B4). Bars represent mean ±SEM values (n=6-21 per group) *p<0.05.

Supplemental References

1. Pagliarini DJ, Calvo SE, Chang B, et al. A mitochondrial protein compendium elucidates complex I disease biology. Cell. 2008;134:112-123.

2. Shevchenko A, Tomas H, Havlis J, Olsen JV, Mann M. In-gel digestion for mass spectrometric characterization of proteins and proteomes. Nat Protoc. 2006;1:2856-2860.

3. Rappsilber J, Ishihama Y, Mann M. Stop and go extraction tips for matrix-assisted laser desorption/ionization, nanoelectrospray, and LC/MS sample pretreatment in proteomics. Anal Chem. 2003;75:663-670.

4. Cox J, Mann M. MaxQuant enables high peptide identification rates, individualized p.p.b.-range mass accuracies and proteome-wide protein quantification. Nat Biotechnol. 2008;26:1367-1372.

5. Millington DS, Kodo N, Norwood DL, Roe CR. Tandem mass spectrometry: a new method for acylcarnitine profiling with potential for neonatal screening for inborn errors of metabolism. J Inherit Metab Dis. 1990;13:321-324.

6. Jensen MV, Joseph JW, Ilkayeva O, Burgess S, Lu D, Ronnebaum SM, Odegaard M, Becker TC, Sherry AD, Newgard CB. Compensatory responses to pyruvate carboxylase suppression in islet beta-cells. Preservation of glucose-stimulated insulin secretion. J Biol Chem. 2006;281:22342-22351.

CHAPTER FIVE:
CONSEQUENCES OF INCREASED KETONE OXIDATION IN HEART FAILURE

Introduction

Heart failure (HF) is a significant public health problem that is growing as a greater proportion of our population ages. Despite current treatments, ~43% of patients die within five years of initial hospitalization (1). Heart failure prevalence is predicted to increase 46% between 2012 and 2030. Realization of this projection amounts to diagnosed heart failure in over 8 million adults (2). Thus, the expectation of pervasive critical illness in the near future necessitates rapid development of therapies to prevent and treat heart failure.

Heart failure refers to a syndrome in which the heart cannot adequately pump blood throughout the body. A multitude of studies indicate that there is a fundamental imbalance in energy transduction to adenosine triphosphate (ATP) and demand in the failing heart. In the healthy adult heart, fatty acid oxidation (FAO) accounts for 70-90% of ATP production (3). The failing heart, though, exhibits a dramatically altered fuel substrate preference. In HF, FAO rates decline concurrent with a decrease in FAO enzyme expression (4). Increased contribution to ATP production from alternative fuel substrates accompanies diminution of FAO. The failing heart, in large part due to the reduction of FAO, increasingly relies on glucose to generate ATP. Many in the field believe that this fuel shift with increased reliance on glucose as a substrate is inadequate to meet the energy demands of the failing heart, further contributing to cardiac dysfunction and effectively creating a “vicious cycle”.

As we have recently described, there is also an increased reliance on ketone metabolism in heart failure (5, 6). Another group concurrently arrived at the same conclusion in human HF, demonstrating translational relevance of our findings. They reported an increase in 3-hydroxybutanoyl-CoA (CoA ester equivalent of C4-OH carnitine) in human HF. Serum ketone levels and decreased levels of ketones in the myocardium were also observed in HF patients. Importantly, they found increased expression of 3-hydroxybutyrate dehydrogenase, type 1 (BDH1) in the failing human heart, confirming our findings in the experimental model of HF (6).

While these collective results demonstrate that ketone oxidation is increasingly relied on in HF, the implications of this fuel substrate switch are more enigmatic. Specifically, it is unknown as to whether the switch to ketone bodies as a fuel is an adaptive response providing an alternative fuel source when FAO is depressed. To address this key question, we sought to investigate the functional impact of ketone utilization in the failing heart. To this end, we generated and assessed a novel cardiac-specific (cs) BDH1 knockout (KO) mouse line. We confirmed that csBDH1 KO mice are unable to produce acetyl-CoA from 3-hydroxybutyrate oxidation in the heart. In response to transverse aortic constriction with a small apical myocardial infarction (TAC/MI), BDH1 KO mice display exaggerated pathological remodeling with severely depressed left ventricular systolic function and dilatation. Given these results, we hypothesize that increased ketone oxidation is an adaptive response in heart failure.

Results

Generation of Cardiac-specific BDH1 KO Mouse

Mice harboring a “floxed” *Bdh1* gene were crossed to mice with Cre-recombinase (Cre) expression regulated by the myosin heavy chain, α isoform (αMHC) gene promoter (αMHC-Cre mice) to produce csBDH1 KO mice (Figure 12A). This strategy deletes exons 3 and 4, which encode the majority of the catalytic domain (7). Subsequent reverse transcription quantitative polymerase chain reaction (RT-qPCR) analysis confirmed loss of *Bdh1* (Figure 12B, left). Likewise, western blot shows near complete knockout of BDH1 protein in hearts of BDH1 KO mice (Figure 12B, right).

BDH1 KO mice did not show any difference in weight, growth rate, or ventricular weight (vw)/ body weight (bw) compared to WT (data not shown). There was also no difference in absolute heart weight (HW) or cardiac function as determined by echocardiograph (echo) (data not shown). Levels of circulating 3-hydroxybutyrate (3OHB) were measured in fed and fasted states and found to be unchanged in BDH1 KO mice compared to WT controls (data not shown). However, assessment of the Mendelian ratio of the crosses revealed a small but significantly lower than predicted number of csBDH1 KO mice at time of weaning (Table 1). These latter results suggest some perinatal or postnatal lethality. We next assessed substrate utilization in the csBDH1 KO mouse heart using nuclear magnetic resonance spectroscopy (NMR). Hearts were isolated and perfused in the Langendorff mode with ^{13}C-labeled R-β-hydroxybutyrate.

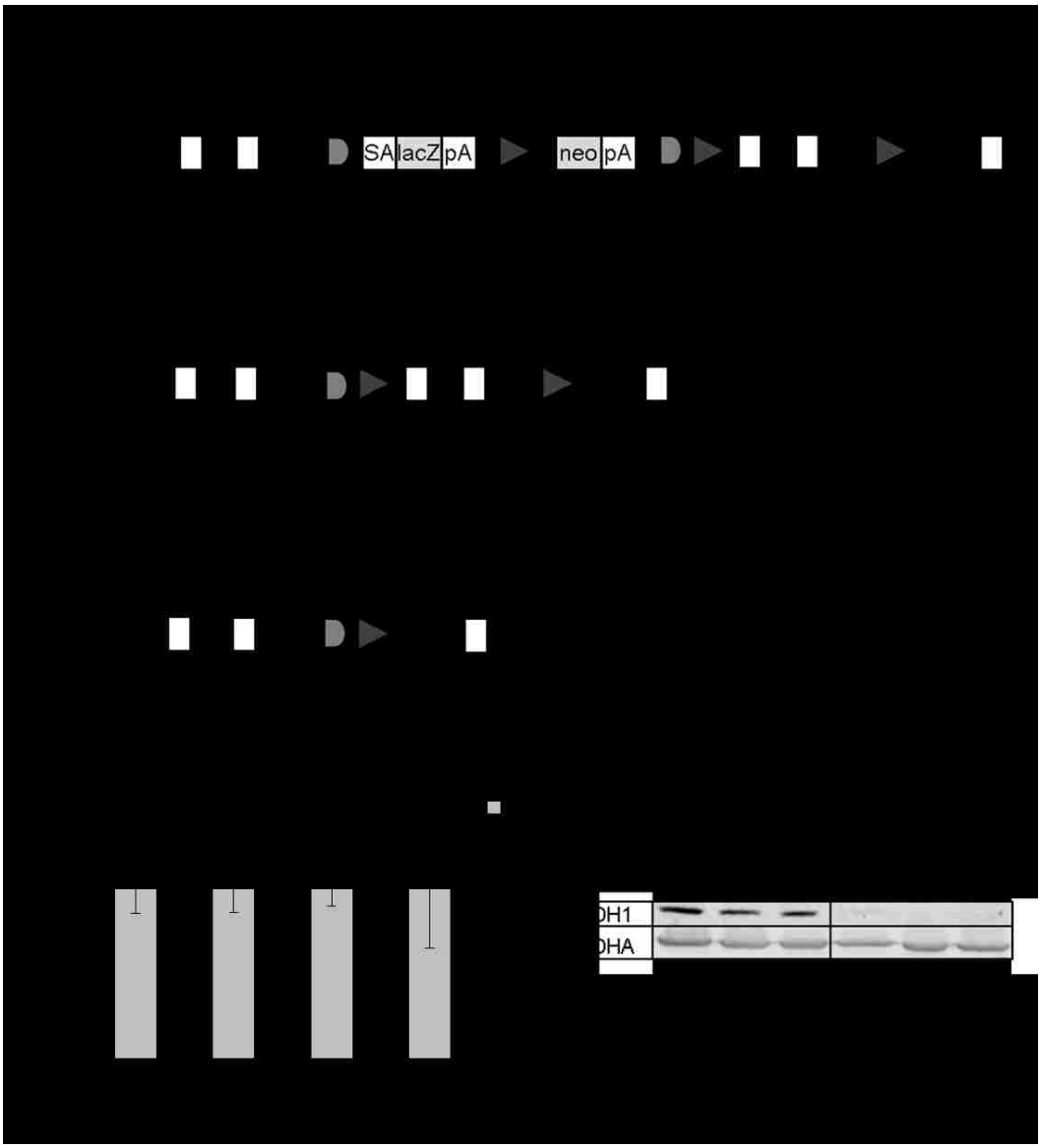

Figure 12. Generation of cardiac-specific (cs) BDH1 KO mice.

(A) Schematic of design for generating csBDH1 KO mice. ES cells with *Bdh1 targeting (Bdh1-)* construct (top row) were injected into blastocysts to generate founder mice. *Bdh1*$^{-}$ construct contains FRT sites flanking cassette with SA sequence, reporter genes *lacZ* and *neo*, and pA signals. Start sites (ATG) for transcript variants of *Bdh1* are indicated. Loxp sites flank *Bdh1* exons 3 and 4. Exon 5-7 are in construct but not shown on diagram. Founder mice mated with Flp mice to produce progeny with *Bdh1*^{flox} *(Functional)* alleles. *Bdh1*^{flox} mice were subsequently mated with αMHC-Cre mice. Offspring from this pairing either inherited Cre-recombinase transgene (Cre^{+}) resulting in αMHC-driven Cre expression and knockout of *Bdh1* or did not (Cre^{-}). The *Bdh1*^{rec} *(Null)* schematic (bottom row) shows the BDH1 KO allele, which has lost exon 3 and 4. RT-qPCR primer sites indicated as P1 (E1), P2-3 (E2-3), P3-4 (E3-4). **(B)**(Left) *Bdh1* mRNA in cardiac tissue of WT (grey) and KO (black) mice . Expression corrected to *36b4* and normalized to WT (=1). Each pair of bars represents the amplicon region of qPCR primer pairs; exon 1 (E1), exon 2-3 (E2-3), exon 3-4 (E3-4), and exon 7 (E7). E2-3 and E3-4 primers were designed to span introns. E1 and E7 were designed within respective exons. Bars represent mean ± SEM (n = 6-12); *p-value<0.05 WT vs. KO with Mann-Whitney test. (Right) Western blot using protein from hearts of *Cre*$^{-}$ *Bdh1*^{flox} (WT) and *Cre*$^{+}$ *Bdh1*^{flox} (KO) mice (n=3). Antibodies used are labeled on the left. Anti-SDHA was used as a mitochondrial protein-loading control. Cs,cardiac specific; BDH1, 3-hydroxybutyrate dehydrogenase, type 1 ; KO, knockout; ES, embryonic stem; FRT, flippase recognition target; SA, splice acceptor; neo, neomycin resistance gene; pA, poly-A; loxp, Locus of Crossover in P1; Flp, Flp1 recombinase; αMHC, myosin heavy chain, a isoform; mRNA, messenger ribonucleic acid; WT, wild-type; 36b4, Ribosomal Protein Lateral Stalk Subunit P0; qPCR, quantitative polymerase chain-reaction; SDHA, succinate dehydrogenase, subunit A

Table 1. Mendelian ratios for offspring from *Cre*$^{-}$*, Bdh1* $^{f/f}$ crossed with *Cre*$^{+}$*, Bdh1* $^{f/f}$.

Cre +/ -	Gender	Number of Mice	Expected Percentage	Actual Percentage
+	M	26	25%	20%
+	F	21	25%	17%

Chi squared =9.031 with 3 degrees of freedom. Two-tailed p-value=0.0289

BDH1 KO hearts were shown to completely lack the ability to form acetyl-CoA from R-β-hydroxybutyrate (Figures 13A,B). Consistent with the substrate oxidation data, levels of 3OHB were markedly increased in csBDH1 KO hearts (Figure 13C).

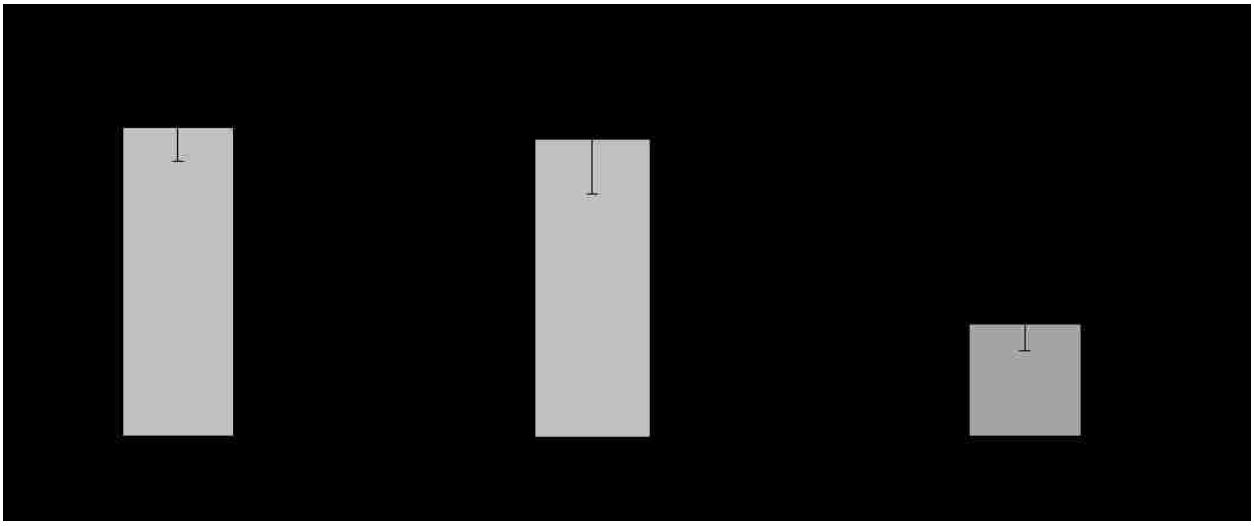

Figure 13. csBDH1 KO mice are unable to oxidize 3OHB.

(A) The fraction of acetyl-CoA formed from ^{13}C-labeled 3OHB is shown. **(B)** The percent of glutamate derived from ^{13}C-labeled 3OHB is shown. **(C)** The total amount of 3OHB in ventricular tissue normalized to wet weight from Sham WT and Sham KO is shown. Bars represent mean ± SEM (n = 3-5); *p-value<0.05 WT vs. KO using Welch's t-test. Cs,cardiac specific; BDH1, 3-hydroxybutyrate dehydrogenase, type 1 ; KO, knockout; 3OHB, 3-hydroxybutyrate; Fc, fractional contribution; WT, wild-type; N.D., not detected; FE, fractional enrichment

BDH1 deficiency results in worsened pathologic cardiac remodeling in context of a pressure-overload stress

We next sought to address the impact of lost ketone oxidation capacity for cardiac response to a pathophysiological stress known to cause heart failure. For these studies, BDH1 WT and KO mice were subjected to (TAC/MI) (8). As we previously reported, the TAC/MI procedure results in left ventricular hypertrophy (LVH) and remodeling in wild-type mice (8). There was no significant difference in mortality rates between the BDH1 WT and KO mice up to 4-weeks following surgery (Figure 14). Echocardiographic analyses were conducted 4-weeks post-surgery to assess cardiac function and remodeling (Table 2). Although the degree of LVH did not differ (Figure 15A), ejection fraction was significantly lower in the BDH1 KO compared to WT controls (Figure 15B). Additionally, end-systolic volume (ESV) and end-diastolic volume (EDV) were both significantly elevated in the BDH1 KO failing heart compared to WT controls (Figures 15C-D).

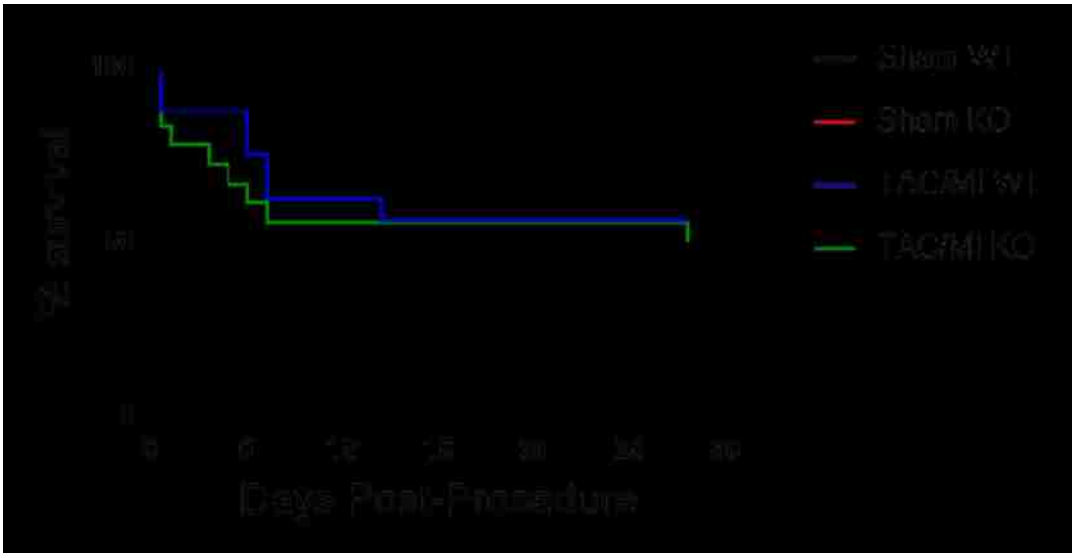

Figure 14. Survival rates following TAC/MI.

Kaplan-Meier plot shows percent of mice surviving (y-axis) at specified time-points (x-axis). Sham WT (black line) n=5, sham KO (red line) n=6, TAC/MI WT (blue line) n=16, and TAC/MI KO (green line) n=18 are shown. Log-rank (Mantel-Cox) test used to determine significance. TAC,transverse aortic constriction; MI, myocardial infarction; WT, wild-type; KO, knockout

Table 2. Echocardiography data 4-weeks post-TAC/MI or sham procedure

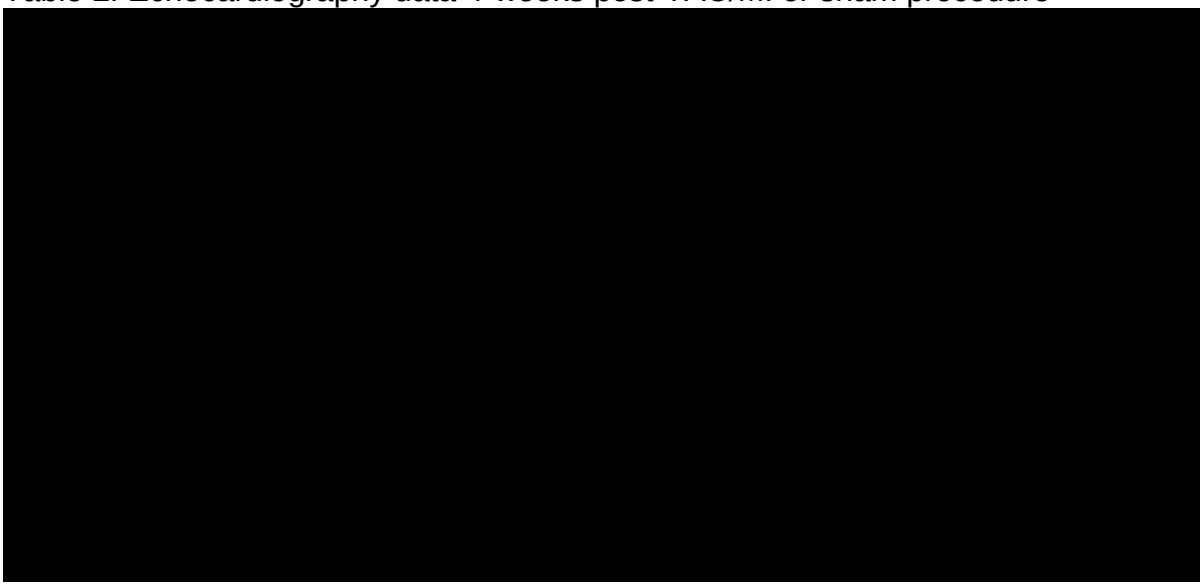

Mean +/- SEM is shown. *p<0.05 WT vs. KO, #p<0.05 Sham vs. HF using ANOVA with Tukey's post-hoc analysis. TAC, transverse aortic constriction; MI, myocardial infarction; HR, heart rate; BW, body weight; Ao, aorta; Prox, proximity; VTI, velocity-time integral; EDV, end diastolic volume; ESV, end systolic volume; EF, ejection fraction; SWMI, segmental wall motion score index; WT, wild-type; HF, heart failure; KO, knockout

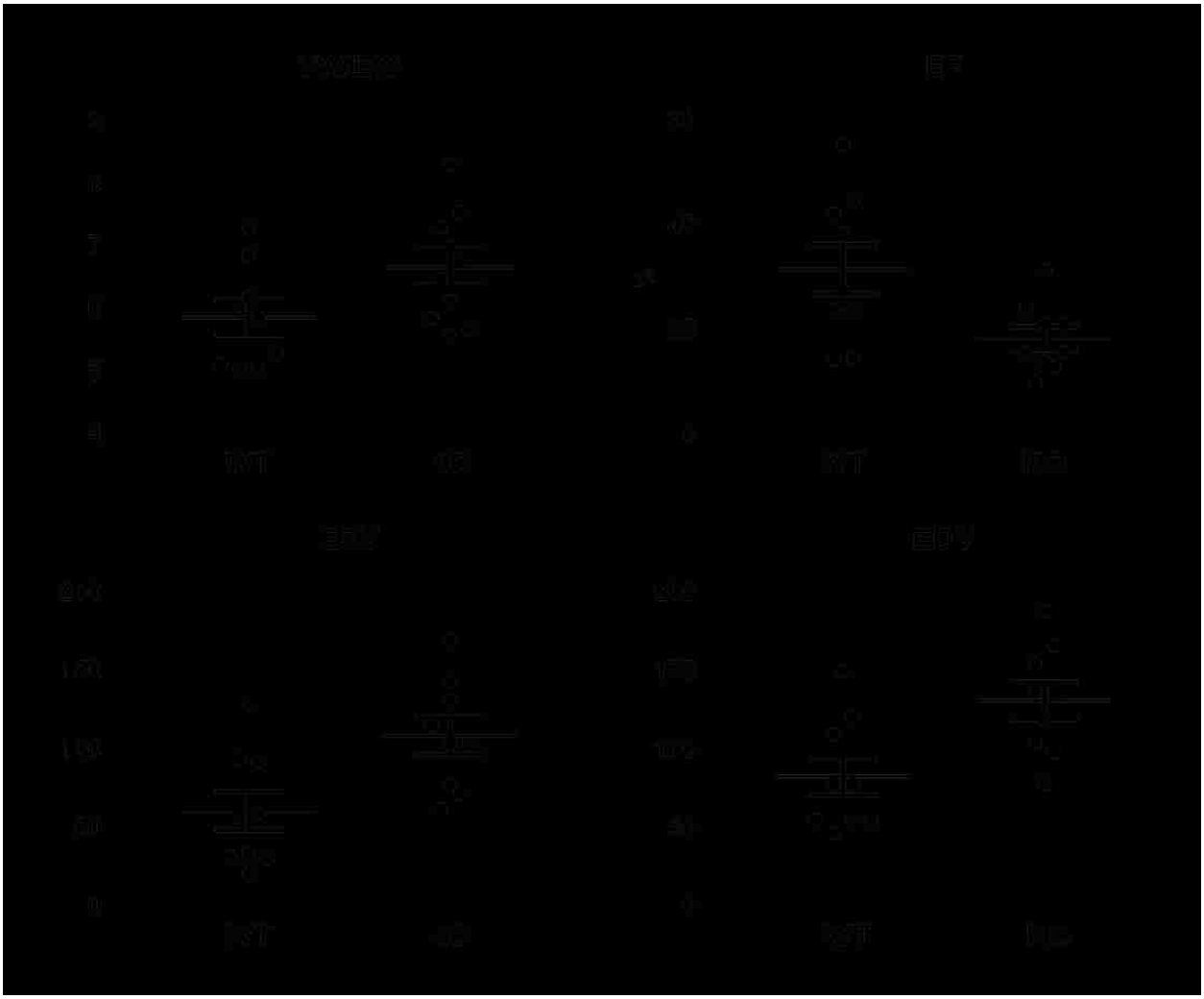

Figure 15. BDH1 KO mice exhibit severe pathological remodeling.

Scatter plots for cardiac remodeling parameters of each TAC/MI mouse that survived to echo (28 days post-surgery). **(A)** VW/BW shown as ratio of (mg/g). **(B)** EF shown as % **(C)** ESV graphed as volume (υl) **(D)** EDV graphed as volume (υl). Values are mean +/- SEM, *p<0.05 WT vs. KO, using ANOVA with Tukey's post-hoc. BDH1 indicates 3-hydroxybutyrate dehydrogenase, type 1 ; KO, knockout; WT, wild-type; TAC, transverse aortic constriction; MI, myocardial infarction; echo, echocardiograph; VW, ventricular weight; BW, body weight; EF, ejection fraction; ESV, end systolic volume; EDV, end diastolic volume

Known gene markers of cardiac hypertrophy and failure were assessed in the hearts of experimental animals. In the TAC/MI groups, cardiac pathological hypertrophy gene markers, encoding contractile proteins and natriuretic peptides, were increased in

the wild-type mice and to a greater extent in csBDH1 KO mice (Figure 16A). Conversely, a similarly exacerbated pathological gene signature was observed for ATPase sarcoplasmic/endoplasmic reticulum Ca^{2+} transporting 2 (*Atp2a2*) and troponin 1, cardiac type (*Tnni3*), whose transcript levels are known to decrease in HF (Figure 16B). Interestingly, some gene expression changes were noted in the sham treated BDH1 KO compared to the BDH1 WT sham mice. Specifically, myosin heavy chain beta isoform (*Myh7*) levels were increased significantly and *Tnni3* levels were significantly decreased in sham BDH1 KO mouse hearts (Figure 16B). In addition, expression of genes involved in fatty acid utilization, which are characteristically downregulated in heart failure (9), was suppressed to a greater extent in csBDH1 KO hearts (Figure 16C). Lastly, we found an increase in BDH1 expression in the WT failing heart, consistent with our previous findings (Figure 16C) (5). Collectively, these data demonstrate that the csBDH1 KO mice exhibit exaggerated cardiac remodeling in response to TAC/MI.

Discussion

Recently, our lab identified an increased reliance on ketone body oxidation in a mouse model of early-stage HF (5). Another group arrived at the same conclusion in human HF (6). However, the consequences of increased ketone oxidation in HF are not well-defined.

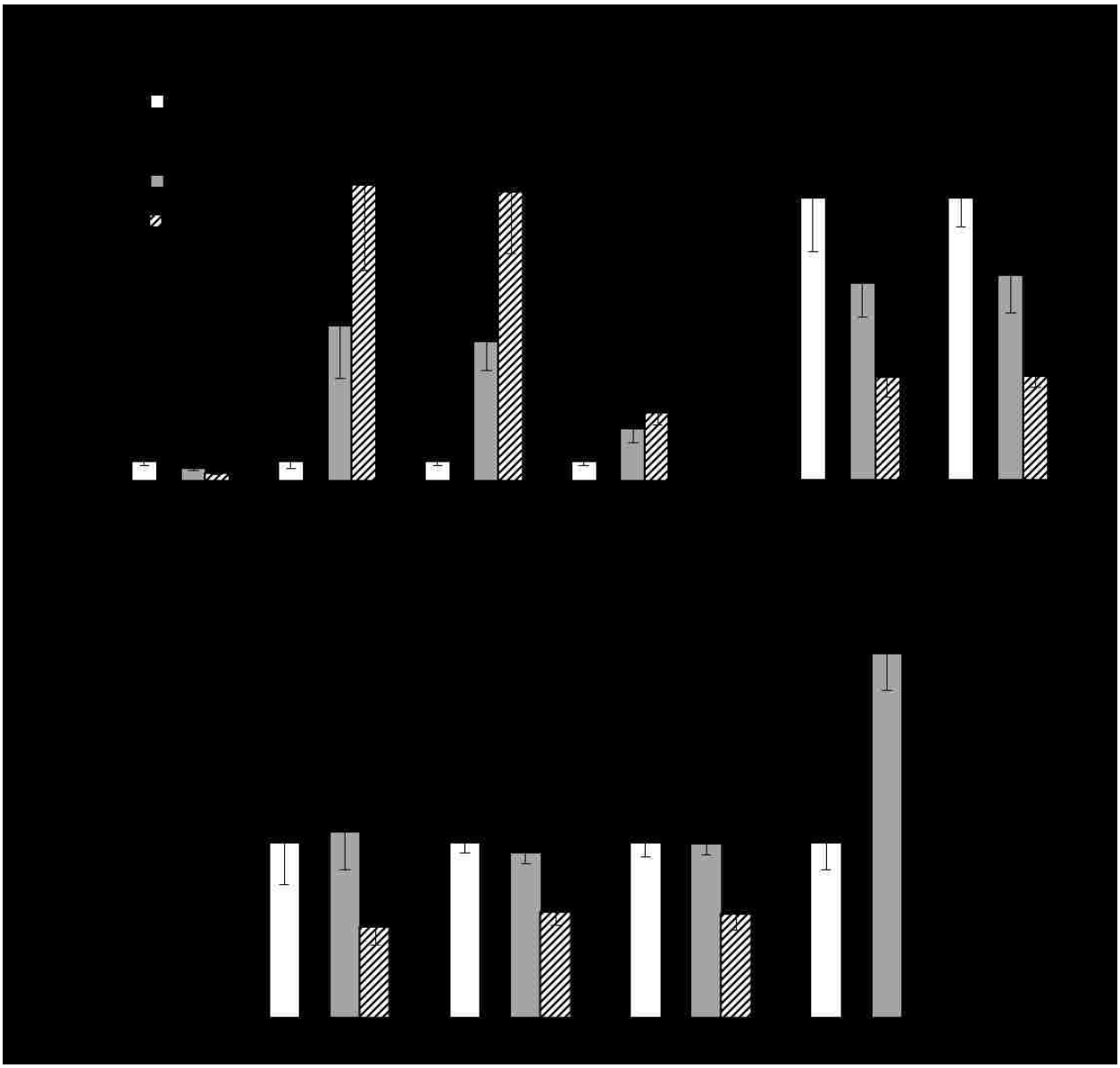

Figure 16. The gene expression signature indicates severe pathological remodeling in the BDH1 KO mouse.

mRNA expression levels in cardiac tissue of Sham WT (white), Sham KO (black), TAC/MI WT (grey) and TAC/MI KO (stripes) mice normalized to *36b4*. **(A)** mRNA levels of *Myh6*, *Myh7*, *Nppa*, *and Nppb* are shown. **(B)** Excitation-contraction coupling *Atp2a2* and *Tnni3* mRNA levels shown. **(C)** Oxidative phosphorylation genes *Ppara*, *Acadm*, *Acsl1*, and *Bdh1* mRNA levels shown. All gene expression levels are normalized to Sham WT (=1). Bars represent mean ± SEM (n=5-16); *p-value<0.05 Sham vs. TAC/MI; #p-value<0.05 WT vs. KO Mann-Whitney. BDH1, 3-hydroxybutyrate dehydrogenase, type 1; KO, knockout;; WT, wild-type; 36b4, Ribosomal Protein Lateral Stalk Subunit P0; Myh6, myosin heavy chain 6; Myh7, myosin heavy chain 7; Nppa, natriuretic peptide A; Nppb, natriuretic peptide B; Atp2a2, ATPase sarcoplasmic/endoplasmic reticulum Ca2+ transporting 2; Tnni3, Troponin I3, cardiac type; Ppara, peroxisome proliferator-activated receptor alpha; Acadm, medium-chain acyl-CoA dehydrogenase; Acsl1, long chain fatty-acid CoA ligase 1

Notably, though, a study using mice with targeted deletion of the gene encoding succinyl-CoA-3-oxaloacid CoA transferase (SCOT) in the heart, which catalyzes the acetoacetate→acetoacetate-CoA reaction, advances pathological progression of pressure-overload induced HF (10). Other investigations report indirect correlations between circulating ketone levels and cardiac health.

Recently, the results of trials with sodium-glucose transporter-2 inhibitors (SGLT2i), new glucose-lowering agents, are of significant interest and may relate to our work. The EMPA-REG OUTCOME trial was originally conducted to determine the cardiovascular effects of empagliflozin, which at the time was indicated as a treatment for type 2 diabetes. This massive study followed 7020 patients for a median of 3.1 years. The results showed a 38% relative risk reduction for cardiovascular related death in patients given empagliflozin (11). Empagliflozin treatment also commonly causes elevated circulating ketone levels (12). The precise reasons for improved cardiovascular mortality are not known, but the correlation between increased ketone levels and cardiac benefits has provoked intense interest in cardiac ketone metabolism (13).

In this study, we sought to directly determine the consequences of increased ketone oxidation in the failing heart. To this end, we generated a cardiac-specific (cs) BDH1 KO mouse. The csBDH1 KO adult mouse exhibits no overt baseline phenotype other than a possible lethality of incomplete penetrance. We suspect that perinatal deaths may account for this difference due to the importance of myocardial ketone oxidation in cardiac maturation (14). Studies monitoring viability of pups at birth are underway to establish if death occurs in neonates disproportionately.

Although it is widely believed that 3-hydroxybutyrate is oxidized solely by BDH1, we sought to verify that csBDH1 KO hearts would be unable to oxidize 3-hydroxybutyrate (7). We reasoned that if an alternate mechanism is capable of oxidizing 3-hydroxybutyrate in absence of BDH1, our experimental premise of eliminating myocardial 3-hydroxybutyrate oxidation by KO of BDH1 would be erroneous. We confirmed the necessity of BDH1 for 3OHB oxidation. Given the degree of compensation typically observed in metabolic enzymes, it is somewhat surprising that no other enzyme accommodates 3OHB oxidation in the BDH1 KO heart (15). Whether BDH1 remains necessary for terminal ketone oxidation with varying substrate concentrations is a question addressed in ongoing experiments. The complete absence of compensation combined with the lack of evident defects in the csBDH1 KO mouse suggests that, at least in basal conditions, cardiac ketone oxidation is not essential for proper function of the adult heart. Indeed, most studies find ketone bodies contribute minimally to normal cardiac energy production (14). Contrary to the aforementioned ostensible insignificance, though, we observed ~40% of the acetyl-CoA produced in the perfusion experiments with BDH1 WT hearts originated from 3-hydroxybutyrate.

Similar experiments using labeled palmitate are planned to assess how absence of ketone oxidation affects FAO. Based on existing literature, we expect fatty acids will have an increased contribution to the acetyl-CoA pool in absence of BDH1 (14). Given that the normal heart generates 70-90% of its ATP from FAO; one could speculate the heart’s capacity to oxidize ketones “on demand” is insurance for periods of nutritive stress (3). The fact that we observe accumulation of 3OHB in the hearts of BDH1 KO

mice suggests continuous 3OHB import irrespective of oxidative capacity further supporting the notion that the heart exists in a perpetual state of preparedness.

The small contribution of 3OHB to the glutamate pool in the csBDH1 KO also provides insight into potential fates of excessive 3OHB. It appears that when the heart is completely prevented from oxidizing 3-hydroxybutyrate, some of the ketone enters the TCA cycle via anaplerosis subverting acetyl-CoA production. To provide further understanding of the fate of accumulated 3OHB in the heart, we are conducting unbiased metabolomics with csBDH1 KO hearts and WT counterparts.

When subjected to TAC/MI surgery, csBDH1 KO mice fare worse than BDH1 WT mice. The significant differences in ejection fraction, ESV, and DSV all demonstrate more severe remodeling in hearts unable to oxidize 3OHB. The gene expression data further corroborates the conclusion that csBDH1 KO mice are at a disadvantage in HF. The combined results from the TAC/MI experiments strongly suggest that the shift to increased myocardial ketone oxidation in HF is an adaptive phenomenon.

The results also raise the important question: what is the basis for the cardiac remodeling phenotype in csBDH1 KO mice? Two primary possibilities are currently being considered to explain the adaptive nature of increased ketone oxidation in HF (Figure 17). Notably, these hypotheses are not mutually exclusive. The simplest explanation for the more severe HF pathology in the csBDH1 KO is that 3OHB oxidation provides additional ATP production when FAO is downregulated. Accordingly, the worsened heart failure phenotype of csBDH1 KO mice could reflect fuel and, thus, energy “starvation”. The other possibility is that loss of BDH1 leads to accumulation of

toxic metabolites related to an elevation in levels of 3-hydroxybutyrate in the myocardium. If this is the causation for the phenotype observed in csBDH1 KO mice post TAC/MI, a number of mechanisms could be factors.

Increased levels of 3-hydroxybutyrate or its downstream metabolites could have a number of ramifications. There is evidence implicating 3OHB in a variety of cellular processes including: redox homeostasis, differentiation, signaling, inflammation, oxidative stress, epigenomic regulation and other post-translational modification of proteins (14). BDH1 KO may effectively poison the cell due to the aberrant effects caused by accumulating 3OHB. Given that BDH1 catalyzes the oxidation of 3-hydroxybutyrate and simultaneously reduces NAD^+ to form NADH, it is possible disturbing this reaction could affect intracellular redox state (14). This possibility will be addressed with experiments measuring the NAD^+ and NADH concentrations in normal and failing hearts of WT and csBDH1 KO mice.

From a mechanistic standpoint, it will be important to distinguish between the “energy starvation” and “metabolite toxin” hypotheses. One approach is to assess the response of csSCOT KO mice to TAC/MI. If the mice do not exhibit a heart failure phenotype, the “metabolite toxin” theory would be implied. Conversely, if csSCOT KO mice phenocopy the csBDH1 KO mice, the “energy starvation” model seems likely.

Given the interest in SGLT2i-mediated positive outcome on cardiovascular events in patients and the potential connection to ketone metabolism, we are planning studies using SGLT2i in our mouse model of HF. These studies will first determine if SGLT2i treatment of non-diabetic mice results in elevated levels of ketones. Once this

determination is made, we will treat TAC/MI mice with SGLT2i and assess their outcome. Follow-up experiments combining SGLT2i with csBDH1 KO and csSCOT KO mice in HF are also planned. This research will elucidate, at least in part, the role of ketone oxidation in the failing heart and potentially provide insight into the cardio-protective effects of empagliflozin.

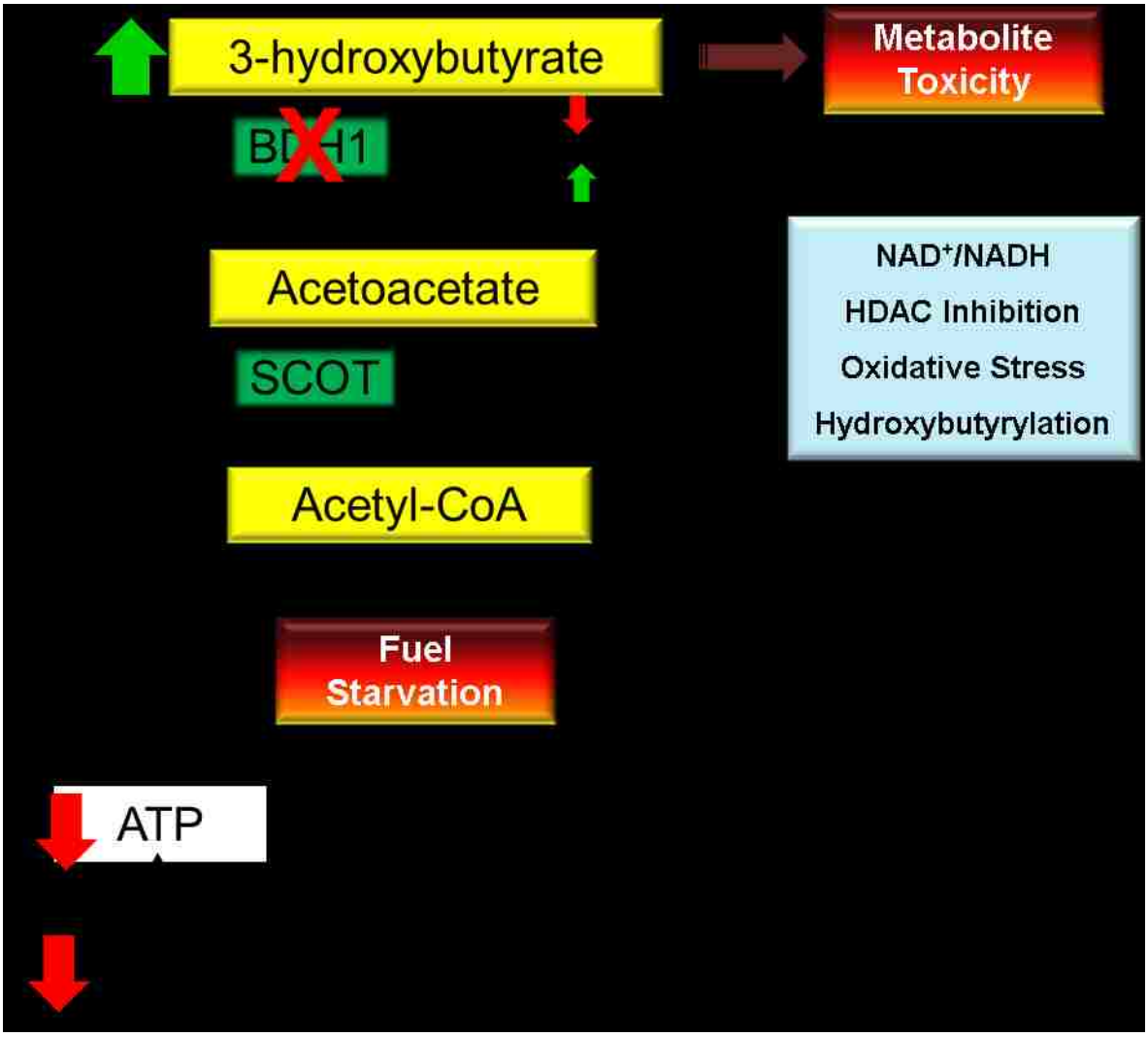

Figure 17. Proposed models for cardiac remodeling in csBDH1 KO mice.

BDH1, 3-hydroxybutyrate dehydrogenase, type 1; NAD^+, nicotinamide adenine dinucleotide; NADH, nicotinamide adenine dinucleotide plus hydrogen; SCOT, succinyl-CoA:3-ketoacid CoA transferase; ATP, adenosine triphosphate; PCr, phosphocreatine; HDAC, histone deacetylase

Methods

Animal Studies

All experiments performed with animals were conducted with protocols approved by Institutional Animal Care and Use Committee at Sanford Burnham Prebys Medical Discovery Institute at Lake Nona. Studies were performed on male C57BL/6N mice 6 to 12 weeks of age on standard chow.

Cardiac specific BDH1 Knockout Mouse Production

We used the αMHC-Cre recombinase system to make an inducible cardiac myocyte specific *Bdh1* knockout mouse (Figure 12). The engineered *Bdh1*$^{-}$ construct contains a FRT flanked cassette comprised of SA, lacZ, and pA sites. Loxp sites flank *Bdh1* exons 3 and 4 (Figure 12A, top). Subsequent mating of *Bdh1*$^{-}$ mice with Flp mice produced progeny with *Bdh1*^{flox} alleles which encode functional BDH1 (Figure 12A, middle). We backcrossed the *Bdh1*^{flox} mice with wild-type C57BL/6N (BL6N) mice to obtain *Bdh1*^{flox} mice on a BL6N genetic background. Final breeding pairs consisted of a *Bdh1*^{flox} BL6N mouse and a hemizygous *αMHC-Cre* BL6N mouse. The litters from final breeding pairs included mice with floxed *Bdh1* allele either with (Cre^{+}) or without (Cre^{-}) (Figure 1A, bottom).

Genotyping

Ear punch samples from 4 week old mice at onset of weaning were used for DNA extraction. DNA was extracted by adding 100ul 25mM NaOH, 0.2mM EDTA pH 12,

heating at 95C for 20mins, then adding 100ul 40mM Tris pH 5 to neutralize. Samples were used immediately following extraction or stored at 4°C. PCR solution used 1μl of extracted DNA with appropriate primers and Tm as listed. PCR products were analyzed using standard gel electrophoresis (1.2% for *Bdh1*, 1.5% *Nnt*, *2*% for *Cre*). Genotyping primers are listed in Table 3.

Table 3. Genotyping Primers

Bdh1 Fwd: TGCAGGAATCAGTGCTCTCTCCTAG
Bdh1 Rev: GGTGTCAGGGCTGAAGGATG
Tm=58°C
Cre Fwd: CCGGTGAACGTGCAAAACAGGCTCTA
Cre Rev: CTTCCAGGGCGCGAGTTGATAGC
Tm=60°C
Nnt Fwd: GTA GGG CCA ACT GTT TCT GCA
Nnt WT Rev: GGG CAT AGG AAG CAA ATA CCA
Nnt MUT Fwd: GTG GAA TTC CGC TGA GAG AAC
Tm=60°C

Heart failure model

HF model was achieved by surgical application of transverse aortic constriction combined with a small apical myocardial infarct (TAC/MI) as described previously (8). Mice were subject to echocardiograph and harvested 28 days post-operation. Hearts were immediately excised from mice deeply anesthetized with pentobarbital. Atriums were removed and ventricles immediately frozen in liquid nitrogen (LN_2). Samples were stored at -80°C until use.

RNA Isolation

One-third of the pulverized heart was partitioned into a Precellys homogenization tube on ice. After addition of 700μl of QIAzol Lysis Reagent to the samples they were secured in the pre-chilled Precellys Homogenizer. The homogenization protocol used three cycles of 20 seconds 6800rpm agitation followed by a 10 second pause. The remainder of the RNA isolation followed the standard Qiagen miRNeasy kit protocol. Isolated RNA was diluted to 0.1ug/μl with ddH2O

RT-qPCR

A two-step protocol was used to assess mRNA expression. For cDNA synthesis, 0.5μg of RNA was used with Agilent Genomics AffinityScript cDNA Synthesis Kit according to manufacturer instructions. Synthesized cDNA was used with Brilliant III Ultra-Fast SYBR Green QPCR Master Mix for qPCR performed in triplicate using Roche LightCycler 480 Instrument II and primers for specific genes. Gene expression was normalized to levels of *36b4*. Primers used are shown in Table 4.

Table 4. . RT-qPCR Primers

Gene Target		Sequence 5'->3'
Bdh1 Exon 3-4	Fwd	TCAGGCAGATGCGGCTA
	Rev	ATGCTTGGCCAGTGAGAAC
36b4	Fwd	TGGAAGTCCAACTACTTCCTCAA
	Rev	ATCTGCTGCATCTGCTTGGAG
Acadm	Fwd	ATGACGGAGCAGCCAATGAT
	Rev	TAATGGCCGCCACATCAGAG
Acsl1	Fwd	CGCCCATATGTTTGAGACCG
	Rev	GTCGTCCATAAGCAGCCTGA
Atp2a2	Fwd	GGAGATGCACCTGGAAGACT
	Rev	CCACACAGCCGACGAAA
Nppa	Fwd	AGTGCGGTGTCCAACACAGA
	Rev	GACCTCATCTTCTACCGGCATCT
Myh7	Fwd	GCCAACTATGCTGGAGCTGATGCC
	Rev	GGTGCGTGGAGCGCAAGTTTGTCATAAG
Tnni3	Fwd	TCTGCCAACTACCGAGCCTAT
	Rev	CTCTTCTGCCTGTCGTTCCAT
Nppb	Fwd	GCTGCTTTGGGCACAAGATAG
	Rev	GCAGCCAGGAGGTCTTCCTA
Ppara	Fwd	ACTACGGAGTTCACGCATGTG
	Rev	TTGTCGTACACCAGCTTCAGC
Myh6	Fwd	GGTCCACATTCTTCAGGATTCTCT
	Rev	CCTTCTCTGACTTTCGGAGGTACT

.

Metabolite Analysis

3-hydroxybutyrate measurements in the heart were obtained from analysis of organic acids using methods described previously (5, 16).

Substrate Oxidation Measurements

Mice were heparinized (100 U) by intraperitoneal (IP) injection and anesthetized with 85 mg/kg ketamine and 12 mg/kg xylazine. Following sacrifice, hearts were isolated and

perfused with a modified Langendorff perfusion protocol (10mM glucose, 0.5mM, sodium D-3-hydroxybutyrate-2,4-$^{13}C_2$, 1mM lactate, 0.4mM 1:3 palmitate/BSA). Following each perfusion, hearts were snap frozen with liquid nitrogen–cooled tongs. NMR spectroscopy was used to quantify the fractional contribution (Fc) of acetyl-CoA and fractional enrichment (FE) of glutamate produced from labeled ketone.

References

1. Benjamin EJ, Blaha MJ, Chiuve SE, et al. Heart Disease and Stroke Statistics-2017 Update: A Report From the American Heart Association. Circulation. 2017;

2. Mozaffarian D, Benjamin EJ, Go AS, et al. Heart Disease and Stroke Statistics-2016 Update: A Report From the American Heart Association. Circulation. 2016;133(4):e38-60.

3. Lopaschuk GD, Jaswal JS. Energy metabolic phenotype of the cardiomyocyte during development, differentiation, and postnatal maturation. J Cardiovasc Pharmacol. 2010;56(2):130-40.

4. Taegtmeyer H, Overturf ML. Effects of moderate hypertension on cardiac function and metabolism in the rabbit. Hypertension. 1988;11(5):416-26.

5. Aubert G, Martin OJ, Horton JL, et al. The Failing Heart Relies on Ketone Bodies as a Fuel. Circulation. 2016;133(8):698-705.

6. Bedi KC, Snyder NW, Brandimarto J, et al. Evidence for Intramyocardial Disruption of Lipid Metabolism and Increased Myocardial Ketone Utilization in Advanced Human Heart Failure. Circulation. 2016;133(8):706-16.

7. Marks AR, Mcintyre JO, Duncan TM, Erdjument-bromage H, Tempst P, Fleischer S. Molecular cloning and characterization of (R)-3-hydroxybutyrate dehydrogenase from human heart. J Biol Chem. 1992;267(22):15459-63.

8. Weinheimer CJ, Lai L, Kelly DP, Kovacs A. Novel mouse model of left ventricular pressure overload and infarction causing predictable ventricular remodelling and progression to heart failure. Clin Exp Pharmacol Physiol. 2015;42(1):33-40.

9. Sack MN, Rader TA, Park S, Bastin J, Mccune SA, Kelly DP. Fatty acid oxidation enzyme gene expression is downregulated in the failing heart. Circulation. 1996;94(11):2837-42.

10. Schugar RC, Moll AR, André d'avignon D, Weinheimer CJ, Kovacs A, Crawford PA. Cardiomyocyte-specific deficiency of ketone body metabolism promotes accelerated pathological remodeling. Mol Metab. 2014;3(7):754-69.

11. Zinman B, Wanner C, Lachin JM, et al. Empagliflozin, Cardiovascular Outcomes, and Mortality in Type 2 Diabetes. N Engl J Med. 2015;373(22):2117-28.

12. Taylor SI, Blau JE, Rother KI. SGLT2 Inhibitors May Predispose to Ketoacidosis. J Clin Endocrinol Metab. 2015;100(8):2849-52.

13. Mudaliar S, Alloju S, Henry RR. Can a Shift in Fuel Energetics Explain the Beneficial Cardiorenal Outcomes in the EMPA-REG OUTCOME Study? A Unifying Hypothesis. Diabetes Care. 2016;

14. Puchalska P, Crawford PA. Multi-dimensional Roles of Ketone Bodies in Fuel Metabolism, Signaling, and Therapeutics. Cell Metab. 2017;25(2):262-284.

15. Vega RB, Kelly DP. Cardiac nuclear receptors: architects of mitochondrial structure and function. J Clin Invest. 2017;

16. Jensen MV, Joseph JW, Ilkayeva O, et al. Compensatory responses to pyruvate carboxylase suppression in islet beta-cells. Preservation of glucose-stimulated insulin secretion. J Biol Chem. 2006;281(31):22342-51.

.

CHAPTER SIX: CONCLUSION

Cardiac metabolism plays a critical role in the vital function of the heart. The heart is essentially a biotic pump that uses tremendous amounts of energy to force blood through circulation. In order to satiate the high energy requirement of heart function, kilograms of adenosine triphosphate (ATP) are produced daily in the heart. The heart has evolved to be an energetic omnivore, allowing it to adapt to changing physiological environments and nutrient conditions. This characteristic metabolic plasticity is quite apparent in the development of the heart. Substantial metabolic reprogramming events also occur when the heart encounters stress.

Several metabolic abnormalities are signatures of the failing heart. The well-documented alterations include decreased phosphocreatine (PCr)/ATP (excellent prognostic indicators) and decreased fatty acid oxidation (FAO) rates. However, the degree to which the metabolic derangements are causative agents in the pathogenesis of heart failure (HF) is largely unknown.

In an effort to begin to understand how metabolic changes contribute to pathogenesis of early-stage HF, an unbiased systems based approach was used to characterize the metabolome, transcriptome, and proteome. In this series of experiments, the following observations were made: 1) transcript and protein levels are positively correlated between compensated hypertrophy (CH) and HF, 2) very little changes in metabolic gene expression outside of lipid metabolism occur, and 3) metabolite profiles between CH and HF vary drastically. Based on this data set, we hypothesized that a post-translational modification (PTM) was likely regulating enzyme

activity accounting for the discrepant alterations in metabolite profiles without coordinate changes in gene expression.

We then sought to identify candidates for a post-translational modification that could be a causative agent. Based on our data showing elevations in acetyl (C2) pools, we hypothesized that acetylation levels of metabolic proteins may be altered in the failing heart. Indeed, subsequent acetylproteomic analysis showed hyperacetylation of mitochondrial proteins specifically in mouse and human HF but not in CH. At this point, we were unsure of the functional consequences of hyperacetylation, so we used an acetyl-mimic mutation of one of the hyperacetylated residues to establish whether these PTM in HF could be causing dysfunction. The lysine 179 (K179) residue of succinate dehydrogenase, subunit A (SDHA) was mutated to glutamine (K179Q). Whole cell respirometry and biochemical assays showed the K179Q mutation resulted in significant loss-of-function. These data suggested that at least some of the hyperacetylation events observed in HF have functional consequences. Currently, we are establishing parameters, including stoichiometry, by which acetylation events are more likely to be functionally relevant.

Our –omics data also revealed elevations in C4-OH, a by-product of ketone oxidation, leading us to investigate ketone oxidation as an alternative fuel source in HF. Our query found increased levels of 3-hydroxybutyrate dehydrogenase, type 1 (BDH1) on both a transcript and protein level. Collaborative efforts led to substrate oxidation experiments in the isolated heart, showing an increased capacity for ketone oxidation. Ketogenic diet studies and *in vitro* studies verified C4-OH carnitine as a valid

representative metabolite for ketone metabolism. Taken together, these data provided evidence for the hypothesis that ketone oxidation is increasingly relied upon as a fuel in HF. Once we established the presence of increased ketone oxidation, we sought to address the consequences of this fuel substrate shift in HF.

In order to determine if the switch to increased ketone oxidation was adaptive, maladaptive, or otherwise inconsequential, we generated a cardiac-specific (cs) BDH1 knockout (KO) mouse. These mice did not display any overt phenotype other than a slight reduction in the Mendelian ratio of KO mice born. However, when subjected to stress of transverse aortic constriction combined with a small apical myocardial infarction (TAC/MI), the csBDH1 KO fared worse than wild-type (WT) counterparts. From these data, we concluded that increased ketone oxidation in the failing heart is likely an adaptive response. Future experiments are planned to further assess the mechanism by which ketone oxidation plays an adaptive role.

The elevations observed in acetyl pools result in hyperacetylation of mitochondrial proteins in the failing heart. While more investigation is needed to establish which hyperacetylation events are deleterious, we show that at least the K179 SDHA hyperacetylation event is detrimental. The research discussed in this dissertation also shows ketone oxidation is increasingly used in the failing heart. Furthermore, the elevation in ketone oxidation is an adaptive event in HF. This could have far-reaching implications especially in light of the EMPA-REG trials. The main conclusion arrived at in this dissertation is that ***short-chain carbon metabolism is a highly consequential factor in the failing heart phenotype.***

APPENDIX: COPYRIGHT PERMISSION

Copyright Permission for Content in Chapter 3

Julie Horton

From: no-reply@copyright.com
Sent: Monday, February 6, 2017 10:58 AM
To: Julie Horton
Subject: Copyright.com Order Confirmation

Do Not Reply Directly to This Email

To ensure that you continue to receive our emails,
please add copyright@marketing.copyright.com to your address book.

Thank You for Your Order with Copyright Clearance Center

Copyright Clearance Center

Dear Julie Horton,

Thank you for placing your order with Copyright Clearance Center.

Order Summary:
Order Date: 02/06/2017
Confirmation Number: 11623716
Items in order: 1
Order Total: $ 0.00

To view or print your order details or terms and conditions, click the following link and log in:
https://www.copyright.com/dispatcher?type=order&target=historydetail&id=11623716

Need additional permissions? Go here.

How was your experience? Click here to give us feedback.

Sign Up Today!

Copyright Fundamentals: One-Module eLearning Certificate Course

OneCopyright Education's single-module certificate course focuses on the basics of U.S. copyright law from a corporate perspective.

January 19, 2017 at 12:2pm EDT | Registration is $125

If you need assistance, please visit our online help (www.copyright.com/help).

Please do not reply to this message. This e-mail address is not monitored for responses.

Toll Free: +1.855.239.3415
Local: +1.978.646.2600
info@copyright.com
www.copyright.com

1

Copyright Clearance Center

Confirmation Number: 11623716
Order Date: 02/06/2017

Customer Information

Customer: Julie Horton
Account Number: 3001109077
Organization: Sanford Burnham Medical Discovery Institute
Email: jhorton@sbpdiscovery.org
Phone: +1 (321)7475910
Payment Method: Invoice

This is not an invoice

Order Details

JOURNAL OF CLINICAL INVESTIGATION. ONLINE

Billing Status: **N/A**

Order detail ID:	70284301
ISSN:	1558-8238
Publication Type:	e-Journal
Volume:	
Issue:	
Start page:	
Publisher:	AMERICAN SOCIETY FOR CLINICAL INVESTIGATION

Permission Status: Granted
Permission type: Republish or display content
Type of use: Republish in a thesis/dissertation
Order License Id: 4043111213223

Requestor type	Academic institution
Format	Electronic
Portion	chapter/article
Title or numeric reference of the portion(s)	Chapter 3
Title of the article or chapter the portion is from	N/A
Editor of portion(s)	N/A
Author of portion(s)	N/A
Volume of serial or monograph	N/A
Page range of portion	
Publication date of portion	05/01/2017
Rights for	Main product
Duration of use	Life of current edition
Creation of copies for the disabled	no
With minor editing privileges	yes
For distribution to	Worldwide
In the following language(s)	Original language of publication
With incidental promotional use	no
Lifetime unit quantity of new product	Up to 499

Made available in the following markets	education
The requesting person/organization	Julie L Horton
Order reference number	
Author/Editor	Julie Horton
The standard identifier of New Work	Horton_Dissertation
The proposed price	0
Title of New Work	Consequences of Altered Short-Chain Carbon Metabolism in Heart Failure
Publisher of New Work	University of Central Florida
Expected publication date	May 2017
Estimated size (pages)	100

Note: This item was invoiced separately through our **RightsLink service.** More info **$ 0.00**

Total order items: 1 **Order Total: $0.00**

Copyright Permission for Content in Chapter 4

WOLTERS KLUWER HEALTH ORDER DETAILS

Feb 24, 2017

Order Number	501239632
Order date	Feb 24, 2017
Licensed content publisher	Wolters Kluwer Health
Licensed content title	Circulation
Licensed content date	Dec 31, 1969
Type of Use	Thesis/Dissertation
Requestor type	Author of requested content
Format	Electronic
Portion	chapter/article
Title or numeric reference of the portion(s)	The Failing Heart Relies on Ketone Bodies as a Fuel
Title of the article or chapter the portion is from	N/A
Editor of portion(s)	N/A
Author of portion(s)	Julie L Horton
Volume of serial or monograph.	133
Page range of the portion	
Publication date of portion	January 27, 2016
Rights for	Main product
Duration of use	Life of current edition
Creation of copies for the disabled	no
With minor editing privileges	no
For distribution to	Worldwide
In the following language(s)	Original language of publication
With incidental promotional use	no
The lifetime unit quantity of new product	Up to 499
Made available in the following markets	education
The requesting person/organization is:	Julie L Horton
Order reference number	
Author/Editor	Julie L Horton
The standard identifier of New Work	Horton_Dissertation
Title of New Work	Consequences of Altered Short-Chain Carbon Metabolism in Heart Failure
Publisher of New Work	N/A
Expected publication date	May 2017
Estimated size (pages)	100

Total (may include CCC user Not Available fee)

Copyright Clearance Center

Special Rightsholder Terms & Conditions

The following terms & conditions apply to the specific publication under which they are listed.

Circulation
Permission type: Republish or display content
Type of use: Thesis/Dissertation

TERMS AND CONDITIONS

The following terms are individual to this publisher:

None

Other Terms and Conditions:

STANDARD TERMS AND CONDITIONS

1. Description of Service; Defined Terms. This Republication License enables the User to obtain licenses for republication of one or more copyrighted works as described in detail on the relevant Order Confirmation (the "Work(s)"). Copyright Clearance Center, Inc. ("CCC") grants licenses through the Service on behalf of the rightsholder identified on the Order Confirmation (the "Rightsholder"). "Republication", as used herein, generally means the inclusion of a Work, in whole or in part, in a new work or works, also as described on the Order Confirmation. "User", as used herein, means the person or entity making such republication.

2. The terms set forth in the relevant Order Confirmation, and any terms set by the Rightsholder with respect to a particular Work, govern the terms of use of Works in connection with the Service. By using the Service, the person transacting for a republication license on behalf of the User represents and warrants that he/she/it (a) has been duly authorized by the User to accept, and hereby does accept, all such terms and conditions on behalf of User, and (b) shall inform User of all such terms and conditions. In the event such person is a "freelancer" or other third party independent of User and CCC, such party shall be deemed jointly a "User" for purposes of these terms and conditions. In any event, User shall be deemed to have accepted and agreed to all such terms and conditions if User republishes the Work in any fashion.

3. Scope of License; Limitations and Obligations.

3.1 All Works and all rights therein, including copyright rights, remain the sole and exclusive property of the Rightsholder. The license created by the exchange of an Order Confirmation (and/or any invoice) and payment by User of the full amount set forth on that document includes only those rights expressly set forth in the Order Confirmation and in these terms and conditions, and conveys no other rights in the Work(s) to User. All rights not expressly granted are hereby reserved.

3.2 General Payment Terms: You may pay by credit card or through an account with us payable at the end of the month. If you and we agree that you may establish a standing account with CCC, then the following terms apply: Remit Payment to: Copyright Clearance Center, Dept 001, P.O. Box 843006, Boston, MA 02284-3006. Payments Due: Invoices are payable upon their delivery to you (or upon our notice to you that they are available to you for downloading). After 30 days, outstanding amounts will be subject to a service charge of 1-1/2% per month or, if less, the maximum rate allowed by applicable law. Unless otherwise specifically set forth in the Order Confirmation or in a separate written agreement signed by CCC, invoices are due and payable on "net 30" terms. While User may exercise the rights licensed immediately upon issuance of the Order Confirmation, the license is automatically revoked and is null and void, as if it had never been issued, if complete payment for the license is not received on a timely basis either from User directly or through a payment agent, such as a credit card company.

3.3 Unless otherwise provided in the Order Confirmation, any grant of rights to User (i) is "one-time" (including the editions and product family specified in the license), (ii) is non-exclusive and non-transferable and (iii) is subject to any and all limitations and restrictions (such as, but not limited to, limitations on duration of use or circulation) included in the Order Confirmation or invoice and/or in these terms and conditions. Upon completion of the licensed use, User shall either secure a new permission for further use of the Work(s) or immediately cease any new use of the Work(s) and shall render inaccessible (such as by deleting or by removing or severing links or other locators) any further copies of the Work (except for copies printed on paper in accordance with this license and still in User's stock at the end of such period).

3.4 In the event that the material for which a republication license is sought includes third party materials (such as photographs, illustrations, graphs, inserts and similar materials) which are identified in such material as having been used by permission, User is responsible for identifying, and seeking separate licenses (under this Service or otherwise) for, any of such third party materials; without a separate license, such third party materials may not be used.

3.5 Use of proper copyright notice for a Work is required as a condition of any license granted under the Service. Unless otherwise provided in the Order Confirmation, a proper copyright notice will read substantially as follows: "Republished with permission of [Rightsholder's name], from [Work's title, author, volume, edition number and year of copyright]; permission conveyed through Copyright Clearance Center, Inc. " Such notice must be provided in a reasonably legible font size and must be placed either immediately adjacent to the Work as used (for example, as part of a by-line or footnote but not as a separate electronic link) or in the place where substantially all other credits or notices for the new work containing the republished Work are located. Failure to include the required notice results in loss to the Rightsholder and CCC, and the User shall be liable to pay liquidated damages for each such failure equal to twice the use fee specified in the Order Confirmation, in addition to the use fee itself and any other fees and charges specified.

3.6 User may only make alterations to the Work if and as expressly set forth in the Order Confirmation. No Work may be used in any way that is defamatory, violates the rights of third parties (including such third parties' rights of copyright, privacy, publicity, or other tangible or intangible property), or is otherwise illegal, sexually explicit or obscene. In addition, User may not conjoin a Work with any other material that may result in damage to the reputation of the Rightsholder. User agrees to inform CCC if it becomes aware of any infringement of any rights in a Work and to cooperate with any reasonable request of CCC or the Rightsholder in connection therewith.

4. Indemnity. User hereby indemnifies and agrees to defend the Rightsholder and CCC, and their respective employees and directors, against all claims, liability, damages, costs and expenses, including legal fees and expenses, arising out of any use of a Work beyond the scope of the rights granted herein, or any use of a Work which has been altered in any unauthorized way by User, including claims of defamation or infringement of rights of copyright, publicity, privacy or other tangible or intangible property.

5. Limitation of Liability. UNDER NO CIRCUMSTANCES WILL CCC OR THE RIGHTSHOLDER BE LIABLE FOR ANY DIRECT, INDIRECT, CONSEQUENTIAL OR INCIDENTAL DAMAGES (INCLUDING WITHOUT LIMITATION DAMAGES FOR LOSS OF BUSINESS PROFITS OR INFORMATION, OR FOR BUSINESS INTERRUPTION) ARISING OUT OF THE USE OR INABILITY TO USE A WORK, EVEN IF ONE OF THEM HAS BEEN ADVISED OF THE POSSIBILITY OF SUCH DAMAGES. In any event, the total liability of the Rightsholder and CCC (including their respective employees and directors) shall not exceed the total amount actually paid by User for this license. User assumes full liability for the actions and omissions of its principals, employees, agents, affiliates, successors and assigns.

6. Limited Warranties. THE WORK(S) AND RIGHT(S) ARE PROVIDED "AS IS". CCC HAS THE RIGHT TO GRANT TO USER THE RIGHTS GRANTED IN THE ORDER CONFIRMATION DOCUMENT. CCC AND THE RIGHTSHOLDER DISCLAIM ALL OTHER WARRANTIES RELATING TO THE WORK(S) AND RIGHT(S), EITHER EXPRESS OR IMPLIED, INCLUDING WITHOUT LIMITATION IMPLIED WARRANTIES OF MERCHANTABILITY OR FITNESS FOR A PARTICULAR PURPOSE. ADDITIONAL RIGHTS MAY BE REQUIRED TO USE ILLUSTRATIONS, GRAPHS, PHOTOGRAPHS, ABSTRACTS, INSERTS OR OTHER PORTIONS OF THE WORK (AS OPPOSED TO THE ENTIRE WORK) IN A MANNER CONTEMPLATED BY USER; USER UNDERSTANDS AND AGREES THAT NEITHER CCC NOR THE RIGHTSHOLDER MAY HAVE SUCH ADDITIONAL RIGHTS TO GRANT.

7. Effect of Breach. Any failure by User to pay any amount when due, or any use by User of a Work beyond the scope of the license set forth in the Order Confirmation and/or these terms and conditions, shall be a material breach of the license created by the Order Confirmation and these terms and conditions. Any breach not cured within 30 days of written notice thereof shall result in immediate termination of such license without further notice. Any unauthorized (but licensable) use of a Work that is terminated immediately upon notice thereof may be liquidated by payment of the Rightsholder's ordinary license price therefor; any unauthorized (and unlicensable) use that is not terminated immediately for any reason (including, for example, because materials containing the Work cannot reasonably be recalled) will be subject to all remedies available at law or in equity, but in no event to a payment of less than three times the Rightsholder's ordinary license price for the most closely analogous licensable use plus Rightsholder's and/or CCC's costs and expenses incurred in collecting such payment.

8. **Miscellaneous.**

8.1 User acknowledges that CCC may, from time to time, make changes or additions to the Service or to these terms and conditions, and CCC reserves the right to send notice to the User by electronic mail or otherwise for the purposes of notifying User of such changes or additions; provided that any such changes or additions shall not apply to permissions already secured and paid for.

8.2 Use of User-related information collected through the Service is governed by CCC's privacy policy, available online here: http://www.copyright.com/content/cc3/en/tools/footer/privacypolicy.html.

8.3 The licensing transaction described in the Order Confirmation is personal to User. Therefore, User may not assign or transfer to any other person (whether a natural person or an organization of any kind) the license created by the Order Confirmation and these terms and conditions or any rights granted hereunder; provided, however, that User may assign such license in its entirety on written notice to CCC in the event of a transfer of all or substantially all of User's rights in the new material which includes the Work(s) licensed under this Service.

8.4 No amendment or waiver of any terms is binding unless set forth in writing and signed by the parties. The Rightsholder and CCC hereby object to any terms contained in any writing prepared by the User or its principals, employees, agents or affiliates and purporting to govern or otherwise relate to the licensing transaction described in the Order Confirmation, which terms are in any way inconsistent with any terms set forth in the Order Confirmation and/or in these terms and conditions or CCC's standard operating procedures, whether such writing is prepared prior to, simultaneously with or subsequent to the Order Confirmation, and whether such writing appears on a copy of the Order Confirmation or in a separate instrument.

8.5 The licensing transaction described in the Order Confirmation document shall be governed by and construed under the law of the State of New York, USA, without regard to the principles thereof of conflicts of law. Any case, controversy, suit, action, or proceeding arising out of, in connection with, or related to such licensing transaction shall

be brought, at CCC's sole discretion, in any federal or state court located in the County of New York, State of New York, USA, or in any federal or state court whose geographical jurisdiction covers the location of the Rightsholder set forth in the Order Confirmation. The parties expressly submit to the personal jurisdiction and venue of each such federal or state court. If you have any comments or questions about the Service or Copyright Clearance Center, please contact us at 978-750-8400 or send an e-mail to info@copyright.com.

v 1.1

Close